NASA Technical Memorandum 1999–206892, Volume 3

SeaWiFS Postlaunch Technical Report Series

Stanford B. Hooker, Editor
NASA Goddard Space Flight Center
Greenbelt, Maryland

Elaine R. Firestone, Senior Technical Editor
SAIC General Sciences Corporation
Beltsville, Maryland

Volume 3, The SeaBOARR-98 Field Campaign

Stanford B. Hooker
NASA Goddard Space Flight Center
Greenbelt, Maryland

Giuseppe Zibordi
Joint Research Centre
Ispra, Italy

Gordana Lazin
Dalhousie University
Halifax, Canada

Scott McLean
Satlantic, Inc.
Halifax, Canada

Abstract

This report documents the scientific activities during the first Sea-viewing Wide Field-of-view Sensor (SeaWiFS) Bio-Optical Algorithm Round-Robin (SeaBOARR-98) experiment, which took place from 5–17 July 1998, at the *Acqua Alta* Oceanographic Tower (AAOT) in the northern Adriatic Sea off the coast of Italy. The ultimate objective of the SeaBOARR activity is to evaluate the effect of different measurement protocols on bio-optical algorithms using data from a variety of field campaigns. The SeaBOARR-98 field campaign was concerned with collecting a high quality data set of simultaneous in-water and above-water radiometric measurements. The deployment goals documented in this report were to: a) use four different surface glint correction methods to compute water-leaving radiances, $L_W(\lambda)$, from above-water data; b) use two different in-water profiling systems and three different methods to compute $L_W(\lambda)$ from in-water data (one making measurements at a fixed distance from the tower, 7.5 m, and the other at variable distances up to 29 m away); c) use instruments with a common calibration history to minimize intercalibration uncertainties; d) monitor the calibration drift of the instruments in the field with a second generation SeaWiFS Quality Monitor (SQM-II), to separate differences in methods from changes in instrument performance; and e) compare the $L_W(\lambda)$ values estimated from the above-water and in-water measurements. In addition to describing the instruments deployed and the data collected, a preliminary analysis of the data is presented, and the kind of follow-on work that is needed to completely assess the estimation of $L_W(\lambda)$ from above-water and in-water measurements is discussed.

1. INTRODUCTION

From 5–17 July 1998, an international group was deployed to the *Acqua Alta* Oceanographic Tower (AAOT) in the northern Adriatic Sea off the coast of Italy. The team consisted of scientists and technicians from the National Aeronautics and Space Administration (NASA) Goddard Space Flight Center (GSFC), the Space Applications Institute (SAI) Marine Environment Unit of the Joint Research Centre (JRC) of the Commission of the European Communities (CEC), the *Istituto per lo Studio della Dinamica delle Grandi Masse* (ISDGM) of the Italian *Consiglio Nazionale delle Ricerche* (CNR), Dalhousie University, and Satlantic, Inc. The science team from these organizations is given in Appendix A. Although most of the institutes involved participated independently, the NASA Sea-viewing Wide Field-of-view Sensor (SeaWiFS) Project provided additional funding to different aspects of the activity to ensure the availability of the needed elements.

The purpose of the deployment was to make in-water and above-water radiometric measurements in support of three activities (listed from highest to lowest priority):

1. Continue an ongoing time series of bio-optical measurements that are used by the European Coastal Atmosphere and Sea Time Series (CoASTS) activity and the SeaWiFS Project;
2. Validate a tower-shading correction methodology for the AAOT that was devised after a previous set of experiments (Zibordi et al. 1999); and
3. Collect a high quality data set of simultaneous in-water and above-water radiometric measurements along with a suite of bio-optical parameters.

The prioritization of the activities was deemed necessary to ensure rational sampling choices in the event of adverse environmental conditions. As it turned out, the weather provided a sufficient amount of environmental conditions to assemble a complete and comprehensive data set. The deployment was called the first SeaWiFS Bio-Optical Algorithm Round-Robin (SeaBOARR-98) experiment, because the ultimate objective is to evaluate the effect of the different measurement protocols on bio-optical algorithms from a variety of field campaigns. This report details the first steps in that long-term analysis.

Spectral water-leaving radiance, $L_W(\lambda)$, is the central physical quantity for bio-optical studies in the upper ocean. Whether determined from below- or above-surface measurements, $L_W(\lambda)$ must be accurately measured. The SeaWiFS Project, for example, requires $L_W(\lambda)$ uncertainties be 5% or less (Hooker et al. 1993a). This is thought to be routinely achievable for in-water measurements in Case-1 waters, but the uncertainty associated with above-water measurements has not been well quantified. The main difficulty for the latter is associated with correcting the above-water observations for the effect of surface waves which introduce significant fluctuations into the glint and reflected sky light components of the surface radiance field. The problem is made more difficult by the presence of clouds which increase the fluctuations and associated uncertainties.

At present, there are several methods for surface glint correction which were developed for different conditions in which remote measurements are made, i.e., clear or cloudy sky, and Case-1 or Case-2 water: Austin (1974); Morel (1980); Carder and Steward (1985); Bukata et al. (1988); Mueller and Austin (1995), the so-called SeaWiFS

protocol; Lee et al. (1996); and Lazin (1998). Hereafter, Morel (1980), Carder and Steward (1985) and as further explained in Lee et al. (1996), the Mueller and Austin (1995) SeaWiFS protocol, and Lazin (1998) are referred to as M80, C85, S95, and L98, respectively.

The in-water analysis techniques currently in use are based primarily on the Smith and Baker (1984) method, hereafter referred to as S84. Variations are derived from what measurement procedures (and platforms) are used to acquire the data, and how the in-water data is propagated to the surface. Two alternative techniques were implemented in the ProSoft† software that is freely available for processing bio-optical data collected with Satlantic, Inc.‡ (Halifax, Canada) instruments. The two alternative ProSoft methods rely on a surface buoy to measure the in-water radiance field close to the sea surface and are categorized according to when the options were added to ProSoft, which occurred in 1994 and 1997, so the two are referred to hereafter as P94 and P97, respectively. The SeaBOARR-98 goals documented here were to:

1. Use four surface glint correction methods (M80, C85, S95, and L98) to compute $L_W(\lambda)$ from above-water data;
2. Use two in-water profiling systems and three in-water analysis methods (S84, P94, and P97) to compute $L_W(\lambda)$ from in-water data;
3. Use radiometers with a common calibration history to minimize intercalibration uncertainties;
4. Monitor the calibration drift of the instruments in the field with a second generation SeaWiFS Quality Monitor, the so-called SQM-II, to separate differences in methodologies from changes in instrument performance; and
5. Compare the results to the $L_W(\lambda)$ values estimated from the above-water and in-water measurements.

2. INSTRUMENTATION

The AAOT is located approximately 15 km east of the city of Venice (12.5083°E,45.3139°N). The water depth immediately below the tower is about 17 m and the composition of the nearby sea floor is primarily sand and silt. The tower was built in 1975 and is owned and operated by CNR/ISDGM in Venice. The tower is composed of four levels supported by four large pillars. Each level is approximately 7.2 m×5.2 m in size with the exception of the lowest level which is 5.2 m×5.2 m.

The first (lowest) tower level, about 4.5 m above the water, has an open grid deck and no facilities. The second level is approximately 7 m above the water and contains a workshop, two 12 kW diesel-powered electrical generators, a portable scientific laboratory, and storage spaces for a large complement of lead-acid batteries, fuel tanks, etc. At this level, a special open grid platform, 3.5 m wide, extends 6.5 m over the sea towards the southeast and provides mounting points for instruments to be deployed above, or into, the sea. The Wire-Stabilized Profiling Environmental Radiometer (WiSPER) package is deployed from this platform. Also located on this level is the water filtering and hydrography laboratory. The third deck contains the main laboratory, which is also the primary accomodations space (with room for five people to stay overnight). The fourth (upper-most) deck, at about 13 m above the water, contains a wind generator, solar panels, a variety of meteorological instruments, communications antennae, plus freshwater and seawater storage tanks.

Although the primary reason for selecting the AAOT for SeaBOARR-98 was the ongoing use of the tower by a rigorous group of optical oceanographers (JRC and CNR), the other reasons were its stability (towers do not pitch and roll like ships), and its proximity to a strong coastal front. The water around the tower can be Case-1 or Case-2 depending on whether the coastal front is pushed onshore or off. The opportunity for sampling different water types within one field campaign was very appealing.

For SeaBOARR-98, the total number of optical systems deployed on the tower was increased from one (WiSPER is permanently installed on the tower) to six:

a) The miniature NASA Environmental Sampling System (miniNESS),
b) The recently modified SeaWiFS Surface Acquisition System (SeaSAS),
c) The WiSPER system,
d) The Dalhousie University SeaWiFS Aircraft Simulator (DalSAS),
e) The Dalhousie University Buoyant Optical Surface Sensor (DalBOSS), and
f) An SQM-II, which was set up in the water filtering and hydrography laboratory.

Detailed descriptions of each system are given in Sections 2.1–2.6, respectively, so only a brief introduction is given here. The two in-water profilers are miniNESS and WiSPER; SeaSAS and DalSAS are above-water instruments, and DalBOSS makes both types of measurements.

The SQM-II and all of the radiometers used with the miniNESS, SeaSAS, WiSPER, DalSAS, and DalBOSS instruments, were manufactured by Satlantic, Inc. This commonality in equipment was not accidental; the SeaBOARR

† ProSoft is a bio-optical data analysis and visualization program from the Department of Oceanography at Dalhousie University (Halifax, Canada); it is written using MatLab™ software from Mathworks, Inc. (Natick, Massachusetts), and is available from `raptor.ocean.dal.ca`.

‡ Identification of commercial equipment to adequately specify or document the experimental problem does not imply recommendation or endorsement, nor does it imply that the equipment identified is necessarily the best available for the purpose.

Table 1. Channel numbers and center wavelengths (in nanometers) for the radiometers used with SeaBOARR-98 radiometric sampling systems. The sensor systems are given with their individual sensor codes which are formed from a one-letter designator for the type of sensor, plus a two-digit serial number (S/N). All of the channels have 10 nm bandwidths except the DalSAS instruments for which the 412, 443, 490, 510, and 555 nm channels have 20 nm bandwidths. Note that the M99 sensor was the solar irradiance reference for both miniNESS and SeaSAS, but it is only shown once for miniNESS.

Channel	*miniNESS*			*SeaSAS*		*WiSPER*		*DalSAS*				*DalBOSS*	
Number	R35	I40	M99	S69	S28	R46	I71	S64	S09	M20	M93	Q33	N48
1	411.1	411.5	411.5	412.6	412.7	412.3	411.3	412.7	412.7	412.6	412.5	406.5	405.1
2	442.9	442.5	442.8	442.4	443.1	442.8	442.9	443.5	444.0	443.2	443.5	412.2	412.4
3	489.9	489.3	489.9	491.3	489.5	490.5	490.2	490.0	491.5	491.5	490.0	435.3	435.6
4	509.7	509.6	510.3	510.3	510.1	510.8	510.1	781.9	780.7	781.6	781.7	443.4	442.9
5	554.8	555.4	554.5	554.1	554.8	554.9	554.8	510.9	510.5	509.8	509.3	455.9	456.1
6	665.0	665.7	664.8	669.8	670.0	665.8	665.6	554.6	554.4	554.6	554.4	489.9	489.3
7	683.1	683.2	683.2	683.6	682.5	683.9	683.6	666.4	665.3	665.6	665.8	510.4	510.4
8												531.6	531.5
9												554.6	554.5
10												590.3	590.4
11												665.1	664.8
12												670.0	670.0
13												700.6	700.6

science team decided this was the easiest way to ensure redundancy and intercalibration. Another reason for relying on one manufacturer was it greatly simplified calibration monitoring with the SQM-II, since all the radiometers had identical outer dimensions, which meant the SQM-II did not have to be repeatedly reconfigured.

SeaSAS, WiSPER, miniNESS, and DalSAS all use 7-channel ocean color radiance series 200 (OCR-200) sensors, as well as 7-channel ocean color irradiance series 200 (OCI-200) sensors. Both radiometers utilize 16-bit analog-to-digital (A/D) converters and are capable of detecting light over a four-decade range. DalBOSS is equipped with both 13-channel OCI and OCR series 1000 radiometers (OCI-1000 and OCR-1000, respectively), which employ 24-bit A/D converters plus gain switching, and are capable of detecting light over a seven-decade range.

A benefit of assembling (nearly) identical equipment from the participating investigators was the wavelengths and bandwidths (10 nm) for the different instruments were very similar. A summary of the radiometer wavelengths and their sensor codes is given in Table 1. This made it much easier to make substitutions in the event of failures. For example, shortly after deploying to the tower, the original irradiance reference for miniNESS malfunctioned (the power and telemetry unit would fail intermittently); a spare reference was used as a substitute with no loss of functionality and no interruption to data acquisition.

The miniNESS profiler measures upwelled radiance and downwelled irradiance as a function of depth, $L_u(z)$ and $E_d(z)$, respectively. A separate sensor measures the total solar irradiance (the direct plus the indirect or diffuse components) just above the sea surface, $E_d(0^+)$. Internal tilt sensors quantify the vertical orientation (φ) of the profiler as it falls through the water. The WiSPER package makes the same measurements as miniNESS, $L_u(z)$ and $E_d(z)$, but it is winched up and down the water column between two taught wires, so it has no need for tilt sensors. In addition, the E_d sensor can be rotated 180° to measure $E_u(z)$. DalBOSS is a floating buoy, so it can measure $E_d(0^+)$ well clear of any perturbative effects associated with the superstructure of the tower. A downward-looking radiance sensor at the bottom of the buoy measures the upwelled radiance at a depth (z_0) close to the sea surface, $L_u(z_0)$.

The SeaSAS instruments measure the indirect (or sky) radiance reaching the sea surface, $L_i(0^+)$, and the (total) radiance right above the sea surface, $L_T(0^+)$. The latter is composed of three terms: the radiance leaving the sea surface from below (the so-called water-leaving radiance), the direct sunlight reflecting off the surface (the so-called sun glint), and the indirect sky light reflecting off the surface (the so-called sky glint). A separate sensor measures $E_d(0^+)$ which, in this case, is the same sensor used with miniNESS (the output of the irradiance sensor is sent to both data acquisition systems). DalSAS makes the same measurements as SeaSAS, $L_i(0^+)$ and $L_T(0^+)$, but the surface-viewing radiometer looks through a square aperture that can be blocked with a gray plaque, so it can also measure the radiance of the plaque, $L_p(0^+)$. Two separate sensors are used to measure the total and indirect (or diffuse) solar irradiance just above the sea surface, $E_d(0^+)$ and $E_i(0^+)$, respectively.

In addition to paying close attention to the optimal viewing capabilities of each instrument system, some instruments were equipped with sensors that measured their

viewing angles. SeaSAS, for example, had an external module that measured the vertical (two-axis) tilts and horizontal (compass) pointing of the radiometers (the so-called DIR-10 unit); miniNESS and DalBOSS had internal sensor modules that measured the vertical (two-axis) tilts of the radiometers. A generalized coordinate system for these pointing systems is given in Fig. 1.

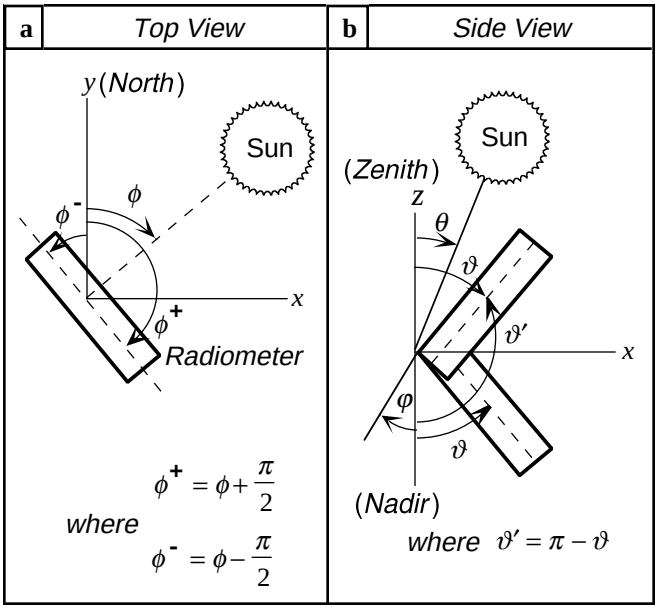

Fig. 1. The coordinate systems used for instrument pointing: **a)** looking down from above (the z-axis is out of the page), and **b)** looking from the side (the y-axis is out of the page). The ϕ coordinate is the solar azimuth angle, θ is the solar zenith angle, and ϑ is the radiometer pointing angle with respect to the vertical axis, z. The perturbations (or tilts) in vertical alignment, which can change the pointing angles, are given by φ.

Note that ϕ is measured with respect to an arbitrary reference, in this case due north, and ϑ is measured with respect to nadir (the direction pointing straight down to the sea surface). The angle ϑ' corresponds to the angle ϑ measured with respect to the zenith (the direction pointing straight up from the sea surface).

The basic data sampling activity involved collecting data from all of the instruments as simultaneously as possible, so hand-held radios were used to coordinate the beginning and ending of sampling intervals. Although it would have been preferable to have all of the instruments sampling the smallest patch of water possible, space limitations on the tower did not permit this. The DalSAS instrument had to be mounted on the top-most deck, which has a number of superstructure obstacles (wind generator, antenna masts, etc.), so to ensure unperturbed viewing of the sea surface during most of the day, two locations were chosen (Fig. 2). Depending on the time of day, this instrument was moved from one site to the other.

To facilitate tracking of the radiometric instruments during SQM-II sessions, each light sensor was assigned a code. A summary of the instruments, along with their primary physical measurements (in terms of vertical sampling) and sensor codes is given in Table 2.

Table 2. A summary of the radiometers used during SeaBOARR-98 along with their primary physical measurement (in terms of their vertical sampling) and their sensor codes.

System	*Sensor*	*Measure*	*Code*
miniNESS	OCR-200	$L_u(z)$	R35
	OCI-200	$E_d(z)$	I40
	OCI-200	$E_d(0^+)$	M99
SeaSAS	OCR-200	$L_i(0^+)$	S69
	OCR-200	$L_T(0^+)$	S28
	OCI-200	$E_d(0^+)$	M99
	DIR-10	ϑ,ϕ	D01
WiSPER	OCR-200	$L_u(z)$	R46
	OCI-200	$E_d(z)$	I71
DalSAS	OCR-200	$L_i(0^+)$	S64
	OCR-200	$L_T(0^+)$	S09
	OCR-200	$L_p(0^+)$	S09
	OCI-200	$E_d(0^+)$	M20
	OCI-200	$E_i(0^+)$	M93
DalBOSS	OCR-1000	$L_u(z_0)$	Q33
	OCI-1000	$E_d(0^+)$	N48

In addition to the above-water and in-water optical measurements, a variety of other data were collected to help characterize the optical properties of the AAOT site:

1. Seawater temperature and salinity by CTD measurements, plus tide level;
2. Seawater attenuation and absorption profiles at nine wavelengths by AC-9 measurements;
3. Pigment analyses using the high performance liquid chromatography (HPLC) technique;
4. Particle size distribution of sea water particles by Coulter Counter analysis with a Multisizer-II;
5. Direct sun irradiance and sky radiance measurements by CE-318 measurements;
6. *In vivo* spectral absorption of particulate matter (PM) and colored dissolved organic matter (CDOM) through spectrophotometric techniques;
7. Atmospheric pressure, humidity, and temperature, plus wind speed and direction; and
8. Total suspended matter (TSM) through gravimetric filter analysis.

2.1 miniNESS

The miniNESS profiler is a tethered free-falling instrument. It is a variant of the Low-Cost NASA Environmental

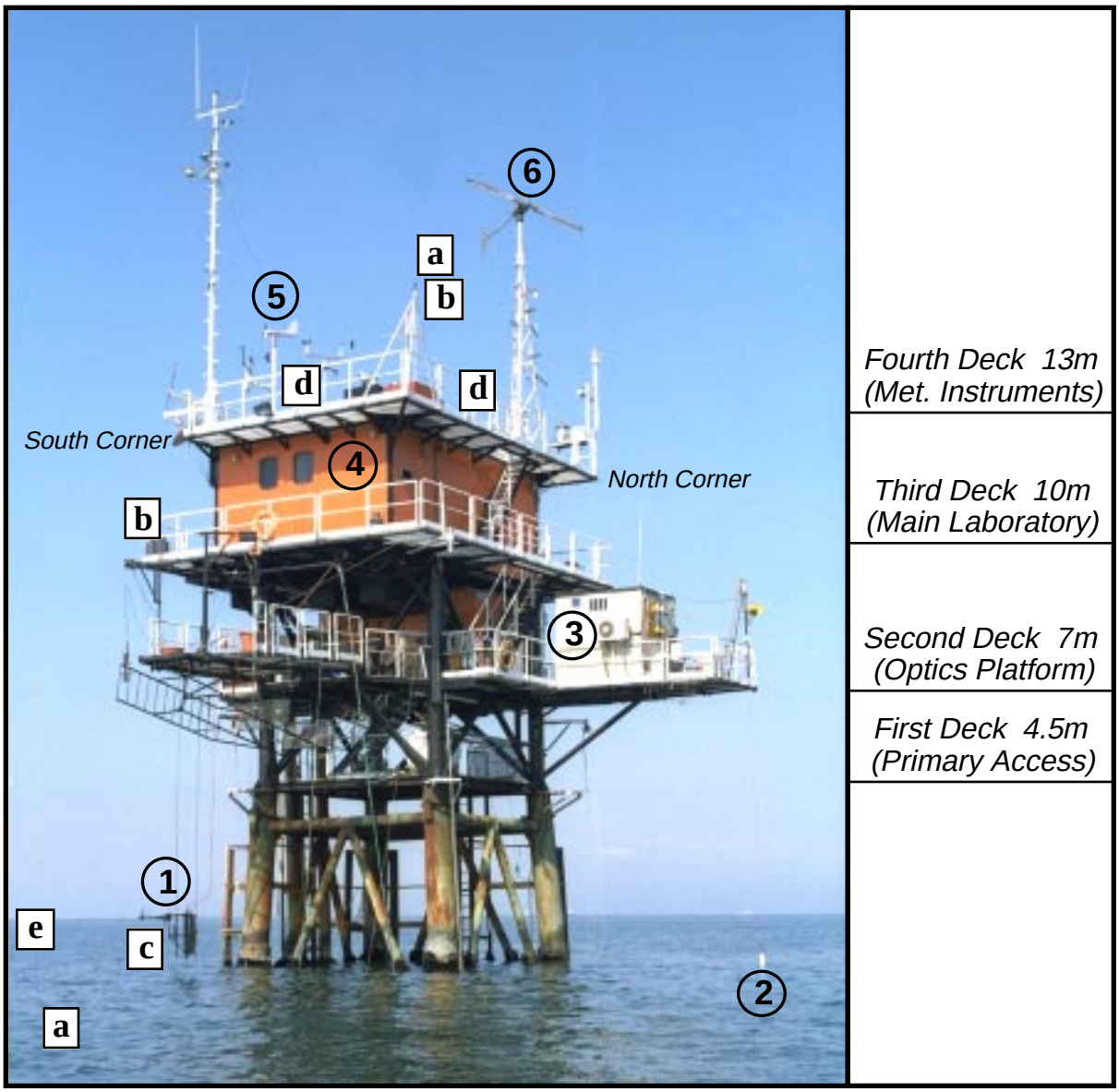

Fig. 2. The AAOT showing the permanently installed equipment (circles with numbers) and the deployment locations of the instruments used during SeaBOARR-98 (squares with letters). The different levels are shown in the right-most panel along with their heights above the water. The installed inventory is as follows: 1) WiSPER, 2) conductivity, temperature, and depth (CTD) profiler, 3) water filtering and hydrography laboratory, 4) main lab and accommodations space, 5) meteorological instruments, and 6) wind generator. The deployment locations for SeaBOARR-98 were a) miniNESS (the irradiance reference sensor for miniNESS and SeaSAS was deployed on a mast located on the eastern corner of the fourth deck), b) SeaSAS, c) WiSPER, d) DalSAS (two deployment points for DalSAS are shown and the irradiance reference sensors were located at the left-most location), and e) DalBOSS.

Sampling System (LoCNESS) which is built up from components used with the SeaWiFS Optical Profiling System (SeaOPS) on Atlantic Meridional Transect (AMT) cruises (Robins et al. 1996). An in-air irradiance sensor (M99) measured the incident solar irradiance just above the sea surface, $E_d(0^+, \lambda)$. The irradiance sensor was packaged with a DATA-100 module (as an integral unit) that converted the analog output of the OCI-200 radiometer to RS-485 serial communications. For SeaBOARR-98, the sensor package was mounted on a mast on the top-most tower deck (eastern corner). The height and location of the mast ensured none of the tower's superstructure shadowed the sensor under almost all illumination conditions. A summary of the data collected with the miniNESS profiler and its reference is presented in Appendix B. A schematic of

the instruments used with the miniNESS profiler is given in Fig. 3.

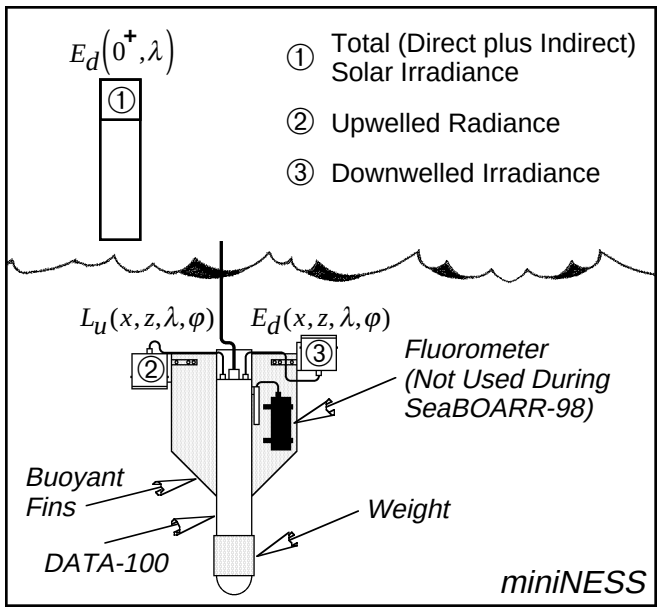

Fig. 3. A schematic of the miniNESS profiler.

The free-fall aspects of the miniNESS design are derived from the SeaWiFS Free-Falling Advanced Light Level Sensors (SeaFALLS) profiler which is based on a Satlantic SeaWiFS Profiling Multichannel Radiometer (SPMR). In the SeaFALLS design, 13-channel OCR-1000 and OCI-1000 sensors are connected in line with power and telemetry modules (24-bit A/D converters for the light sensors) to form a 1.24 m long cylinder. The OCR-1000 is oriented as the *nose* to measure $L_u(z,\lambda)$, and the OCI-1000 as the *tail* to measure $E_d(z,\lambda)$. The addition of weight to the nose and buoyant (foam) fins to a tail bracket produces a rocket-shaped package that falls through the water column with minimum tilts (less than 2°). The power and telemetry cable extends through the field of view of the irradiance sensor, but the small diameter of the cable (7 mm) minimizes any negative effects on the measured light field.

The LoCNESS profiler is built out of modular, low-cost components: a DATA-100 (with 16-bit A/D converters) for power and telemetry, and 7-channel OCR-200 and OCI-200 sensors. In the LoCNESS configuration, the DATA-100 and the two light sensors are connected in line using extension brackets, with the OCR-200 at the nose, and the OCI-200 at the tail. The LoCNESS profiler can also be built with the Three-Headed Optical Recorder (THOR) option, in which case an adapter plate is used on the nose to permit the mounting of two sensors rather than one: the usual $L_u(z,\lambda)$ sensor plus an additional $E_u(z,\lambda)$ sensor. The two nose sensors do not disturb the stability of the profiler during descent. In fact, THOR has the smallest and most stable tilts of all the profilers. This stability, and the fact that three components of the light field are measured during each profile, makes it one of the most versatile profilers in use today.

The LoCNESS profiler is 1.78 m long with the light sensors separated by the DATA-100 and the extension brackets. This is not an optimal configuration for the shallow, Case-2 water frequently encountered at the AAOT site, so a more compact (0.73 m long) profiler was produced by mounting a radiance sensor (R35) on one fin, an irradiance sensor (I40) on the fin opposite the radiance sensor, and dispensing with the extension brackets. As with LoCNESS, the light sensors send their analog signals to a DATA-100 (S/N 8), which digitizes them (16 bits) and converts the counts to RS-485 serial communications. A comparison of miniNESS with LoCNESS and SeaFALLS is shown in Fig. 4.

A three-headed version of miniNESS capable of also measuring E_u was recently built (for JRC). This profiler is longer than the two-headed version, because the DATA-100 needs another A/D module and an extension bracket must be added to the nose to accommodate the E_u sensor. A flared metal cage is also added to the nose to protect the E_u sensor against accidental bottom impact.

Putting light sensors on the fins destabilizes the profiler (although, tilts less than 2° have been regularly achieved on AMT cruises by carefully trimming the profiler with the added weight), and it makes the L_u sensor more susceptible to shading. This problem was minimized by choosing where the mechanical termination was with respect to the sensors and the sun. In general, the two sensor fins, which are 180° apart, will align perpendicular to the mechanical termination when the cable is pulled in to bring the profiler to the surface (before a profile). To minimize L_u sensor shading, all that is required is to choose which of the other two fins should be used for the mechanical termination, so the L_u sensor aligns towards the sun.

The RS-485 signals from the two DATA-100 units were combined in a Satlantic deck box and converted to RS-232 communications for computer logging. The deck box also provided the (computer-controlled) power for all the sensors and was designed to avoid instrument damage due to improper power-up sequences over varying cable lengths. The RS-232 data were logged on a Macintosh PowerBook computer using software developed at the University of Miami Rosenstiel School for Marine and Atmospheric Science (RSMAS) and the SeaWiFS Project.

The software time stamps the two data streams (in-water and above-water measurements) and writes them to disk simultaneously. The data is stored as American Standard Code for Information Interchange (ASCII), tab-delimited (spreadsheet) files. The software controls the logging and display of the data streams as a function of the data collection activity being undertaken: dark data (caps on the radiometers), down cast, SQM calibration monitoring, etc. The selection of the execution mode automatically sets the file name, so all the operator has to

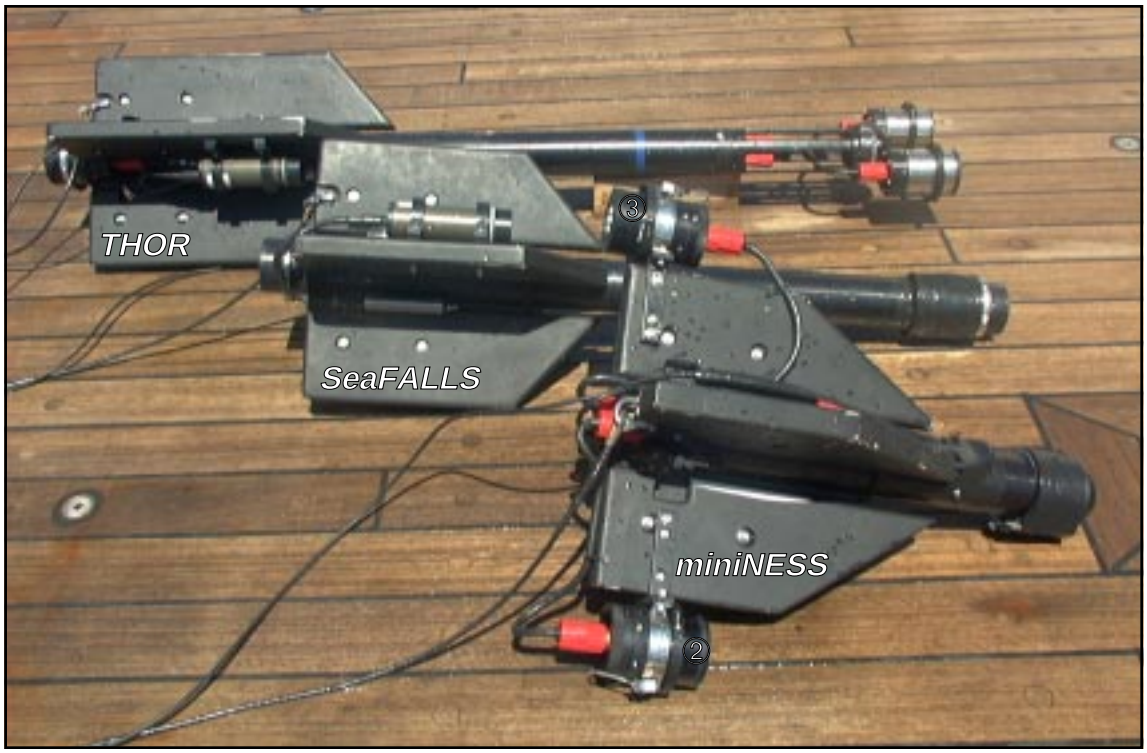

Fig. 4. A side-by-side comparison of the three free-falling profilers discussed in this report: THOR (back), SeaFALLS (middle), and miniNESS (front). THOR is 1.78 m long, SeaFALLS is 1.24 m long, and miniNESS is 0.73 m long. The numbered bullets on the miniNESS sensors correspond to the same bullets in Fig. 3.

do is push buttons to initiate and terminate data acquisition. All of the telemetry channels can be displayed in real time, and the operator can select from a variety of plotting options to visualize the data being collected.

2.2 SeaSAS

SeaSAS was equipped with three radiometers. One radiance sensor (S69) measured the indirect (or sky) radiance, $L_i(0^+)$; a second radiance sensor (S28) measured the total radiance right above the sea surface, $L_T(0^+)$; and a separate irradiance sensor (M99) measured $E_d(0^+)$ (this was the same sensor used with miniNESS). In addition to the radiometers, SeaSAS was equipped with a DIR-10 which measured the pointing geometry and stability (vertically and horizontally) of the SeaSAS frame.

The SeaSAS frame is a unique device consisting of a pedestal and two rails with sensor mounting plates connected to a gear box which is free to rotate in the horizontal (azimuthal) plane. The gear box allows the two rails to move in a scissor-like fashion (i.e., when one is moved up a certain amount, the other moves down by the same amount); thus, if one rail is positioned 40° up from the vertical, the other rail will be 40° down from the vertical. A DATA-100 was mounted on the rail pointed skyward, so it could digitize the $L_i(0^+)$ and the DIR-10 signals. The other rail was pointed seaward and contained the $L_T(0^+)$ sensor fitted to a second DATA-100 in a single, integral package. A generalized schematic of what SeaSAS measured is presented in Fig. 5 and two views of the SeaSAS system deployed in the field is presented in Fig. 6. A summary of the data collected with the SeaSAS instruments is given in Appendix C.

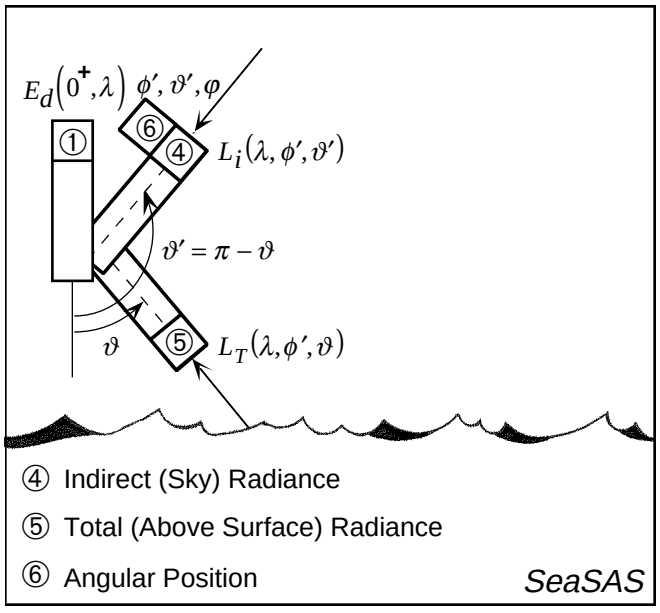

Fig. 5. A schematic of the SeaSAS instruments.

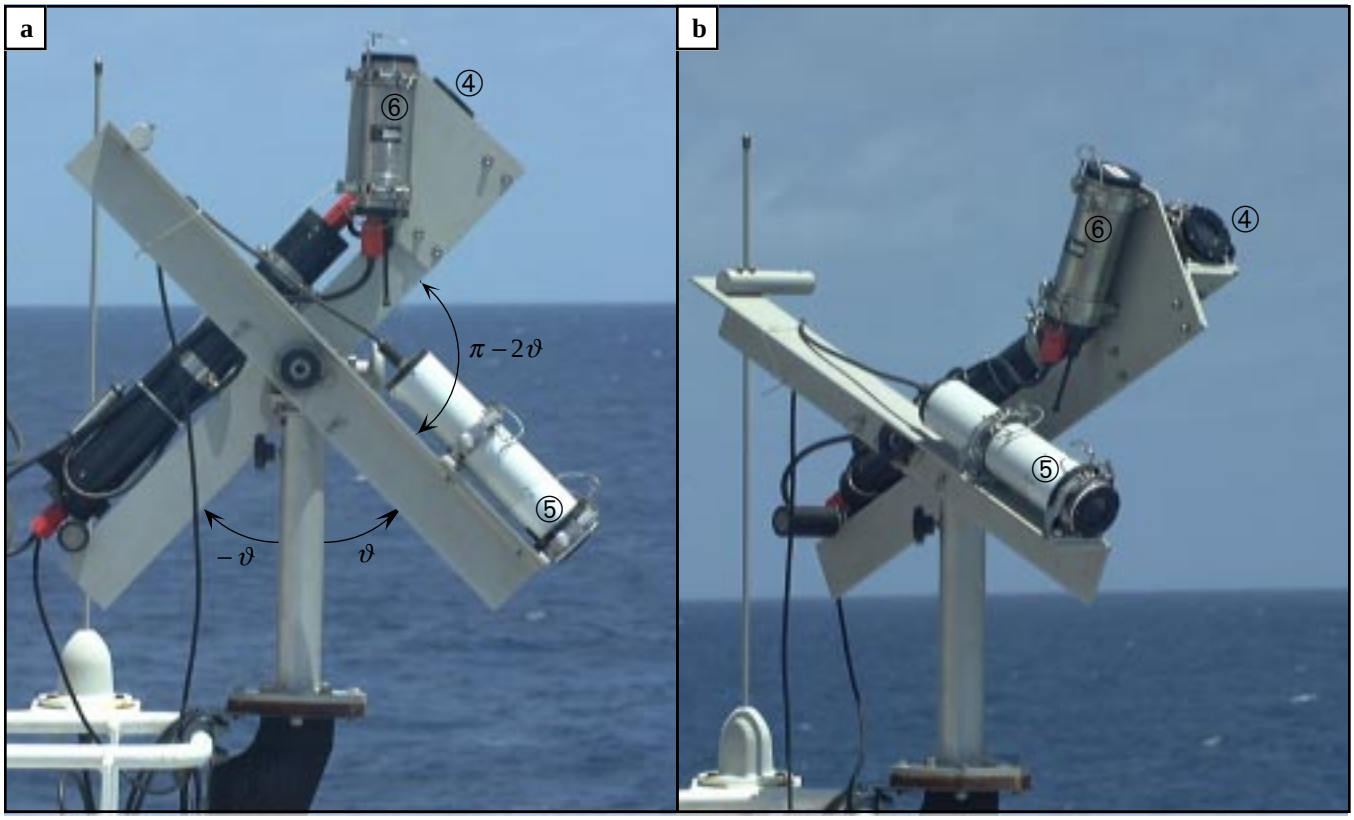

Fig. 6. The SeaSAS frame in two different angular configurations during AMT-6: **a)** $\vartheta \approx 40°$, and **b)** $\vartheta \approx 60°$ (the exaggerated tilting is for demonstration purposes only, although, the saturation threshold of the DIR-10 sensors permits tilts up to 67°). The numbered bullets on, or near, the sensors correspond to the same bullets in Fig. 5. The long black cylinder is the DATA-100 which takes the data from the L_i and DIR-10 sensors. The L_T sensor is permanently attached to its (white) DATA-100 module. When not in use, the two rails can be locked together in the $\vartheta = 90°$ position which prevents large accelerations during adverse environmental conditions.

As with the in-water profilers, the SeaSAS light sensors sent their data to DATA-100 units which sent the digitized data back to the deck box that was providing power for the equipment. The RS-485 signals from the two DATA-100 units were combined in the deck box and converted to RS-232 communications for computer logging. The RS-232 data were logged on a Macintosh PowerBook computer using a variant of the software developed for the profiling instruments. The software time stamped the two data streams (in-water and above-water measurements) and wrote them to disk simultaneously. The data was stored as ASCII, tab-delimited (spreadsheet) files.

One of the design objectives of the SeaSAS frame was to be able to make the sea and sky radiance measurements with only one radiometer. Although this has the disadvantage of increasing the amount of time to make a complete set of measurements, it has the advantage of eliminating any intercalibration differences between the sensors. It also means a smaller (and, therefore, less costly) amount of equipment is needed to make the measurements. The SeaSAS frame can be readily moved in between the two viewing stations, so the only other requirement is to have execution modes in the software that distinguish between these data collection scenarios.

The software controls the logging and display of the data streams as a function of the data collection activity being undertaken: dark data (caps on the radiometers), sea and sky viewing, sea-only viewing, sky-only viewing, SQM calibration monitoring, etc. As with the miniNESS software, the selection of the execution mode automatically sets the file name, so all the operator has to do is push buttons to initiate and terminate data aquisition. This makes it very easy for one operator to control the acquisition of several data streams. All of the telemetry channels are displayed in real time, and the operator can select from a variety of plotting options to visualize the data being collected. The user can also choose to collect data over a three-minute interval (three minutes at 6 Hz produces 1,080 data samples, which is a sufficient amount for standard time series spectral analysis). This feature was used repeatedly during SeaBOARR-98 to synchronize the different acquisition systems.

2.3 WiSPER

The WiSPER system is permanently installed on the AAOT and is operated from the 6.5 m platform extension on the second level. WiSPER uses a custom-built profiling rig, and the positioning of the equipment on the rig was developed with a geometry that ensures the radiometers do not view any part of the mechanical supports. The radiometers are mounted on an extension boom, which puts them 1 m away from the main part of the frame and approximately 7.5 m from the nearest tower leg (the boom can be raised to permit easy access to the sensors).

Two taut wires anchored between the tower and the sea bottom prevent the movement of the rig out of the vertical plane defined by the wires. The narrow geometry of the rig was designed to provide a minimal optical cross section. The field of view of the irradiance sensor is obstructed by the power and telemetry cable, as well as the stabilization wires, but all of these have very small cross sections and the cables are more than 1 m away from the sensors, so any negative effects are minimized. The rigidity and stability of the rig was carefully considered, so there was no need for tilt or roll sensors.

WiSPER uses the same kind of optical sensors as mini-NESS: one OCI-200 (I71) to measure $E_d(z,\lambda)$ and one OCR-200 (R46) to measure $L_u(z,\lambda)$. The former is held in a special bracket that can be rotated 180°, so E_d or E_u measurements can be made with this sensor. Usually three sets of up and down profiles are made each time a measurement sequence is initiated: the first and third to collect E_d and L_u profiles, and the second for E_u and L_u. The E_u measurements were used for Q-factor estimation. A generalized schematic of what WiSPER measured is presented in Fig. 7 and a diagram of the tower shading experiments showing the equipment and their relative positioning with respect to one another is shown in Fig. 8.

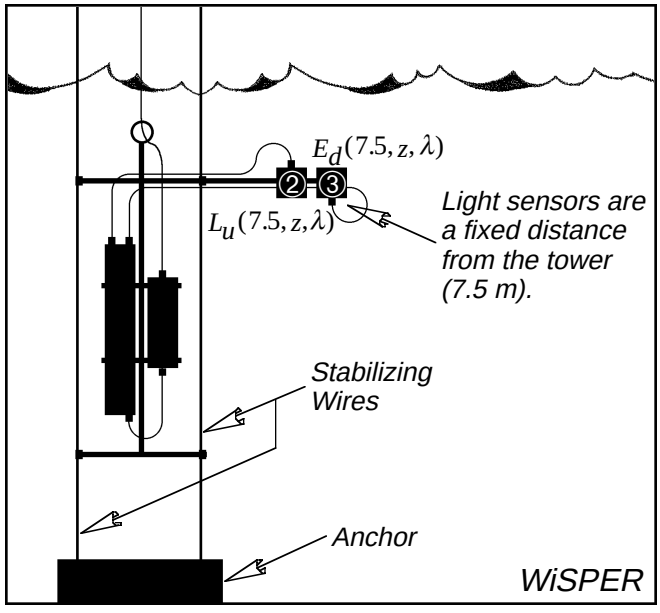

Fig. 7. A schematic of the WiSPER system.

A DATA-100 (S/N 5) provides the A/D and telemetry capability for the WiSPER instruments. The equipment is powered directly from 12 V lead-acid batteries which are stored and kept charged on the tower. WiSPER is raised and lowered from the southeastern side of the tower by an electrical winch, although, the power and telemetry cables are spooled out and taken in by hand (an easy exercise because of the shallow water depth). The typical speed of the winch is approximately $0.1\,\mathrm{m\,s^{-1}}$. In addition to the light sensors, the WiSPER frame also contains an AC-9. The light sensor and AC-9 data are logged on PCs using software supplied by the manufacturers. A picture of the system being deployed is shown in Fig. 9, and a summary of the data collected with the WiSPER system is presented in Appendix D and Appendix E.

The self-shading correction of WISPER data required two extra data sets: a) a Multi-Filter Rotating Shadow-Band Radiometer (MFR-6) which automatically collected $E_d(0^+,\lambda)$ and $E_i(0^+,\lambda)$, and b) *in vivo* absorption of particulate matter and CDOM. Both of the latter are needed to apply the Gordon and Ding (1992) correction scheme as parameterized by the sun zenith angle by Zibordi and Ferrari (1995), and further parameterized as a function of the size of the radiometer by Mueller and Austin (1995).

A field campaign was performed from 3–21 July 1997, to estimate the shading effect induced on in-water radiance and irradiance measurements taken in the immediate vicinity of the AAOT (Zibordi et al. 1999). Sequences of downwelling irradiance and upwelling radiance profiles were collected at varying distances from the tower to evaluate the tower shading effects as a function of the deployment distance (these measurements were performed with the first LoCNESS instrument).

The experimental data, as well as results from a Monte Carlo model, indicated the shading effect at 555 nm during clear-sky conditions was negligible for both downwelling irradiances and upwelling radiances at deployment distances greater than 15 m and 20 m, respectively. At closer distances, for example at the 7.5 m deployment distance regularly used at the AAOT for the collection of WiSPER data, the shading effect was much larger: at 555 nm during clear-sky conditions and a relatively low sun zenith angle of 22°, the shading effect was approximately 2% for downwelling irradiance and about 8% for upwelling radiance. These large effects indicated a correction method was needed for in-water optical data collected near the tower, if the 5% uncertainty objectives of the SeaWiFS Project were to be achieved. Consequently, a correction method based on Monte Carlo simulations was formulated.

The evaluation of the capability of the Monte Carlo model in simulating radiance and irradiance measurements at the tower site produced satisfactory results. The intercomparison between experimental and theoretical data showed mean differences within 2.4% for radiance and 3.1% for irradiance. Although the code validation with field data was restricted to a single experiment (because of the

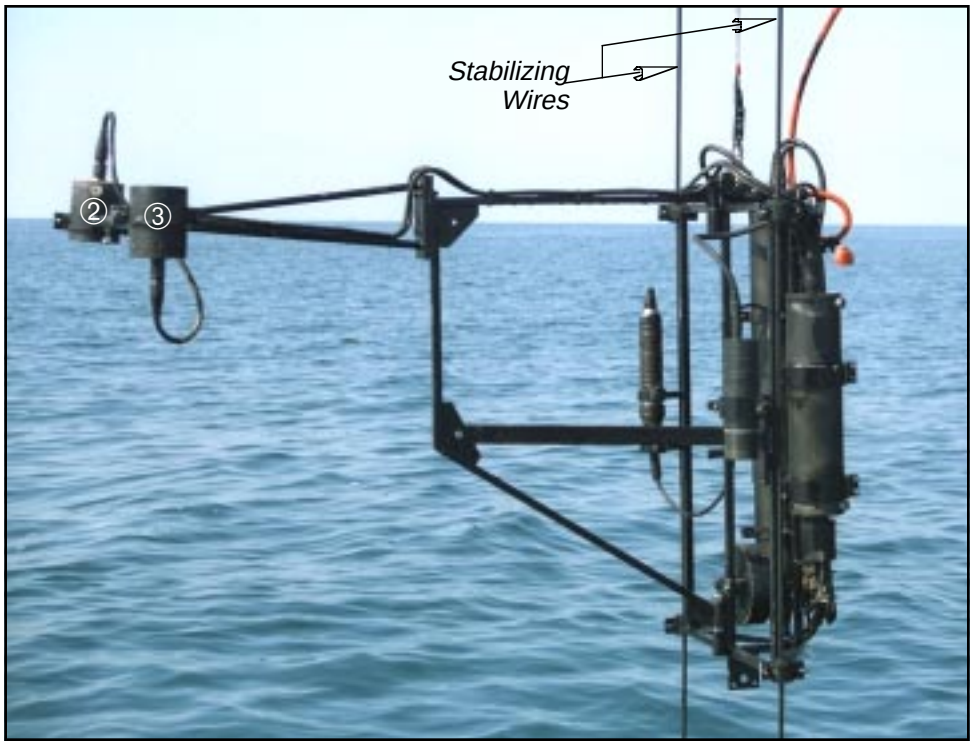

Fig. 8. The WiSPER package being lowered into the water. The numbered bullet on the sensors corresponds to the same bullets in Fig. 7.

difficulty in performing the needed measurements under the required environmental conditions), the result of the intercomparison suggested a viable operational correction method can be constructed for tower shading effects based on the Monte Carlo simulations. One of the SeaBOARR-98 objectives was to validate this correction methodology.

2.4 DalSAS

The DalSAS system is similar in design to the SeaSAS, but is optimized for aircraft remote sensing applications and was specially modified for this campaign. The DalSAS instrument telemeters a full scan of all channels every 100 ms (all channels are sampled within a 400 μs period) as opposed to 167 ms for SeaSAS. All data from this system were logged at full temporal resolution to allow for optimal correction of glint contaminated signals. The irradiance sensors have a cosine response for each wavelength, but the radiance sensors have a 3° half-angle field of view. When the latter were mounted on the tower (13.5 m above the water), the viewing spot on the sea surface was approximately 2 m for all seven channels at a distance of 11.3 m from the tower base.

The DalSAS frame provided the same functionality as the SeaSAS frame, but with a less sophisticated design. The light sensors were mounted on movable plates which were mechanically secured at the desired viewing angle (a protractor was used to set the viewing angles during SeaBOARR-98). The largest mounting plate was designed to accommodate the light sensor that measured the total radiance just above sea surface (S09). A square aperture was situated in the field of view of this sensor, so a gray plaque could be inserted before (or after) each surface-viewing sequence. This permitted the sequential measurement of L_T and L_p with the same radiometer. The L_i sensor (S64) was fitted to a smaller plate that was always pointed skyward. Two in-air irradiance sensors measured the total solar irradiance just above the sea surface (M20), $E_d(0^+, \lambda)$, and the indirect (or diffuse) irradiance just above the sea surface (M93), $E_i(0^+, \lambda)$.

The gray plaque used in this campaign was a 25 cm (10 inch) gray Spectralon™ plaque from Labsphere, Inc. (North Sutton, New Hampshire), with a nominal 10% reflectance (SRT–10–100). This reflectance value permits radiometers with typical above-water saturation values to make this measurement without saturating (approximately $6\,\mu\mathrm{W\,cm^{-2}\,nm^{-1}\,sr^{-1}}$). Unlike the 99% reflectance of pure (white) Spectralon plaques, which are usually used for radiometric calibration, gray plaques are much less lambertian, because of the added impurities of the black doping material. Variations in viewing and illumination geometries, as are naturally found in the field, are likely to add significant variance in this measurement. According to the Labsphere product catalog, for example, a 20% plaque will have a 2% higher reflectance at 45° (compared to 8°) and +5% at 61° for $\lambda = 600$ nm (for a 99% plaque these values are −0.6% at 45°, and −0.5% at 61°).

The use of a 99% plaque and sky-viewing radiometers (the latter have typical saturation values of approximately $60\,\mu\mathrm{W\,cm^{-2}\,nm^{-1}\,sr^{-1}}$) would reduce the uncertainty in measurements, because of the significant nonlambertian reflectivity of gray plaques. The homogeneity of the plaque should be checked at a minimum of four spots on the plaque surface, and variations greater than 2% between the spots should eliminate the use of the plaque for any validation work. A directional/directional (i.e., 0°/45°) plaque calibration, instead of the standard directional/hemispherical calibration was used for this campaign, since this was closer to the actual field geometry (25–45° illumination/50° viewing).

Although Spectralon is very hydrophobic, it readily absorbs grease and oil which are very difficult to remove and can cause significant variance in calibrations. Special precautions must be taken to avoid touching the diffusive material and to avoid long exposure to marine aerosols. During this campaign, the plaque was kept in a padded, air tight enclosure when not in use and only exposed during the measurement sequences. It was always wrapped in acid-free paper during transport and storage before and after the field campaign.

A generalized schematic of what DalSAS measured is shown in Fig. 9. The two irradiance sensors were mounted on the top of the tower, but in a location that allowed an operator to occult the E_i diffusers with a *lollipop*. A side view of the DalSAS from deployed on the tower is shown in Fig. 10. The latter shows the plaque frame with the square aperture centered in the field of view of the L_T sensor (the plaque is not present in the picture). A summary of the data collected with DalSAS is presented in Appendix F.

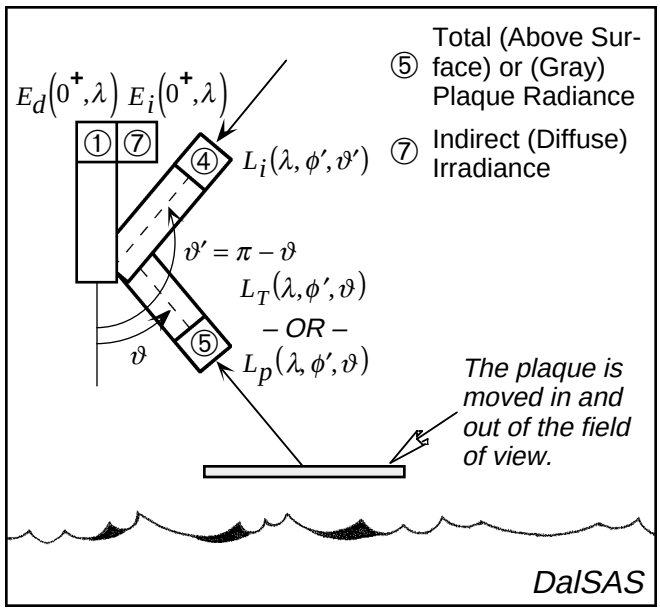

Fig. 9. A schematic of the DalSAS system.

Like SeaSAS, the radiometers used with DalSAS were connected in a modular fashion. The two radiance sensors were connected to the same DATA-100. The S09 sensor was integral to the DATA-100, and the S64 sensor was cabled into an extra port. With this arrangement, the two sensors took and reported data (via RS-485 serial communications) simultaneously. The irradiance sensors were also connected to one DATA-100. The M20 sensor was integral to the DATA-100, and the M93 sensor was cabled into an extra port. Again, this arrangement allowed the two sensors to take and report data (via RS-485 serial communications) simultaneously.

2.5 DalBOSS

DalBOSS is a variant of the SeaWiFS Buoyant Optical Surface Sensor (SeaBOSS) which was first deployed on the AMT-5 cruise (Aiken et al. 1998). SeaBOSS is based on a Satlantic SeaWiFS Multichannel Surface Reference (SMSR) and is composed of an in-air OCI-1000 sensor (N46) which measures the incident solar irradiance immediately above the sea surface, $E_d(0^+,\lambda)$. DalBOSS is basically the same as SeaBOSS: an in-air OCI-1000 sensor (N48) measures $E_d(0^+,\lambda)$, but an additional OCR-1000 sensor (Q33) is fitted to the bottom of the sensor package. This downward-looking sensor measures the upwelled radiance right below the sea surface, $L_u(z_0,\lambda)$. For SeaBOSS and DalBOSS, the sensor package is fitted inside a removable buoyant collar, so it can be deployed on a mast or as a tethered buoy. The irradiance sensor protrudes up above the flotation collar, so one of the difficulties with this system is keeping the irradiance sensor dry during each deployment session.

During the AMT-5 cruise, several experiments were conducted with SeaBOSS to determine how best to cheaply and effectively float an in-air sensor away from a ship while keeping it dry and minimizing tilts while it was deployed. Experiments were also conducted with another type of surface reference called the SeaWiFS Square Underwater Reference Frame (SeaSURF), which is composed of an in-water irradiance sensor, $E_d(z_0,\lambda)$, suspended below a tethered, square floating frame. Rigging SeaSURF with elastic stabilizing cords greatly minimized the tilts associated with the ambient wave field, so it was decided to combine the two flotation systems with SeaBOSS. After several trials, an acceptable arrangement was engineered wherein two sets of elastic stabilizing cords fitted between the frame and the body of the irradiance housing: one at the top of the flotation collar and one at the bottom of the sensor cylinder. The elastic cords significantly absorbed the wave motion and kept the sensor package more oriented towards the vertical. It was also noted that the flotation collar can be moved down the cylinder to expose a retaining plate that normally keeps the flotation collar from working up the cylinder. If this is done, the retaining plate acts like a splash plate, and helps keep water off the irradiance diffusers.

A generalized schematic of what DalBOSS measured during SeaBOARR-98 is presented in Fig. 11.

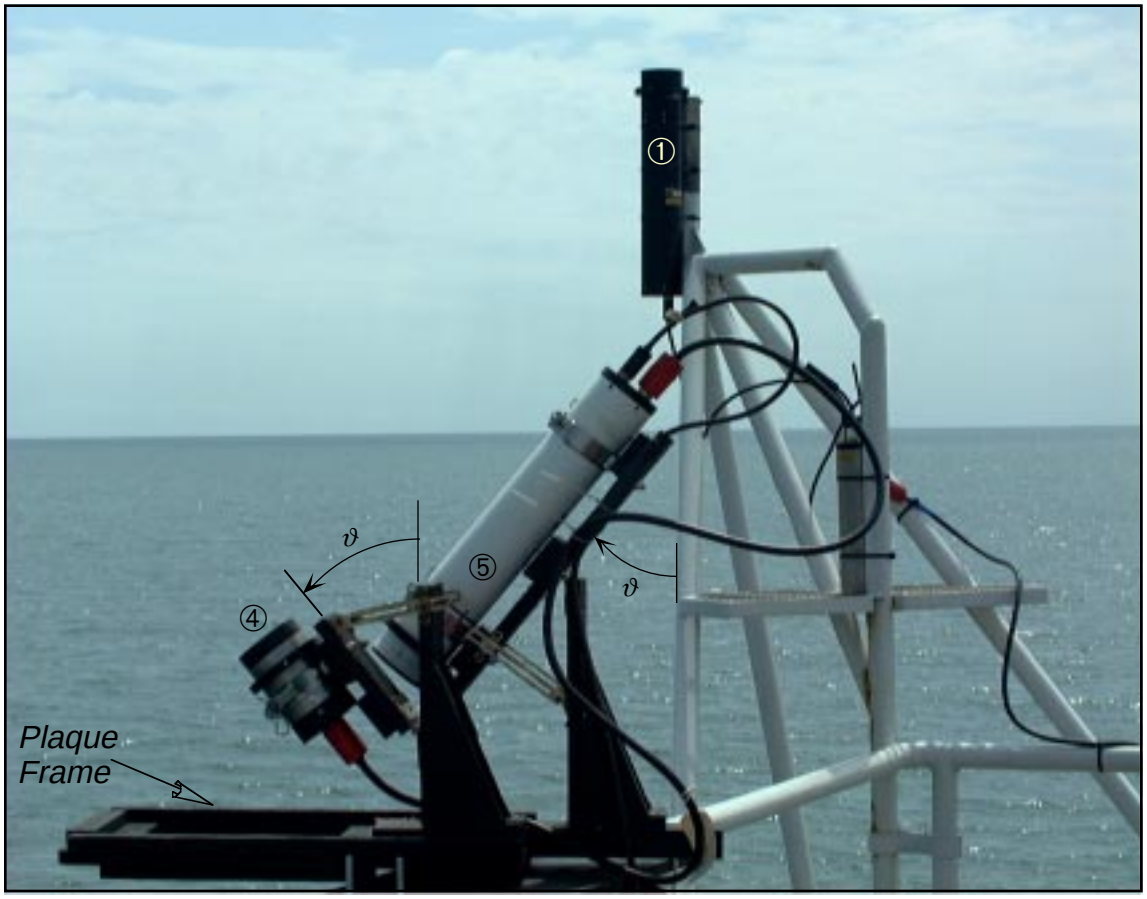

Fig. 10. The DalSAS frame on the northeast side of the tower. The numbered bullets on or near the sensors correspond to the same bullets in Fig. 9. The long white cylinder is the DATA-100 which is integral with the L_T (and L_p) sensor. The L_i sensor is attached to a movable plate which can be secured at the desired viewing angle. A similar mechanical system is used with the DATA-100. The long black cylinder in the background is the $E_d(0^+, \lambda)$ sensor for miniNESS and SeaSAS.

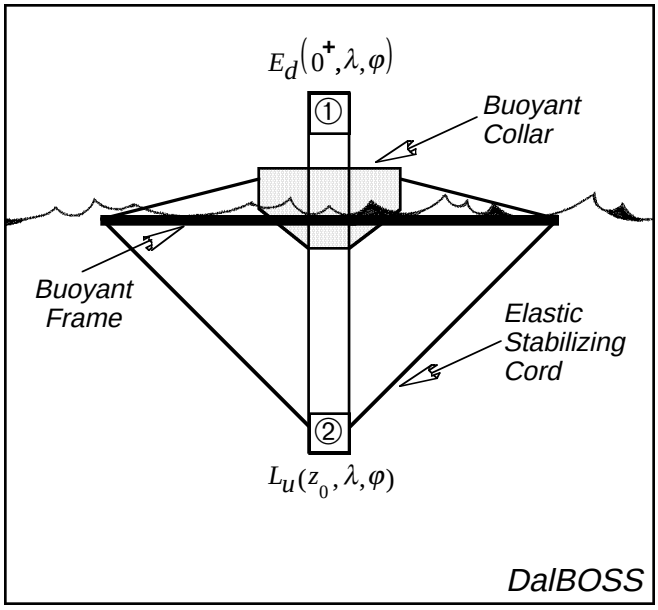

Fig. 11. A schematic of the DalBOSS system.

During SeaBOARR-98, DalBOSS was deployed in the AMT-5 SeaBOSS configuration (Fig. 12). It was lowered into the water from the southwestern side of the tower and taken away by small boat, whereupon, it was tied to an anchor approximately 50 m from the tower. The sea and wave field was usually minimal, so there was little chance that the DalBOSS buoy would pull against the marker buoy (which would accentuate the tilting of the sensor package), and there was no need to push the flotation collar down and use it as a splash plate. A summary of the data collected with the DalBOSS system is presented in Appendix G.

The RS-485 signals from the SMSR unit were combined in a Satlantic deck box and converted to RS-232 communications for computer logging. The deck box also provided the (computer-controlled) power for the sensors. The RS-232 data were logged on a Macintosh PowerBook computer using the aforementioned software developed by RSMAS and the SeaWiFS Project. The two data streams (in-water and above-water measurements) are time stamped and written to disk simultaneously. The software controls the logging and display of the data streams as a function

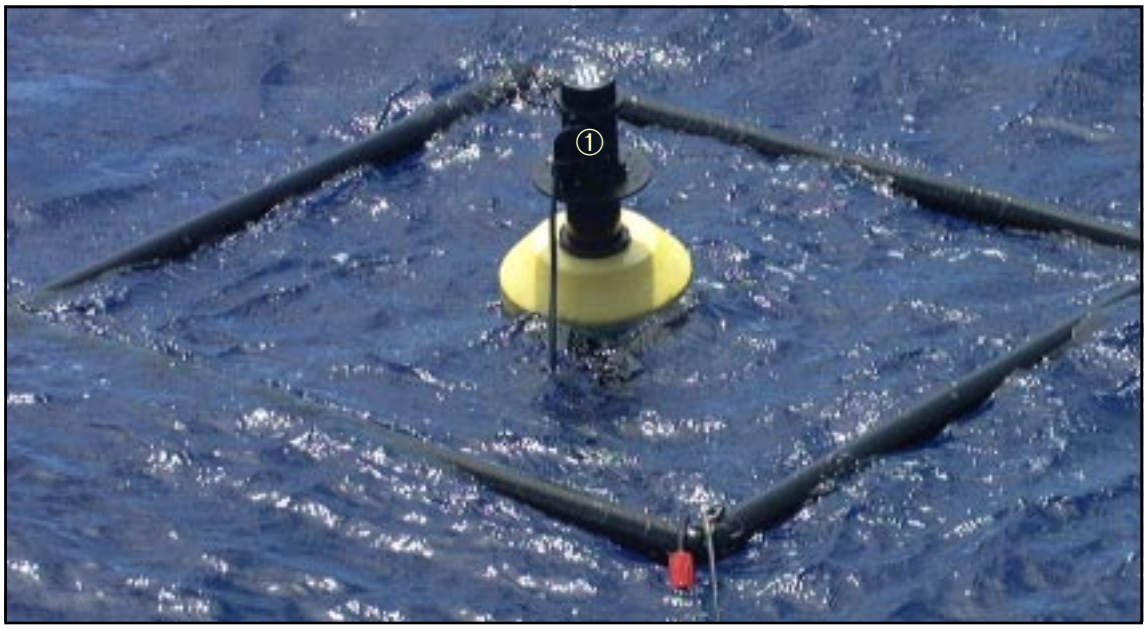

Fig. 12. SeaBOSS deployed during AMT-6. The numbered bullet on the sensor corresponds to the same bullet in Fig. 11. Note the splash plate right above the flotation collar.

of the data collection activity being undertaken: dark data (caps on the radiometers), down cast, constant depth soak, up cast, etc. All of the telemetry channels are displayed in real time, and the operator can select from a variety of plotting options to visualize the data being collected.

2.6 SQM-II

The SQM is a compact light source developed by NASA and NIST for monitoring the radiometric stability of radiometers used to measure the *in situ* optical properties of seawater while they are being deployed in the field. The engineering design and characteristics of the SQM are described by Johnson et al. (1998), so only a brief description is given here. A separate rack of electronic equipment, composed principally of two computer-controlled power supplies and a multiplexed, digital voltmeter (DVM), are an essential part of producing the stable light field. The SQM does not have, nor does it require, an absolute calibration, but it has design objectives of better than 2% stability during field deployments.

The SQM has two sets of halogen lamps with eight lamps in each set; both lamp sets are arranged symmetrically on a ring and operate in series, so if one lamp fails, the entire set goes off. The lamps in one set are rated for 1.05 A (4.2 V) and are operated at 0.95 A, and the lamps in the other set are rated for 3.45 A (5.0 V) and are operated at 3.1 A; the lamp sets are hereafter referred to as the 1 A and 3 A lamps, respectively. The lamps are operated at approximately 95% of their full amperage rating to maximize the lifetime of the lamps.

A low, medium, and high intensity flux level is provided when the 1 A, 3 A, and both lamp sets are used, respectively. Each lamp set was *aged* for approximately 50 hours before deploying the SQM to the field. The interior light chamber has bead-blasted aluminum walls, so the diffuse component of the reflectance is significant. The lamps illuminate a circular plastic diffuser protected by safety glass and sealed from the environment by o-rings. The diffuser is resilient to ultraviolet yellowing, but can age nonetheless. The exit aperture is 20 cm in diameter and has a spatial uniformity of 98% or more over the interior 15 cm circle.

A faceplate or *shadow collar* provides a mounting assembly, so the device under test (DUT), usually a radiance or irradiance sensor, can be positioned in the shadow collar. The DUT has a D-shaped collar fitted to it at a set distance, 3.81 cm (1.5 inch), from the front of the DUT. This distance was chosen based on the most restrictive clearance requirement of the radiometers used in the different deployment rigs. The D-shaped collar ensures the DUT can be mounted to the SQM at a reproducible location and orientation with respect to the exit aperture each time the DUT is used. The former minimizes uncertainties (principally with irradiance sensors) due to distance differences between measurement sessions, while the latter minimizes uncertainties (principally with radiance sensors) due to inhomogeneities in the exit aperture light field. In either case, the D-shaped collar keeps these sources of uncertainties below the 1% level.

The SQM faceplate can be changed to accept a variety of instruments from different manufacturers. Radiometers above a certain size, approximately 15 cm, would be difficult to accomodate, but the entire mounting assembly can be changed to allow for reasonable viewing by seemingly difficult to handle radiometers. To date, three radiometer designs have been used with the SQM, and there were

no problems in producing the needed faceplates, D-shaped collars, or support hardware to accomodate these units.

The SQM light field can change because of a variety of effects; for example, the presence of the DUT, the aging of the lamps, a deterioration in the plastic diffuser, a change in the transmittance of the glass cover, a drift in the control electronics, a repositioning of a mechanical alignment, etc. To account for these changes, three photodiodes, whose temperatures are kept constant with a precision thermoelectric cooler (±0.01 K), measure the exit aperture light level: the first has a responsivity in the blue part of the spectrum, the second in the red part of the spectrum, and the third has a broad-band or *white* response. All three internal monitors view the center portion of the exit aperture. The back of the SQM is cooled by a fan to prevent a build up in temperature beyond what the thermoelectric cooler can accomodate. The SQM has an internal heater to help maintain temperature stability in colder climates and to shorten the time needed for warming up the SQM.

Another SQM quality control procedure is provided by three special DUTs called *fiducials:* a white one, a black one, and a black one with a glass face (the glass is the same as that used with the field radiometers). A fiducial has the same size and shape of a radiometer, but is nonoperational. The reflective surface of a fiducial is carefully maintained, both during its use and when it is not being used. Consequently, the reflective surface degrades very slowly, so over the time period of a field expedition, it remains basically constant. A field radiometer, by comparison, has a reflective surface that is changing episodically from the wear and tear of daily use. This change in reflectivity alters the loading of the radiometer on the SQM and is a source of variance for the monitors inside the SQM that are viewing the exit aperture, or the radiometer itself when it is viewing the exit aperture. The time series of a fiducial, as measured by the internal monitors, gives an independent measure of the temporal stability of the light field.

The SQM has been used to track changes in instruments between calibrations and on four cruises lasting approximately 5–6 weeks each (Hooker and Aiken 1998). Although there was some controversy at the design stage about running the lamps below their rated current (approximately 95% of rating), there has been no observable degradation in the performance of the lamps as a result of this—indeed, they have survived long shipment routes (US to UK to Falkland Islands and back) on repeated occasions, as well as the high vibration environment of a ship. The SQM is clearly a robust instrument well suited to the task of calibration monitoring in the field.

Satlantic, Inc., developed the SQM-II as a commercial version of the SQM and based the design on the original. The main difference with the new unit is the high degree of integration. The entire system consists of two components, a deck box that provides DC power to the SQM-II, and the SQM-II itself. The latter contains the lamp rings (which use the same lamps as the original SQM), heating and cooling subsystems, control circuitry, the system computer, plus display and data storage.

The SQM-II system is designed to be self contained and does not require a PC to operate. Only two cables are required to complete system assembly (an AC power cord for the deck box and a DC power cord to link the deck box to the SQM-II). Although this integration reduces system complexity, it comes with increased vulnerability: a failure in any one of the subsystems can render the entire system inoperable with no opportunity for simply swapping in a new (external) subassembly, like a power supply or DVM. As was done with the original SQM, Satlantic recommends running the SQM-II on an uninterruptable power supply (UPS), and this was done during SeaBOARR-98. A picture of the SQM-II in the water filtering and hydrography laboratory on the AAOT with DalBOSS mounted to the front is shown in (Fig. 13). A summary of the data collected with the SQM-II is presented in Appendix H.

User input to start and monitor the system is via a simple 4-button keypad and a 4×20 fluorescent display at the rear of the device. Commands can be entered using the menus on the display or remotely from a PC. A PC can also be connected to the system to log data during a calibration evaluation and radiometric testing (CERT) session, or the data can be stored internally in a flash card and downloaded later.

The differences between the two SQM units are not restricted to their control architecture. The SQM-II has many improvements that use of the original unit has shown to be desirable under different circumstances:

1. The bulbs are mounted at the front, facing away from the exit aperture, which increases the average path length of the light emitted by each bulb, and it makes it easier to service the lamps (individually and as a subassembly);
2. The light chamber is lined with Spectralon, so the emitted flux is higher, and the aperture uniformity is greater; and
3. At 490 nm, the SQM-II is about seven times more intense than the SQM (the apparent blackbody temperature of the SQM-II is 3,100 K, whereas, the SQM is about 2,400 K);

Although the greater flux of the SQM-II is a desireable attribute for the blue part of the spectrum, the high output in the red saturates many in-water field radiometers. This was subsequently corrected by adding a blue filter to the exit aperture.

2.7 AC-9

Spectral attenuation $c(\lambda)$ and absorption $a(\lambda)$ of seawater particulate plus dissolved matter were measured at 412, 440, 488, 510, 555, 650, 675, 715, and 750 nm making use of an AC-9 with a 25 cm pathlength. AC-9 profiles

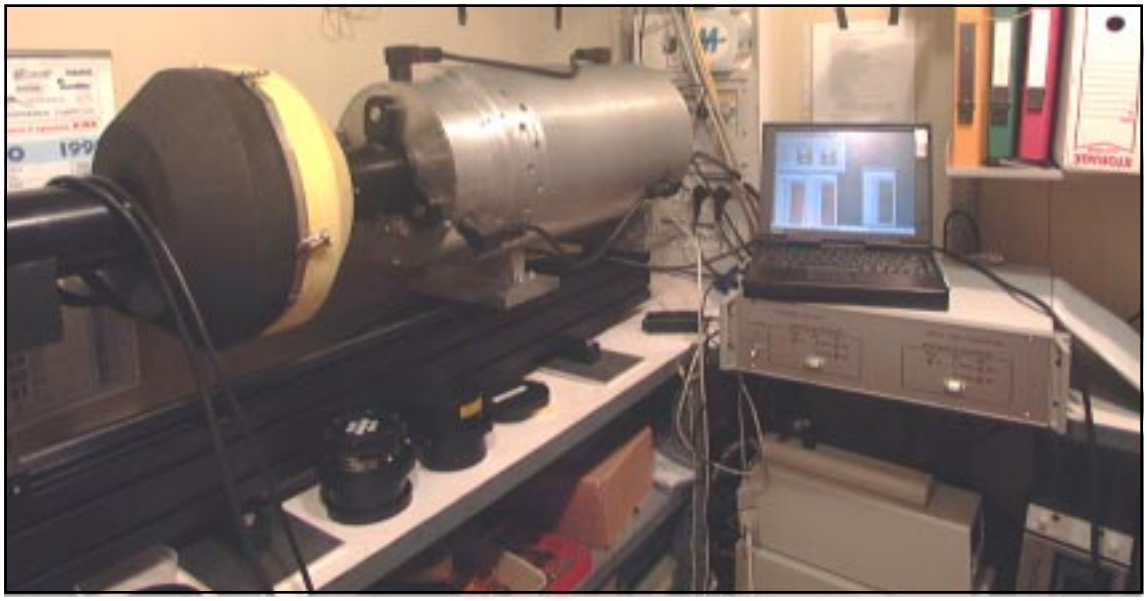

Fig. 13. The SQM-II in the water filtering and hydrography laboratory on the AAOT with DalBOSS mounted to the front.

were taken at the same time as the WiSPER profiles (and also temporally overlapped the miniNESS profiles) as summarized in Appendix E. Data were calibrated making use of the factors provided by the manufacturer, WETLabs, Inc. (Philomath, Oregon). The calibrated absorption and attenuation data were corrected for temperature (T) and salinity (S) effects. These, induced by T-S differences between seawater and the pure water used for laboratory calibration, have been removed by applying

$$\hat{m}(\lambda) \;=\; m(\lambda) \;-\; \big[C_0(\lambda)(T-T') + C_1(\lambda)\,S\big], \tag{1}$$

where $m(\lambda)$ is the measured absorption $a(\lambda)$ or attenuation $c(\lambda)$ at wavelength λ, $\hat{m}(\lambda)$ is the corresponding value corrected for temperature and salinity effects, T and S are the temperature and salinity of seawater during field measurements, T' is the temperature of water during calibration, and C_0 and C_1 are spectral constants provided by the manufacturer.

Absorption coefficients were corrected for scattering effects, which induce overestimate of absorption because of the finite acceptance angle of the instrument. The scattering effects, by assuming that the absorption coefficient of particulate and dissolved material is zero at the reference wavelength $\lambda_0 = 715\,\mathrm{nm}$ and that the shape of the volume scattering function is independent of wavelength (Zaneveld et al. 1992), have been removed by applying

$$\breve{a}(\lambda) \;=\; \hat{a}(\lambda) \;-\; \frac{\hat{a}(\lambda_0)\big(\hat{c}(\lambda)-\hat{a}(\lambda)\big)}{\hat{c}(\lambda_0)-\hat{a}(\lambda_0)}, \tag{2}$$

where ($\breve{}$) means scattering corrected and ($\hat{}$) means salinity and temperature corrected.

2.8 HPLC

Phytoplankton pigment concentrations were analyzed using the HPLC method (Joint Global Ocean Flux Study 1994 and Jeffrey et al. 1997). Seawater samples (2 l) were filtered immediately after collection through glass fiber filters (GF/F with a nominal pore size of 0.7 μm) and stored in liquid nitrogen for successive analysis in the laboratory. Pigment extraction was carried out by placing each filter in 5 mL of 100% acetone (accounting for the 0.8 mL of water retained on the filter, the final volume was 5.8 mL with 86% of acetone).

To correct for any error induced by evaporation or experimental losses during the extraction and centrifugation, 100 mL of Canthaxenthin (used as an internal standard) were added to each sample. The samples were then ground and left for 4 hours in the dark at -20°C for pigment extraction. Samples were successively centrifuged for 5 minutes and filtered using a syringe with a 0.45 μm filter. Five minutes before the injection, 500 mL of the filtrated extract were mixed with 150 mL of MilliQ water and injected into the HPLC system through a 200 mL loop.

From the peak pigmented area (A_p) obtained from the HPLC chromatogram, the concentration C_p ($\mu g\,\mathrm{L}^{-1}$) of each pigment was computed from

$$C_p \;=\; \frac{A_p W_s f_p}{A_s V_f}, \tag{3}$$

where A_p is the peak pigment area (square meters), W_s is the internal standard weight (micrograms), V_f is the volume filtered (liters), A_s is the internal standard area (square meters), and f_p is the relative response factor for

each pigment. The list of analyzed pigments include chlorophyll *a*, chlorophyll *b*, chlorophyll *c*, chlorophyllide *a*, 19′-butanoyloxyfucoxanthin, 19′-hexanoyloxyfucoxanthin, fucoxanthin, zeaxanthin, alloxanthin, peridinin, diadinoxanthin, diatoxanthin, and carotene. A summary of the samples collected for pigment analyses are given in the HPLC Pigment Log (Appendix E).

2.9 PM Absorption

The *in vivo* absorption coefficient of aquatic particles retained on filters, $a_p(\lambda)$ (per meter), were determined with a dual-beam spectrophotometer (a Perkin-Elmer Lambda 19) equipped with a 60 mm diameter integrating sphere. Water samples (2 l) were filtered through GF/F filters under low vacuum pressure (less than 120 mm Hg) to prevent particle breakage and pigment degradation. The filters were placed on petri slides and stored in liquid nitrogen. The measurement methodology described by Tassan and Ferrari (1995) was used to determine the total absorption, $a_p(\lambda)$, of equivalent particle suspension in the 400–750 nm spectral range (with 1 nm resolution). For completeness, the whole suite of relationships applied to spectrophotometric measurements made for deriving $a_p(\lambda)$, are presented here.

According to Tassan and Ferrari (1995), $a_p(\lambda)$ is obtained from

$$a_p(\lambda) \;=\; 2.3\,\frac{A_{\rm sus}(\lambda)}{F_A V_w} \tag{4}$$

where V_w is the volume (cubic meters) of filtered water, F_A is the filter clearance area (square meters), and $A_{\rm sus}(\lambda)$ is the absorbance of the equivalent particle suspension given by

$$A_{\rm sus}(\lambda) \;=\; 0.423\,\hat{a}_s(\lambda) \;+\; 0.479\,\hat{a}_s^2(\lambda), \tag{5}$$

where

$$\hat{a}_s(\lambda) \;=\; \log\left[\frac{1}{1-a_s(\lambda)}\right], \tag{6}$$

and

$$a_s(\lambda) \;=\; \frac{1 \;-\; \rho_T(\lambda) \;+\; R_f(\lambda)\big[\rho_T(\lambda)-\rho_R(\lambda)\big]}{1 \;+\; R_f(\lambda)\rho_T(\lambda)\tau(\lambda)}. \tag{7}$$

In this formulation, (7), $R_f(\lambda)$ is the filter reflectance, $\rho_T(\lambda)$ and $\rho_R(\lambda)$ result from the measurements in transmimssion and reflectance modes, respectively, and τ, an instrument-dependent function, is given by

$$\tau \;=\; 1.171 \;-\; 0.2615\,\gamma(\lambda) \;+\; 0.00013\,\gamma^2(\lambda) \tag{8}$$

where

$$\gamma \;=\; \log\left[\frac{1}{\rho_T(\lambda)}\right] \;-\; 0.5\log\left[\frac{1}{\rho_T(750)}\right]. \tag{9}$$

A summary of the samples collected during SeaBOARR-98 for particulate analyses are given in the Particulate Absorption Log (Appendix E).

2.10 CDOM Absorption

The CDOM or yellow substance absorption coefficient, $a_{\rm ys}(\lambda)$ [$\rm m^{-1}$], was determined using a dual-beam spectrometer (Perkin-Elmer Lambda 12). Water samples (700 mL) were filtered through 0.22 μm cellulose membrane filters and refrigerated at 4°C in an amber glass bottle with the addition of a solution of 10 g $\rm L^{-1}$ of $\rm NaN_3$ to inhibit aerobic bacteria. The laboratory analyses, which were carried out within a few days, were performed in the spectral range 350–750 nm with 1 nm resolution. Spectrometric measurements were taken by placing a 10 cm cuvette containing MilliQ water in the optical path of the reference beam, and a 10 cm cuvette containing CDOM in the optical path for the samples.

The spectral absorption coefficient, $a_{\rm ys}(\lambda)$, was derived from the measured absorbance $A_{\rm ys}(\lambda)$ resulting from the difference between the sample absorbance and the reference absorbance (Ferrari et al. 1996), from

$$a_{\rm ys}(\lambda) \;=\; 2.3\,\frac{A_{\rm ys}(\lambda)}{L_c}, \tag{10}$$

where L_c is the pathlength of the cuvette. A summary of the CDOM Log is given in Appendix E.

2.11 TSM

TSM was obtained from the net weight of the material collected on GF/F filters following the technique of Strickland and Parsons (1972). A volume of seawater (2 l) was filtered through pre-washed, pre-ashed and pre-weighed GF/F filters. During filtration, 1 mL of 4% formalin per liter of seawater was added to the water sample to prevent any plankton from multiplying (which would change the composition of the sample).

After seawater filtration, the filter (i.e., filtration area and border) was washed with distilled water, dried in an oven at 65°C for 24 hours, and then stored in a desiccator before being weighed on an electrobalance. The concentration of TSM (grams per cubic meter) was calculated from the weight difference of the filters before and after filtration divided by the volume of the sampled water.

2.12 Sun Photometer

The CE-318 sun photometer is made by CIMEL Electronique (Paris, France) and is an automatic system measuring the direct sun irradiance plus the sky radiance in the sun and almucantar planes. The system, powered by solar panels and batteries, is composed of three parts: a) a sensor installed in a alto-azimuthal platform; b) an alto-azimuthal platform with the rotational axes (azimuthal and zenithal) controlled by stepping motors; and c) a programmable unit controlling measurement sequences, sun and sky pointing, and data logging. A summary of the Sun Photometer Log is given in Appendix E.

The optical part of the sensor is composed of two collimators with 1.2° full angle field of view (one used for sky radiance measurements and the other used for both sky radiance and direct sun irradiance measurements), a filter wheel with six filters (with 10 nm bandwidth and center wavelengths at 340, 380, 440, 670, 870, and 1,020 nm), and a dark mask for dark current measurements. Two ultraviolet-enhanced silicon detectors (one for each collimator) ensure a reliable measurement range between 340–1,020 nm (Fig. 14).

Fig. 14. A picture of the CIMEL system.

The direct sun irradiance measurements (for the aerosol optical thickness retrievals) are taken at regular air mass intervals in all of the spectral channels. Sky radiance measurements are only performed at 440, 670, 870 and 1,020 nm. Basic sky radiance measurements are taken at different airmasses in the almucantar and sun plane at a broad range of zenith angles for aerosol particle size distribution and phase function retrieval (Holben et al. 1998). Collected data are downloaded into the Aerosol Robotic Network (AERONET) data bank every 30 minutes through the Meteorological Satellite (METEOSAT) Data Collection Platform (DCP) telemetry system.

2.13 Rotating Shadow-Band Radiometer

The MFR-6, manufactured by Yankee Environmental Systems, Inc. (Turners Falls, Massachusetts), automatically measures the total and indirect (or diffuse) components of spectral solar irradiance (Harrison et al. 1994) in six spectral bands (10 nm wide and centered at 415, 500, 615, 673, 870 and 940 nm) and in one broad band (approximately ranging from 400–1,100 nm). The detector is composed of a filter-photodiode mounted in a temperature-controlled enclosure whose input aperture is a cosine collector made of a Spectralon disc coupled to a Spectralon integrating cavity. The non-cosine response of the collector, characterized by the manufacturer, is automatically accounted for by the system software and isused to correct measurements for deviations from ideal cosine response of the input optics.

The total and diffuse components are measured by alternatively exposing and shading the entrance aperture of the instrument. The direct normal component is then computed from the difference of the two measurements. The detector shading from the direct sun component is obtained through an automated shadow band aligned with respect to the north–south direction. The shadow band is a metal strip modeled in an arc shape moving above the center of the instrument's entrance aperture and blocking a portion of sky with a 3.3° angle. The shadow band movement and data logging are controlled by the acquisition unit with a 13-bit A/D converter (Fig. 15).

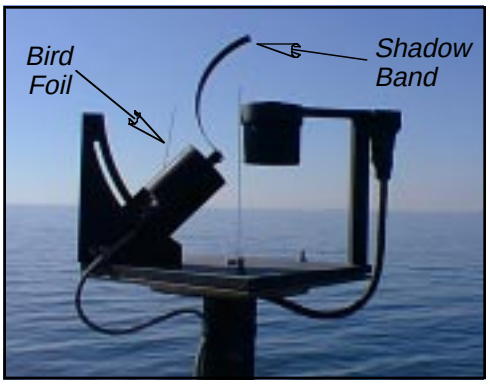

Fig. 15. A picture of the MFR-6 system.

The system, powered by batteries, automatically performs sequences of measurements with a maximum frequency of three measurement cycles every minute. Each measurement sequence, carried out after computation of the sun zenith angle, includes four independent measurements: the total horizontal irradiance with the band at its nadir position, the indirect (diffuse) irradiance with the sun blocked by the band, and two more measurements with the band at +9° and −9° with respect to the sun position. The last two measurements are automatically used to correct the diffuse irradiance measurement for the sky radiance blocked by the band when the sun irradiance is shaded to the sensor.

Data transfer from the acquisition unit to a PC is ensured by an RS-232 serial communication port. During the SeaBOARR-98 experiment, the MFR-6 measurements were taken at 10 minute intervals. A summary of the MFR-6 Log is given in Appendix E.

3. METHODS

The SeaWiFS Project sponsored a workshop from 9–12 April 1991, which was held at the Naval Postgraduate School (Monterey, California) for the expressed purpose of establishing a set of protocols for measuring optical properties, and other environmental variables, to validate the radiometric performance of the SeaWiFS instrument, and to develop and validate bio-optical algorithms for use with SeaWiFS data. The proceedings of the workshop, as interpreted and expanded by the authors and reviewed by the workshop participants and other members of the bio-optical research community, became the SeaWiFS Ocean Optics Protocols (SOOP) and were published as Volume 5 of the (prelaunch) *SeaWiFS Technical Report Series* (Mueller and Austin 1992).

The protocols were intended to establish foundations for a measurement strategy to verify the SeaWiFS uncertainty goals of 5% in water-leaving radiances and 35% in chlorophyll *a* concentration (Hooker et al. 1992). The protocols specified a) the variables which must be measured, briefly reviewed the rationale for measuring each variable, and presented methods of making measurements in the field; b) the protocols for instrument performance specifications (including characterizing and calibrating instruments); and c) the approved methods of data analysis. In general, the SOOP set forth simply described and adapted instrument specifications and procedures that were common practice in the ocean optics community.

From the very beginning, the protocols were considered an evolving prescription that would allow the research community to approach the unprecedented measurement uncertainties implied by the SeaWiFS goals (Hooker and Esaias 1993); research and development activities were acknowledged to be important elements for improving the state of the art in specific areas. It was always the intent of the SeaWiFS Project and the SeaWiFS Working Groups (Hooker et al. 1993b) that the SOOP would be periodically evaluated and revised to reflect technical advances during the SeaWiFS Project cycle. In agreement with such an objective, three different in-water methods and four different above-water methods for determining $L_W(0^+, \lambda)$ were intercompared during SeaBOARR-98: S84, P94, and P97 for the former; and M80, C85, S95, and L98 for the latter.

3.1 In-Water Methods

The experimental setup began with siting a black buoy approximately 30 m from the southeast tower leg; the buoy was perpendicular to the southeastern side of the tower and displaced approximately 2 m to the side of the WiSPER instrument. A pulley was then attached to the buoy and the tower, and a closed loop of line (60 m long with marks on it every 1 m) was attached to the pulleys. A cable ring was linked to one of the cable marks which defined the current position of the profiler (the power and telemetry cable for the profiler passed through the ring). The ring and, thus, the miniNESS profiler, was moved to a selected distance from the tower leg by pulling on the closed loop of line until the desired number of cable marks between the ring's position and the tower leg was achieved. A schematic of the experimental setup is given in Fig. 16.

The miniNESS profiler is sufficiently easy to handle that it can be deployed by one person. Under normal circumstances, the handler keeps a few coils of the power and telemetry cable in the water, so the profiler can fall freely through the water column; once the desired depth has been reached, the cast is terminated and the profiler is pulled back to the surface. For the tower deployments, the profiler was slowly lowered by hand to control the descent rate (approximately $0.4\,\mathrm{m\,s^{-1}}$). A cable block, which could not pass through the cable ring, was used to prevent the profiler from going deeper than 15 m and accidently impacting the sea floor (theoretically this would not damage the profiler, since the light sensors are mounted on the fin assemblies).

An experiment was defined as a sequence of profile deployments going away or towards the platform during a relatively short period of time (typically 20 minutes). While the miniNESS casts were being sequentially collected, the WiSPER system was also repeatedly lowered and raised. For the tower deployments, 20 different experiments were conducted during almost clear sky conditions: 18 with variable miniNESS deployment distances with respect to the tower, and 2 (experiments 7 and 13) with the deployment distance fixed at 7.5 m (the same distance the WiSPER measurements were made with respect to the tower). The latter data were collected for comparison with WiSPER and to estimate temporal variability at the site (from advection). Note that the miniNESS experiments give another estimate of spatial variability.

A summary of the in-water methods to be used (S84, P94, and P97) is presented in Table 3.

3.1.1 S84

The subsurface profile of $L_u(z, \lambda)$ is used to estimate the spectral diffuse attenuation coefficient, $K_u(\lambda)$, and the subsurface signal is propagated to the sea surface using $K_u(\lambda)$; the upwelled radiance is then transmitted across the sea surface to produce $L_W(0^+, \lambda)$. The steps involved with this methodology are as follows:

1. Bin the profiler data in 1 m intervals.
2. Compute $K_u(z_0, \lambda)$ from vertical profiles of $L_u(z, \lambda)$ as the local slope of $\ln\left[L_u(z, \lambda)\right]$ in a depth interval of a few meters centered on depth z_0 (Smith and Baker 1984 and 1986):

$$\ln\left[L_u(z, \lambda)\right] \;=\; \ln\left[L_u(z_0, \lambda)\right] \;-\; K_u(z_0, \lambda)\delta z \quad (11)$$

where $\delta z = z - z_0$. The unknowns $\ln\left[L_u(z_0, \lambda)\right]$ and $K_u(z_0, \lambda)$ are determined as the intercept and

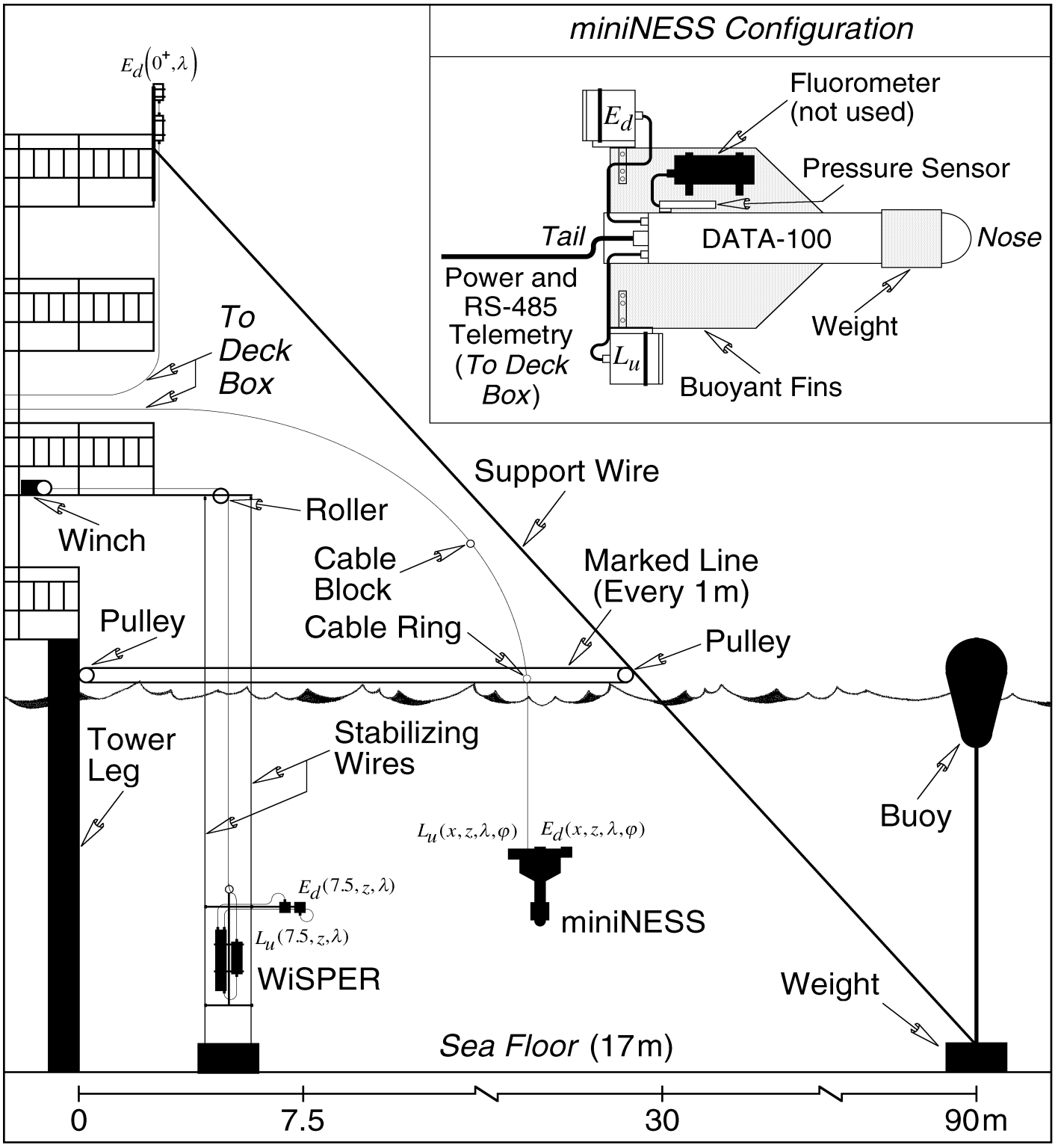

Fig. 16. A schematic of the tower shading experiments showing the equipment and their relative positioning with respect to one another. The WiSPER instrumentation is shown in a slightly distorted view, so all components are visible; in reality, the two radiometers and the two stabilizing wires are aligned in a plane perpendicular to the page, which means the light data is collected approximately 7.5 m away from the tower leg. Details of the miniNESS instrument are shown in the inset panel.

Table 3. A summary of the three in-water methods for calculating $L_W(0^+,\lambda)$.

Method	*Assumptions*	*Input Variables*	$L_W(0^+,\lambda)$ *Calculation*
S84	$z_0-\Delta z \le z < z_0+\Delta z$ $\Delta z \approx$ 4 to 10 m	$K_u(z,\lambda)$ from $L_u(z,\lambda)$ $L_u(0^-,\lambda) = L_u(z_0,\lambda)\exp\left[z_0 K_u(z_0,\lambda)\right]$	$L_W(0^+,\lambda) = 0.544\,L_u(0^-,\lambda)$
P94	$z_0-\Delta z \le z < z_0+\Delta z$ $\Delta z \approx$ 4 to 10 m	$K_u(z,\lambda)$ from $L_u(z,\lambda)$ $L_u(0^-,\lambda) = L_u(0.7,\lambda)\exp\left[0.7\,K_u(\lambda)\right]$	$L_W(0^+,\lambda) = 0.544\,L_u(0^-,\lambda)$
P97	$K_u = K_d, K_u(490,520)$ from $L_u(443,550)$, and C from $K_u(490,520)$	$\chi(\lambda)$ and $e(\lambda)$ using Morel (1988) $K_u(\lambda) = K_w(\lambda)+\chi_c(\lambda)C^{e(\lambda)}$ $L_u(0^-,\lambda) = L_u(0.7,\lambda)\exp\left[0.7\,K_u(\lambda)\right]$	$L_W(0^+,\lambda) = 0.544\,L_u(0^-,\lambda)$

slope of a least-squares linear regression to the measured $\ln\left[L_u(z,\lambda)\right]$ data within the depth interval $z_0-\Delta z \le z < z_0+\Delta z$. The half interval Δz is somewhat arbitrary, although Smith and Baker (1984 and 1986) suggest $\Delta z \approx$ 4–10 m.

3. Extrapolate $L_u(z_0,\lambda)$ to the surface according to

$$L_u(0^-,\lambda) = L_u(z_0,\lambda)\exp\left[z_0 K_u(z_0,\lambda)\right]. \quad (12)$$

4. Transmit $L_u(0^-,\lambda)$ through the sea surface according to Austin (1974):

$$L_W(0^+,\lambda) = \frac{1-\rho(\lambda)}{n_w^2(\lambda)}\,L_u(0^-,\lambda), \quad (13)$$

where $\rho(\lambda)$ is the Fresnel reflectance and $n_w(\lambda)$ is the refractive index of seawater. Austin (1980) notes the $\big(1-\rho(\lambda)\big)n_w^{-2}(\lambda)$ expression can be replaced by the constant 0.544, because the wavelength dependence of the variables is very weak. This substitution is made for this method and the other two in-water methods discussed below (P94 and P97).

3.1.2 P94

The subsurface upwelling radiance measured at z = 70 cm is propagated to the sea surface using $K_u(\lambda)$ estimated from simultaneous profiles of $L_u(z,\lambda)$ (following the techniques in S84), and then across the sea surface to produce $L_W(0^+,\lambda)$. The steps involved with this method are as follows:

1. Propagate the subsurface upwelling radiance measured at z = 70 cm depth to the sea surface using $K_u(\lambda)$ estimated from simultaneous profiles of $L_u(z,\lambda)$ (following the techniques in S84):

$$L_u(0^-,\lambda) = L_u(0.7,\lambda)\exp\left[0.7\,K_u(\lambda)\right]. \quad (14)$$

2. Transmit $L_u(0^-,\lambda)$ through the sea surface according to Austin (1974)

$$L_W(0^+,\lambda) = 0.544\,L_u(0^-,\lambda). \quad (15)$$

Note that (15) is the same as (13), except a constant has been used for the $\big(1-\rho(\lambda)\big)n_w^{-2}(\lambda)$ expression.

3.1.3 P97

$K_u(\lambda)$ is estimated using a combination of the Morel (1988) and Austin and Petzold (1981) algorithms. The ratio of $L_u(443)$ to $L_u(550)$ is used to estimate $K_u(490)$ and $K_u(520)$ as described by Austin and Petzold (1981). The computed $K_u(490)$ and $K_u(520)$ values are used to compute the chlorophyll concentration, C, by inverting the algorithm for $K_d(\lambda)$ as detailed by Morel (1988) and assuming $K_u(\lambda) = K_d(\lambda)$. Once C is computed, $K_u(\lambda)$ for the other wavelengths can be computed by applying the Morel (1988) technique.

The subsurface upwelling radiance at z = 70 cm is propagated to the sea surface using the estimated $K_u(\lambda)$, and then across the sea surface to produce $L_W(0^+,\lambda)$:

1. Compute $K_u(490)$ and $K_u(520)$ from $L_u(443)$ and $L_u(550)$ using the Austin and Petzold (1981) algorithms:

$$K_u(490) = 0.022 + 0.0883\left[\frac{L_u(443)}{L_u(550)}\right]^{-1.491}$$
and (16)
$$K_u(520) = 0.044 + 0.0663\left[\frac{L_u(443)}{L_u(550)}\right]^{-1.398}.$$

2. Compute C from (16) by inverting the model relating $K_u(\lambda)$ for Case-1 waters to the mean C value (Morel 1988) while assuming $K_u(\lambda) = K_d(\lambda)$:

$$C_{490} = \left[\frac{K_u(490)-K_w(490)}{\chi_c(490)}\right]^{e^{-1}(490)},$$
$$C_{520} = \left[\frac{K_u(520)-K_w(520)}{\chi_c(520)}\right]^{e^{-1}(520)}, \quad (17)$$
and
$$C = \frac{C_{490}+C_{520}}{2},$$

where $K_w(\lambda)$ represents the spectral attenuation coefficient for pure water, and the coefficients $\chi_c(\lambda)$ and $e(\lambda)$ are regression coefficients determined by statistical analysis of $K_d(\lambda)$ in Case-1 water (Morel 1988).

3. The algorithm for computing $K_u(\lambda)$ is as follows:

$$K_u(\lambda) \;=\; K_w(\lambda) \;+\; \chi_c(\lambda) C^{e(\lambda)}. \qquad (18)$$

4. Propagate the subsurface upwelling radiance measured at $z = 70\,\mathrm{cm}$ depth to the sea surface using the estimated $K_u(\lambda)$ and (14).
5. Transmit $L_u(0^-, \lambda)$ through the sea surface using (15).

3.2 Above-Water Methods

The surface glint correction methods (M80, C85, S95, and L98) for $L_W(\lambda)$ measurements, require the existence of a spectral band in the NIR (λ_r) for which $L_W(\lambda_r) = 0$. In the case of open ocean water (Case-1 with $C < 0.25\,\mathrm{mg\,m^{-3}}$), the assumption $L_W(670) = 0$ can be used (Gordon 1981). For all other Case-1 waters, the wavelengths 765 and 865 nm should be considered for correction (Gordon and Wang 1994). For Case-2 water, the assumption $L_W(1012) = 0$ has been found to be appropriate even in waters heavily loaded with sediment (Bukata et al. 1995). If $L_W(\lambda_r)0$, the amount of glint will be overestimated, which will result in an underestimation of L_W.

A summary of the above-water methods to be used (M80, C85, S95, and L98) is presented in Table 4.

3.2.1 M80

Sky glint correction is based on the assumption that $L_W(\lambda)$ in a near-infrared (NIR) band, $L_W(\lambda_r)$, is equal to zero (Gordon 1981). Consequently, the above-water radiance measured at λ_r is entirely due to surface reflection. The infrared estimates of sky glint are then extended over the whole spectrum by using the measured wavelength dependence of the incident sky radiance. Estimated sky glint is subtracted from the total signal in order to recover $L_W(\lambda)$. The steps for implementing the method are as follows:

1. Remove the temporal sun glint from the high frequency spectra before averaging, so the final mean spectrum incorporates sky glint only.
2. Assume $L_W(\lambda_r) = 0$.
3. Extend the NIR estimate of the sky glint over the whole spectrum by using the measured wavelength dependence of the incident sky radiance, and subtract the estimated sky glint from the total signal:

$$L_W(0^+, \lambda) \;=\; L_T(\lambda, \phi', \vartheta) \;-\; L_i(\lambda, \phi', \vartheta')\delta_r. \qquad (19)$$

where $\phi' = \phi \pm \frac{\pi}{2}$ (90° away from the sun in either direction, i.e., ϕ^+ or ϕ^- in Fig. 1) and $\delta_r = L_T(\lambda_r, \phi', \vartheta)/L_i(\lambda_r, \phi', \vartheta')$.

3.2.2 C85

The C85 method uses data averaged over 10 s intervals, so each spectrum of sea surface radiance incorporates the contribution of temporal sun glint which have to be removed by a correction algorithm. The above-water measurements are corrected for sky glint assuming specular reflection of sky radiance at the sea surface. The residual reflection of downwelling radiation from the wave facets is computed assuming the residual signal in the NIR region is entirely due to surface reflection, i.e., $L_W(\lambda_r) = 0$. Measurements of a horizontally oriented gray reflectance plaque are used to compute the plaque downwelling total irradiance, $E_p(\lambda)$. The steps involved are as follows:

1. Compute $E_p(\lambda)$ as

$$E_p(\lambda) \;=\; \pi \frac{L_p(\lambda, \phi', \vartheta)}{\rho_p(\lambda, \phi', \vartheta)}. \qquad (20)$$

2. Correct for the specular reflection of sky light and for the residual reflection of downwelling radiation from the wave facets by calculating

$$\Delta L \;=\; \big[L_T(\lambda_r) - \rho(\lambda, \phi) L_i(\lambda_r, \phi', \vartheta')\big] \frac{E_p(\lambda)}{E_p(\lambda_r)} \qquad (21)$$

and then deriving

$$\begin{aligned} L_W(0^+, \lambda) \;&=\; L_T(\lambda, \phi', \vartheta) \\ &\quad -\; \rho(\lambda, \phi) L_i(\lambda, \phi', \vartheta') \;-\; \Delta L. \end{aligned} \qquad (22)$$

3.2.3 S95

The first revision of the SOOP incorporated new protocols in several areas, including expanded protocol descriptions for Case-2 waters and other improvements, as contributed by several members of the SeaWiFS Science Team (Mueller and Austin 1995). The version 1 revision required the following for making above-water radiometric measurements for estimating $L_W(0^+, \lambda)$:

1. The radiometer measuring water-leaving radiance should point to the sea surface with an angle of about $\vartheta = 20°$ from nadir and away from the solar azimuth angle (ϕ) by at least 90°, i.e., ϕ'.
2. Foam and floating material must be avoided during measurements, and because of temporal variability due to waves, it is important to record a number of spectra within a period of a few seconds (e.g., 30 spectra within 15 s).
3. Before calculating final mean and standard deviation spectra, outliers should be removed by computing initial estimates of these statistics and rejecting radiance spectra containing values more than 1.5 standard deviations ($1.5\,\sigma$) from the estimated mean (μ).

Table 4. A summary of the four surface glint correction methods applied to the above-water radiance measurements. The assumptions of each method and the input measurements required by the method are given in the second and third columns, respectively. The algorithms for calculating $L_W(\lambda)$ are shown in the fifth column. All of the methods require ideal sky conditions (cloud free or uniformly overcast), except L98, which can be used under a variable sky. The assumption for S95 is that $\rho(\lambda,\phi)$ can be approximated by a flat sea surface. Note that M80, S95, and L98 require the removal of temporal sun glint from the high frequency $L_T(\lambda)$ spectra, whereas C85 uses averaged (10 s) $L_T(\lambda)$ spectra. For all of the SeaBOARR-98 data, $\lambda_r = 780$ nm.

Method	*Assumptions*	*Input Variables*	$L_W(0^+,\lambda)$ *Calculation*
M80	$L_W(\lambda_r)=0$ and Ideal Sky	$L_T(\lambda)$ and $L_i(\lambda)$	$L_W(0^+,\lambda) = L_T(\lambda,\phi',\vartheta) - L_i(\lambda,\phi',\vartheta')\left[\frac{L_T(\lambda_r,\phi',\vartheta)}{L_i(\lambda_r,\phi',\vartheta')}\right]$
C85	$L_W(\lambda_r)=0$ and Ideal Sky	$L_T(\lambda)$, $L_i(\lambda)$, and $L_p(\lambda)$	$L_W(0^+,\lambda) = L_T(\lambda,\phi',\vartheta) - \rho(\lambda,\phi)L_i(\lambda,\phi',\vartheta') - \Delta L$ *where* $\Delta L = \left[L_T(\lambda_r) - \rho(\lambda,\phi)L_i(\lambda_r,\phi',\vartheta')\right]E_p(\lambda)/E_p(\lambda_r)$ *and* $E_p(\lambda) = \pi L_p(\lambda,\phi',\vartheta)/\rho_p(\lambda,\phi',\vartheta)$
S95	$\rho(\lambda,\phi)$ and Ideal Sky†	$L_T(\lambda)$ and $L_i(\lambda)$	$L_W(0^+,\lambda) = L_T(\lambda,\phi',\vartheta) - \rho(\lambda,\phi)L_i(\lambda,\phi',\vartheta')$
L98	$L_W(\lambda_r)=0$	$L_T(\lambda)$ and $E_i(\lambda)$	$L_W(0^+,\lambda) = L_T(\lambda,\phi',\vartheta) - \left[\frac{L_T(\lambda_r)}{E_i(\lambda_r)}\right]E_i(\lambda)$

† The SOOP indicates S95 can "probably" be used under variable cloud conditions.

4. $L_T(\lambda)$ must be corrected for sky glint using measurements of sky radiance, $L_i(\lambda)$, in the direction appropriate for the specular reflection from the sea surface into the sensor. $L_i(\lambda)$ measurements can be made either by looking at a horizontal *first surface* mirror (a mirror with no layers other than the reflective surface) at the same nadir and azimuth angles used for the $L_T(\lambda)$ observations, or by pointing the radiometer into the sky at a zenith angle equal to the nadir angle of the $L_T(\lambda)$ observations (or as in Fig. 1, $\vartheta' = \pi - \vartheta$) and with the same azimuth angle. The sky glint is removed using ρ:

$$L_W(0^+,\lambda) = L_T(\lambda,\phi',\vartheta) - \rho(\lambda)L_i(\lambda,\phi',\vartheta'). \quad (23)$$

3.2.4 L98

Sky glint correction for this method is also based on the assumption that $L_W(\lambda_r) = 0$, so the signal received in the λ_r part of the spectrum is entirely due to surface reflection. The L98 method uses the wavelength dependence of diffuse sky irradiance to extend the estimate of sky glint at λ_r over the whole spectrum. Estimated sky glint is subtracted from the total signal in order to recover $L_W(\lambda)$.

The advantage of this method is that it incorporates the effect of clouds. The technical advantage is that $E_d(0^+,\lambda)$ and $E_i(0^+,\lambda)$ can be measured with the same instrument: an upward-viewing radiometer where the diffuse component can be determined by cyclically blocking the sun disc to the radiometer, so $E_d(0^+,\lambda)$ and $E_i(0^+,\lambda)$ can be continuously monitored during remote sensing observations. The steps involved are as follows:

1. Remove the temporal sun glint from the high frequency spectra before averaging, so the final mean spectrum incorporates sky glint only.
2. Assume $L_W(\lambda_r) = 0$.
3. Extend the estimate of sky glint at λ_r over the entire spectrum by using the measured wavelength dependence of $E_i(0^+)$ and subtract the estimated sky glint from the total signal to calculate

$$L_W(0^+,\lambda) = L_T(\lambda,\phi',\vartheta) - \left[\frac{L_T(\lambda_r)}{E_i(\lambda_r)}\right]E_i(\lambda). \quad (24)$$

3.2.5 Method Revisions

From 11–12 December 1997, the Normalized Remote Sensing Reflectance Workshop was held at the Center for Coastal Physical Oceanography (CCPO), Old Dominion University (Norfolk, Virginia). The meeting was sponsored by the GSFC Sensor Intercomparison and Merger for Biological and Interdisciplinary Ocean Studies (SIMBIOS) Project. The goal of the workshop was:

> *Determination of the uncertainty budgets of normalized remote sensing reflectance (NRSR), in and between the various methods used to measure it, and because of uncertainties in calibration (radiometer and reflectance target), environmental variance, and the treatments of Fresnel reflectance of skylight and the ocean's bidirectional reflectance distribution function (BRDF).*

The goal was to be realized through three objectives:

1. Review current results and data (begin tabulating uncertainty budgets);
2. Define a unified data set for NRSR and begin populating it; and
3. Plan experimental comparisons to explore the uncertainty sources associated with each method of measuring NRSR.

It was proposed that the group accept as a baseline, for purposes of discussion, that the uncertainty in NRSR determined from in-water $L_u(z,\lambda)$ profiles, combined with above-water measurements of $E_d(0^+,\lambda)$, is approximately 5% for $\lambda < 600\,\mathrm{nm}$ and $K(490) < 0.1$.

In later discussions it was agreed to limit planned intercomparisons between above- and below-water determinations of NRSR to these conditions. This uncertainty estimate is based on results from the first Data Analysis Round-Robin (DARR-94) activity (Siegel et al. 1995) and the third SeaWiFS Intercalibration Round-Robin Experiment (SIRREX-3), and SIRREX-4 (Mueller et al. 1996 and Johnson et al. 1996, respectively).

Radiative transfer simulations of remote sensing reflectance measurements above a wave-roughened surface were undertaken by Curt Mobley from Sequoia Scientific, Inc. (Seattle, Washington). The results showed the increase with wind speed (and resulting surface wave slope) of sky radiance and sun glint reflectance in total radiance viewed at the sea surface, relative to radiance from beneath the surface. At wind speeds approaching $10\,\mathrm{m\,s^{-1}}$, his results suggested the best nadir viewing angle would be 40°, rather than the 30° used by many of the participants (and the 20° given in the original publication of S95). At lower wind speeds and a 40° viewing angle, Mobely recommended using an effective surface reflectance of 0.028.

There was a consensus that more analyses could and should be done in four general areas of remote sensing reflectance (R_{rs}) measurements:

1. Uncertainties in and between $E_d(0^+)$ determined by a) direct measurement of $E_d(0^+)$ with a calibrated radiometer, b) estimation of $E_d(0^+)$ by measuring reflected radiance (calibrated or uncalibrated, since calibration coefficients cancel in R_{rs} formed in this way) from a gray target of known (calibrated) reflectance, and c) $E_d(0^+)$ modeled for clear sky conditions, with and without independent measurements of aerosol and ozone optical thicknesses;
2. Uncertainties between different above-water methods for measuring R_{rs};
3. Uncertainties between R_{rs} values determined from above- and in-water radiance measurements; and
4. Comparative analyses of measured R_{rs} (above water or in water), modeled R_{rs} based on measured inherent optical properties (IOPs), and models based on water-column constituents (e.g., chlorophyll *a*) contributing to IOP.

For these analyses, the following restrictions on data entries were agreed to: $\lambda < 600\,\mathrm{nm}$; $K(490) < 0.1\,\mathrm{m^{-1}}$; percent cloud cover less than 20%; wind speed less than $10\,\mathrm{m\,s^{-1}}$ (higher wind speed data can be submitted, but should not be included in the simpler comparisons), solar zenith angle from 30–60°(again data outside this range may be submitted, but should probably be excluded from the simpler methods of intercomparison).

Based on the consensus reached at the meeting, all of the above-water methods used in the SeaBOARR-98 field campaign used a viewing angle of 40° from nadir. Every effort was made to adhere to the agreed upon sampling restrictions, but the most important criteria was to collect data during stable illumination conditions, i.e., clear sky, calm sea, low wind speed, etc.

3.4 SQM-II Protocols

To monitor the stability (in the field) of the in-water and above-water radiometers used during SeaBOARR-98, and to quantify the performance of the SQM-II during its field commissioning, the procedures given in Hooker and Aiken (1998) were followed where applicable: a calibration evaluation and radiometric testing (CERT) session was defined and a sequence of procedures was implemented for each CERT session. In summary, each CERT session involved the following steps:

1. The number of hours on each lamp set were tracked by recording the starting number of hours on each lamp set.
2. One radiometer (S09) was selected to monitor the powering and warming up of the SQM-II. The first data collected during a CERT session were the dark voltages for this radiometer, which was achieved by putting an opaque cap on the radiometer and collecting data for 3 minutes during the collection of the SQM-II internal dark voltages.
3. Once the SQM-II was powered up at the selected lamp level, it was allowed to warm up for at least 1 hour. During this time, internal monitor voltages, lamp voltages, and internal temperatures of the SQM-II were recorded. The warm-up period was considered completed when the internal SQM-II monitors were constant to within 0.1%. The radiometric stability usually coincided with a thermal equilibrium as denoted by the internal thermistors.
4. After the warm-up period, each fiducial was measured, and then the individual radiometric sensors were tested sequentially. First, the previous DUT was removed and replaced with a glass fiducial. Second, dark voltages for the radiometer and SQM-II monitor data for the glass fiducial were simultaneously collected for 3 minutes. Third, the glass fiducial was removed and replaced with the radiometer. Finally, data from the SQM-II internal detector and

Table 5. A summary of the environmental characteristics of the AAOT site during the SeaBOARR-98 stations. All of the time information is given as the sequential day of the year (SDY) and Greenwich Mean Time (GMT), where 7 July is SDY 188 and 13 July is SDY 195. Sea state (SS), cloud cover (CC), and light stability (LS) are all given as coded values: 0–12, 0–8, and 0–2, respectively. The SS entries are for the World Meteorological Organization (WMO) Code M scale (WMO–N.8), the CC entries are in eighths of coverage, and the LS entries are as follows: 0 for stable light, 1 for slightly changing illumination, and 2 for variable conditions. Wind speed (WS) and many of the other values are shown for the time period in which they were collected, but are applicable for the entire station. The ratio of $E_i(0^+,\lambda)$ to $E_d(0^+,\lambda)$ is given by r. The $a_{\rm ys}$, a_p, r, and K_d values are all for $\lambda = 490$. The Ångström exponent and coefficients are given by α and β, respectively.

Station			WS	SS	CC	LS	β	α	C_{a+a}	$C_{\rm TSM}$	$a_{\rm ys}$	a_p	R	K_d	θ
Code	SDY	Time	$[\mathrm{m\,s^{-1}}]$		*[Coded]*				$[\mathrm{mg\,m^{-3}}]$		$[\mathrm{m^{-1}}]$			$[\mathrm{m^{-1}}]$	[°]
46s1	188	1034–1104	2.4	1	4	0	0.22	1.3	1.22	1.91	0.039	0.065	0.76	0.27	23
46s2	189	1014–1042	4.9	2	3	0	0.02	1.4	0.51	0.93	0.019	0.028	0.14	0.10	25
46s2a	189	1241–1305		2	3	0	0.01	2.1					0.16	0.09	30
46s3	190	1300–1329	5.3	1	7	1			1.74	4.21	0.049	0.111	7.30	0.44	33
46s4	191	0854–0916	4.3	1	6	1	0.06	1.6	1.84	3.16	0.031	0.087	0.43	0.37	36
46s5	191	1124–1150	5.3	1	0	0	0.07	1.6	1.55	2.84	0.027	0.094	0.32	0.30	23
46s5a	191	1159–1125		1	0	0	0.07	1.6					0.29	0.30	25
46s5b	191	1247–1313		1	0	0	0.07	1.5					0.32	0.31	31
46s5c	191	1321–1351		1	0	0	0.06	1.6					0.33	0.30	36
47s1	194	1026–1043	7.3	1	0	0	0.23	1.5	0.27	0.84	0.051	0.024	0.89	0.09	25
47s1a	194	1104–1130		1	0	0	0.15	1.6					0.69	0.08	23
47s1b	194	1133–1200		1	0	0	0.15	1.6					0.61	0.08	24
47s1c	194	1215–1242		2	0	0	0.14	1.6					0.59	0.07	27
47s1d	194	1250–1315		2	0	0	0.08	1.8					0.48	0.08	31
47s1e	194	1428–1500		1	0	0	0.07	1.8					0.53	0.09	48
47s2	195	0810–0836	2.4	1	8	1			0.92	1.93	0.081	0.055		0.24	42
47s3	195	0943–1009	3.0	0	8	0			0.68	1.87	0.091	0.061		0.22	28

the radiometer were recorded for 3 minutes. Each time a DUT was used, SQM-II lamp voltages and internal temperatures were recorded. Each data collection event (3 minutes) is referred to here as a data acquisition sequence (DAS) and represents approximately 1,080 radiometer samples and 450 SQM-II (internal monitor) samples.

5. Before the SQM-II was shut down, the fiducials were measured again. These measurements, plus the fiducial data acquired using the glass fiducial in between radiometer dark and light (SQM-II) measurements, are the primary sources for tracking the stability of the SQM-II flux. In some cases, a radiometer recorded the powering down of the lamps. After the lamps were powered down, the ending number of hours on each lamp set were recorded.
6. The internal monitor dark voltages were recorded by putting an opaque cap over the SQM-II exit aperture and collecting data for 3 minutes.

It is important to note the warmup process only involved the SQM-II and it was done only once before the individual DUTs were measured; the DUTs were not warmed up per se, although, they were kept in the same room as the SQM-II, so they were at room temperature.

4. PRELIMINARY RESULTS

A summary of the environmental characteristics of the AAOT site during the SeaBOARR-98 stations is given in Table 5. Although one of the data collection objectives was to collect as much data as possible following the restrictions agreed to at the NRSR meeting, the opportunities for data collection were dictated by the weather, and the primary objective was simply to collect the best data possible under the conditions at the time. Nonetheless, many of the acquisition events are within the workshop restrictions.

The nomenclature used to distinguish the water-leaving radiances derived from the in-air and in-water methods is $\hat{L}_W^A(0^+,\lambda)$ and $\tilde{L}_W^B(0^+,\lambda)$, respectively, where the A and B codes identify the above-water and below-water methods used, i.e., water-leaving radiances estimated using the in-water S84 method are identified as $\tilde{L}_W^{\rm S84}(0^+,\lambda)$.

In this preliminary analysis, only the data collected during clear sky, calm sea, and Case-2 water are considered (Lazin et al. 1998). Figure 17 shows the water-leaving radiances obtained from the four above-water methods compared to the values estimated from the WiSPER data using the S84 in-water method. The latter are corrected for instrument self-shading, but are not corrected for the perturbation effects of the tower. The above-water data set is

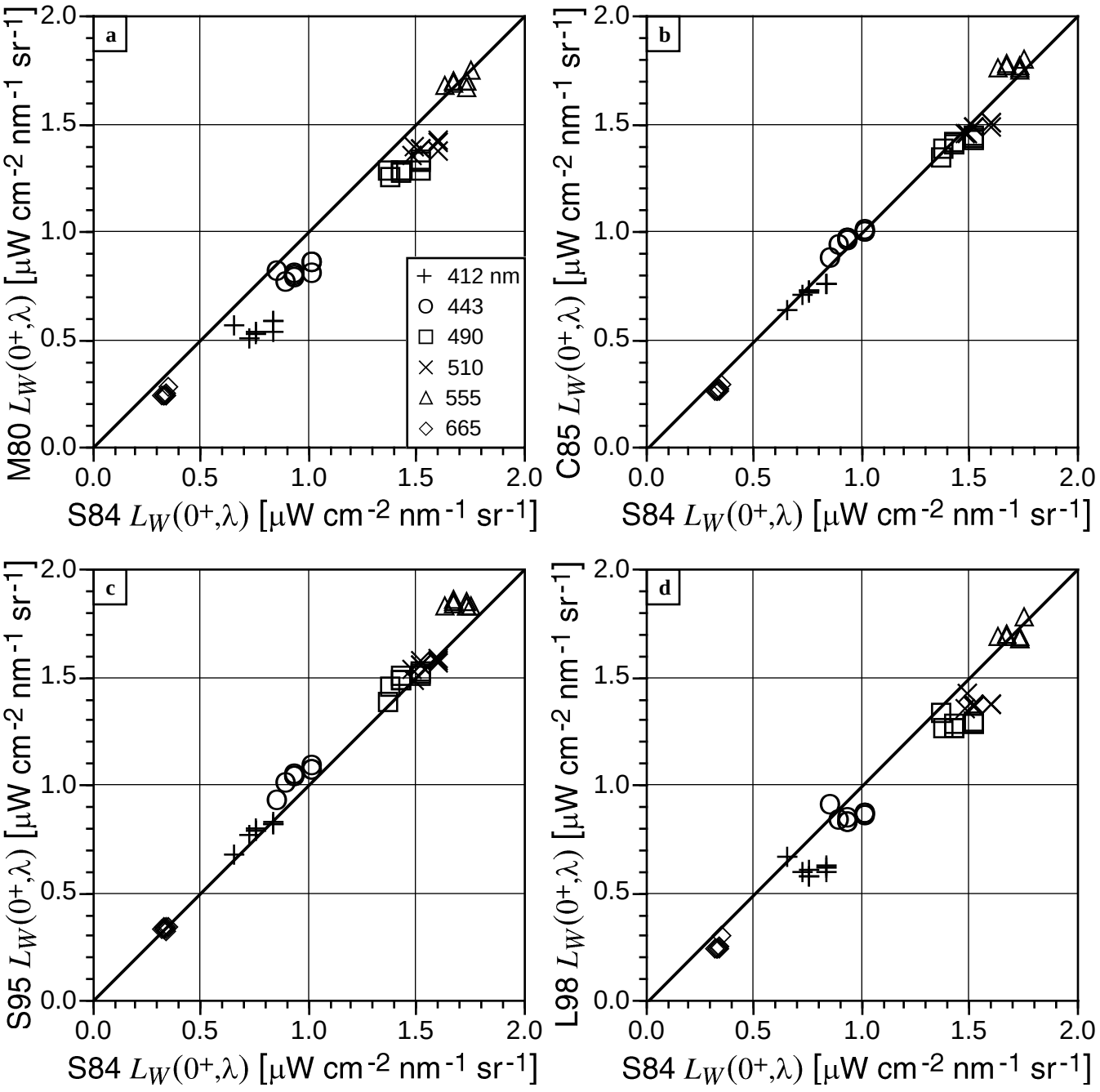

Fig. 17. A comparison of the S84 in-water $L_W(0^+,\lambda)$ method with four above-water estimation methods: **a)** M80, **a)** C85, **a)** S95, and **a)** L98. The wavelength codes are shown as an inset panel in **a**.

also not corrected for tower shading effects.

The root mean square difference (RMSD) was computed for each method and wavelength as:

$$\psi^B = 100\left[\sum \frac{1}{N}\left[\frac{\hat{L}_W^A(0^+,\lambda) - \tilde{L}_W^B(0^+,\lambda)}{\tilde{L}_W^B(0^+,\lambda)}\right]^2\right]^{\frac{1}{2}} \quad (25)$$

where N is the number of measurements and the ψ values are categorized by the in-water method used. Depending on wavelength, ψ^{S84} for the L_W values was in the range of 3–6% for the S95 method, 7–12% for the C85 method, 7–20% for the L98 method, and 11–22% for the M80 method.

The L98 and M80 methods systematically underestimated $L_W(0^+,\lambda)$, because the $L_W(780) = 0$ assumption was not appropriate for the water type involved (very turbid Case-2). The glint estimate from the 780 nm band was, therefore, too high, which produced low $L_W(0^+,\lambda)$ values. The C85 method uses Fresnel reflectance for sky

glint correction, as well as the $L_W(780) = 0$ assumption for the minor correction of the residual reflection of global radiance from the waves. This method was not greatly influenced by the actual existence of $L_W(780)$ and water quality. The S95 method, which assumes clear sky and specular reflection of sky radiance from the calm sea, is in excellent agreement with the in-water estimates, as expected regarding the experienced conditions.

Preliminary SQM-II analyses have been completed for 1 of the 16 radiometers used during SeaBOARR-98 (S09). For the four CERT sessions completed at the tower, the data shows S09 was stable to better than 0.5% for all channels (McLean et al. 1998). Hooker and Aiken (1998) reported similar overall stability for Satlantic radiance sensors, so there is no reason to believe the other sensors will show substantially different characteristics. They also showed Satlantic irradiance sensors were slightly less stable, but the sensors were usually stable to within 1.0%. Given these facts, the expectation is that differences in methods above the 1.0% level are real and are not due to instrument performance problems.

5. DISCUSSION

To provide a quick look at the data collected during SeaBOARR-98, only one part of the data collected in the experiment was analyzed. The preliminary results from this effort indicate the following:

1. The methods based on the simple concept of specular reflection that employ Fresnel reflectance values were the most appropriate for clear sky and Case-2 water (S95 and C85);
2. The best results were obtained if the temporal sun glint outliers were removed from the data before computing final mean spectra (S95), which emphasizes the importance of high frequency measurements of sea surface radiance;
3. The corrections based on the assumption of a *black* sea in the 780 nm band (M80 and L98), are not recommended for Case-2 water, but these two methods might be improved by using a correction band centered more in the infrared part of the spectrum;
4. The only surface glint correction method that met the required 5% accuracy of $L_W(0^+, \lambda)$ (compared to the in-water estimates) was the S95 method; and
5. The SQM-II data, plus the results of Hooker and Aiken (1998), indicate differences in methods above the 1.0% level are real and are not due to instrument performance problems.

It is important to note polarization sensitivity has only been semiqualitatively assessed using the practices given in the SOOP: a radiance sensor was rotated about its axis 90° from the sun in the sun–zenith plane on a cloud- and haze-free day. No noticable changes were observed, although, no quantitative results were recorded. A polarization characterization for all of the above water radiance sensors will be perfomed in the laboratory during SIRREX-7 (March 1999) to quantify this effect.

Future activities will also include analysis of the second part of the data (overcast conditions, variable sky, and clear water), a completion of the SQM-II data, an inclusion of the additional in-water methods for computing $L_W(0^+, \lambda)$, an examination of the tower shading effect on the subsurface and above-water measurements, and a quantification of how the differences in the various measurement protocols effect bio-optical algorithms. Ultimately, the latter is the most important for SeaWiFS validation activities (Hooker and McClain 1999). The next field activity will be concerned with a) using the four above-water and the three in-water methods at sea while the ship is stopped (but, nonetheless, moving in the ambient wave field), and b) using as many of the above-water methods as possible while the ship is underway. One of the primary emphases will be to collect as much data as possible in Case-1 water while adhering to as many of the sampling restrictions agreed to at the NRSR meeting as possible.

Acknowledgments

SeaBOARR-98 could not have been executed at the high level that was achieved without the competent contributions of the AAOT crew: Armando and Daniele Penzo, and Narciso and Gianni Zennaro. The logistics were substantially more involved than the usual CoASTS field campaigns, so the enthusiastic assistance from the CNR scientific staff led by Luigi Alberotanza was essential. In particular, Perluigi Cova was responsible for the CTD profiles as well as the meteorological data collection, and Sandro Vianello was responsible for water filtration.

Acknowledgements are also due to the JRC scientists: Dirk van der Linde for the support provided in preparing the optical devices for deployment and the TSM analyses, John Doyle for miniNESS deployment assistance, Jean-François Berthon for providing the AC-9 processed data, Cristina Targa for the HPLC analyses, and Stefania Grossi for the dissolved and particulate matter absorption analyses. The JRC and CNR participation in the experiment was mainly supported by the European Commission through contracts ENV4–CT96–0307 and MAS3–CT97–0087.

The miniNESS, SeaSAS, DalSAS, and DalBOSS data were all acquired and recorded using software developed by Jim Brown (University of Miami) and the SeaWiFS Project. The SeaWiFS Project (Charles McClain) also provided additional funding, directly or indirectly, to most of the participants which was critical in bringing all of the needed elements together as scheduled.

Appendices

A. SeaBOARR-98 Science Team
B. The miniNESS Deployment Log
C. The SeaSAS Deployment Log
D. The WiSPER Deployment Log
E. The Ancillary Data Collection Logs
F. The DalSAS Deployment Log
G. The DalBOSS Deployment Log
H. The SQM-II Deployment Log

Appendix A

SeaBOARR-98 Science Team

The SeaBOARR-98 science team members are presented alphabetically.

Jean-François Berthon
JRC/SAI/ME T.P. 272
Ispra, I–21020 (VA)
ITALY
Voice: 39–0–332–789–934
Fax: 39–0–332–789–034
Net: jean-francois.berthon@jrc.it

Pierluigi Cova *and*
Sandro Vianello
CNR/ISDGM
San Polo 1364
I–30125 Venice
ITALY
Voice: 39–0–41–521–6840
Fax: 39–0–41–260–2340
Net: claudia@neuro.isdgm.ve.cnr.it

John Piero Doyle
JRC/SAI/ME T.P. 272
I–21020 Ispra (VA)
ITALY
Voice: 39–0–332–786–052
Fax: 39–0–332–789–034
Net: john.doyle@jrc.it

Stefania Grossi
JRC/SAI/ME T.P. 272
I–21020 Ispra (VA)
ITALY
Voice: 39–0–332–785–834
Fax: 39–0–332–789–034
Net: stefania.grossi@jrc.it

Stanford Hooker
NASA/GSFC/Code 970.2
Bldg. 28, Room W121
Greenbelt, Maryland 20771
USA
Voice: 301–286–9503
Fax: 301–286–1775
Net: stan@ardbeg.gsfc.nasa.gov

Gordana Lazin
Dept. of Oceanography
Dalhousie University
Halifax, Nova Scotia B3H 4J1
CANADA
Voice: 01–902–494–3655
Fax: 01–902–494–2039
Net: gogo@raptor.ocean.dal.ca

Dirk van der Linde
JRC/SAI/ME T.P. 272
I–21020 Ispra (VA)
ITALY
Voice: 39–0–332–785–362
Fax: 39–0–332–789–034
Net: dirk.vanderlinde@jrc.it

Scott McLean
Satlantic, Inc.
Richmond Terminal, Pier 9
3295 Barrington Street
Halifax, Nova Scotia B3K 5X8
CANADA
Voice: 01–902–492–4780
Fax: 01–902–492–4781
Net: scott@satlantic.com

Cristina Targa
JRC/SAI/ME T.P. 272
I–21020 Ispra (VA)
ITALY
Voice: 39–0–332–785–834
Fax: 39–0–332–789–034
Net: cristina.targa@jrc.it

Giuseppe Zibordi
JRC/SAI/ME T.P. 272
I–21020 Ispra (VA)
ITALY
Voice: 39–0–332–785–902
Fax: 39–0–332–789–034
Net: giuseppe.zibordi@jrc.it

Appendix B

The miniNESS Deployment Log

The miniNESS Deployment Log is summarized in Table B1.

Appendix C

The SeaSAS Deployment Log

The SeaSAS Deployment Log is summarized in Table C1.

Appendix D

The WiSPER Deployment Log

The WiSPER Deployment Log is summarized in Table D1.

Appendix E

The Ancillary Data Collection Logs

A summary of the deployment logs for the AC-9, CE-318, and MFR-6 instruments along with the HPLC pigment, yellow substance absorption (a_{ys}), and particulate absorption (a_p) logs are presented in Table E1.

Appendix F

The DalSAS Deployment Log

The DalSAS Deployment Log is summarized in Table F1.

Appendix G

The DalBOSS Deployment Log

The DalBOSS Deployment Log is summarized in Table G1.

Appendix H

The SQM-II Deployment Log

The SQM-II Deployment Log is summarized in Table H1.

Table B1. A summary of the miniNESS deployment log for SeaBOARR-98. The data are organized according to sequential casts and experiments (*Exp.*). The deployment distance from the tower is given by x, and this column is also used to indicate when the darks were recorded for the profiler and the reference together (*Bdarks*) or individually (*Pdarks* and *Rdarks*, respectively). The filenames for the profiler and reference data are in the columns with the same name. All times are in GMT.

Cast	*Exp.*	*SDY*	*Time*	x [m]	*Profiler*	*Reference*	*Cast*	*Exp.*	*SDY*	*Time*	x [m]	*Profiler*	*Reference*
1	0	190	0825	*Bdarks*	J02MC001.SHO	J02MC001.SHM	51	5	191	1251	13.0	J02MD051.SHO	J02MD051.SHM
2	1	191	0740	*Pdarks*	J02MC002.SHO		52	5	191	1252	15.0	J02MD052.SHO	J02MD052.SHM
2	1	191	0834	*Rdarks*		J02MC002.SHM	53	5	191	1253	17.0	J02MD053.SHO	J02MD053.SHM
2	1	191	0855	3.0	J02MD002.SHO	J02MD002.SHM	54	5	191	1254	19.0	J02MD054.SHO	J02MD054.SHM
3	1	191	0856	5.0	J02MD003.SHO	J02MD003.SHM	55	5	191	1255	21.0	J02MD055.SHO	J02MD055.SHM
4	1	191	0857	7.0	J02MD004.SHO	J02MD004.SHM	56	5	191	1256	23.0	J02MD056.SHO	J02MD056.SHM
5	1	191	0859	7.5	J02MD005.SHO	J02MD005.SHM	57	6	191	1258	23.0	J02MD057.SHO	J02MD057.SHM
6	1	191	0902	9.0	J02MD006.SHO	J02MD006.SHM	58	6	191	1259	21.0	J02MD058.SHO	J02MD058.SHM
7	2	191	1128	3.0	J02MD007.SHO	J02MD007.SHM	59	6	191	1300	19.0	J02MD059.SHO	J02MD059.SHM
8	2	191	1129	5.0	J02MD008.SHO	J02MD008.SHM	60	6	191	1301	17.0	J02MD060.SHO	J02MD060.SHM
9	2	191	1130	7.0	J02MD009.SHO	J02MD009.SHM	61	6	191	1302	15.0	J02MD061.SHO	J02MD061.SHM
10	2	191	1130	7.5	J02MD010.SHO	J02MD010.SHM	62	6	191	1303	13.0	J02MD062.SHO	J02MD062.SHM
11	2	191	1131	9.0	J02MD011.SHO	J02MD011.SHM	63	6	191	1304	11.0	J02MD063.SHO	J02MD063.SHM
12	2	191	1132	11.0	J02MD012.SHO	J02MD012.SHM	64	6	191	1305	11.0	J02MD064.SHO	J02MD064.SHM
13	2	191	1133	13.0	J02MD013.SHO	J02MD013.SHM	65	6	191	1307	9.0	J02MD065.SHO	J02MD065.SHM
14	2	191	1135	15.0	J02MD014.SHO	J02MD014.SHM	66	6	191	1310	7.5	J02MD066.SHO	J02MD066.SHM
15	3	191	1151	3.0	J02MD015.SHO	J02MD015.SHM	67	6	191	1311	7.0	J02MD067.SHO	J02MD067.SHM
16	3	191	1152	5.0	J02MD016.SHO	J02MD016.SHM	68	6	191	1312	5.0	J02MD068.SHO	J02MD068.SHM
17	3	191	1153	7.0	J02MD017.SHO	J02MD017.SHM	69	6	191	1313	3.0	J02MD069.SHO	J02MD069.SHM
18	3	191	1153	7.5	J02MD018.SHO	J02MD018.SHM	70	7	191	1316	7.5	J02MD070.SHO	J02MD070.SHM
19	3	191	1154	9.0	J02MD019.SHO	J02MD019.SHM	71	7	191	1318	7.5	J02MD071.SHO	J02MD071.SHM
20	3	191	1156	11.0	J02MD020.SHO	J02MD020.SHM	72	7	191	1319	7.5	J02MD072.SHO	J02MD072.SHM
21	3	191	1158	13.0	J02MD021.SHO	J02MD021.SHM	73	7	191	1320	7.5	J02MD073.SHO	J02MD073.SHM
22	3	191	1159	15.0	J02MD022.SHO	J02MD022.SHM	74	7	191	1322	7.5	J02MD074.SHO	J02MD074.SHM
23	3	191	1201	22.0	J02MD023.SHO	J02MD023.SHM	75	7	191	1323	7.5	J02MD075.SHO	J02MD075.SHM
24	3	191	1206	17.0	J02MD024.SHO	J02MD024.SHM	76	7	191	1325	7.5	J02MD076.SHO	J02MD076.SHM
25	3	191	1207	19.0	J02MD025.SHO	J02MD025.SHM	77	7	191	1326	7.5	J02MD077.SHO	J02MD077.SHM
26	3	191	1210	21.0	J02MD026.SHO	J02MD026.SHM	78	7	191	1327	7.5	J02MD078.SHO	J02MD078.SHM
27	3	191	1212	23.0	J02MD027.SHO	J02MD027.SHM	79	7	191	1328	7.5	J02MD079.SHO	J02MD079.SHM
28	3	191	1213	25.0	J02MD028.SHO	J02MD028.SHM	80	7	191	1329	7.5	J02MD080.SHO	J02MD080.SHM
29	3	191	1216	27.0	J02MD029.SHO	J02MD029.SHM	81	8	194	1016	*Bdarks*	J02MC081.SHO	J02MC081.SHM
30	3	191	1220	29.0	J02MD030.SHO	J02MD030.SHM	81	8	194	1037	3.0	J02MD081.SHO	J02MD081.SHM
31	4	191	1222	27.0	J02MD031.SHO	J02MD031.SHM	82	8	194	1038	5.0	J02MD082.SHO	J02MD082.SHM
32	4	191	1223	25.0	J02MD032.SHO	J02MD032.SHM	83	8	194	1038	7.0	J02MD083.SHO	J02MD083.SHM
33	4	191	1224	23.0	J02MD033.SHO	J02MD033.SHM	84	8	194	1039	7.5	J02MD084.SHO	J02MD084.SHM
34	4	191	1225	21.0	J02MD034.SHO	J02MD034.SHM	85	8	194	1042	9.0	J02MD085.SHO	J02MD085.SHM
35	4	191	1227	19.0	J02MD035.SHO	J02MD035.SHM	86	8	194	1043	11.0	J02MD086.SHO	J02MD086.SHM
36	4	191	1228	17.0	J02MD036.SHO	J02MD036.SHM	87	8	194	1044	13.0	J02MD087.SHO	J02MD087.SHM
37	4	191	1229	15.0	J02MD037.SHO	J02MD037.SHM	88	8	194	1045	15.0	J02MD088.SHO	J02MD088.SHM
38	4	191	1229	13.0	J02MD038.SHO	J02MD038.SHM	89	8	194	1046	17.0	J02MD089.SHO	J02MD089.SHM
39	4	191	1230	11.0	J02MD039.SHO	J02MD039.SHM	90	8	194	1047	19.0	J02MD090.SHO	J02MD090.SHM
40	4	191	1231	9.0	J02MD040.SHO	J02MD040.SHM	91	8	194	1048	21.0	J02MD091.SHO	J02MD091.SHM
41	4	191	1232	7.5	J02MD041.SHO	J02MD041.SHM	92	8	194	1050	21.0	J02MD092.SHO	J02MD092.SHM
42	4	191	1233	7.0	J02MD042.SHO	J02MD042.SHM	93	9	194	1104	3.0	J02MD093.SHO	J02MD093.SHM
43	4	191	1234	5.0	J02MD043.SHO	J02MD043.SHM	94	9	194	1105	5.0	J02MD094.SHO	J02MD094.SHM
44	4	191	1235	3.0	J02MD044.SHO	J02MD044.SHM	95	9	194	1105	7.0	J02MD095.SHO	J02MD095.SHM
45	5	191	1245	3.0	J02MD045.SHO	J02MD045.SHM	96	9	194	1106	7.5	J02MD096.SHO	J02MD096.SHM
46	5	191	1246	5.0	J02MD046.SHO	J02MD046.SHM	97	9	194	1107	9.0	J02MD097.SHO	J02MD097.SHM
47	5	191	1247	7.0	J02MD047.SHO	J02MD047.SHM	98	9	194	1108	11.0	J02MD098.SHO	J02MD098.SHM
48	5	191	1248	7.5	J02MD048.SHO	J02MD048.SHM	99	9	194	1109	13.0	J02MD099.SHO	J02MD099.SHM
49	5	191	1249	9.0	J02MD049.SHO	J02MD049.SHM	100	9	194	1110	15.0	J02MD100.SHO	J02MD100.SHM
50	5	191	1250	11.0	J02MD050.SHO	J02MD050.SHM	101	9	194	1111	17.0	J02MD101.SHO	J02MD101.SHM

Table B1. (cont.) A summary of the miniNESS deployment log for SeaBOARR-98. The data are organized according to sequential casts and experiments (*Exp.*). The deployment distance from the tower is given by x, and this column is also used to indicate when the darks were recorded for the profiler and the reference together (*Bdarks*) or individually (*Pdarks* and *Rdarks*, respectively). The filenames for the profiler and reference data are in the columns with the same name. All times are in GMT.

Cast	*Exp.*	*SDY*	*Time*	x [m]	*Profiler*	*Reference*	*Cast*	*Exp.*	*SDY*	*Time*	x [m]	*Profiler*	*Reference*
102	9	194	1111	19.0	J02MD102.SHO	J02MD102.SHM	154	14	194	1224	13.0	J02MD154.SHO	J02MD154.SHM
103	9	194	1112	21.0	J02MD103.SHO	J02MD103.SHM	155	14	194	1227	15.0	J02MD155.SHO	J02MD155.SHM
104	10	194	1113	21.0	J02MD104.SHO	J02MD104.SHM	156	14	194	1228	17.0	J02MD156.SHO	J02MD156.SHM
105	10	194	1115	19.0	J02MD105.SHO	J02MD105.SHM	157	14	194	1230	19.0	J02MD157.SHO	J02MD157.SHM
106	10	194	1115	17.0	J02MD106.SHO	J02MD106.SHM	158	14	194	1231	21.0	J02MD158.SHO	J02MD158.SHM
107	10	194	1116	15.0	J02MD107.SHO	J02MD107.SHM	159	15	194	1246	3.0	J02MD159.SHO	J02MD159.SHM
108	10	194	1117	13.0	J02MD108.SHO	J02MD108.SHM	160	15	194	1247	5.0	J02MD160.SHO	J02MD160.SHM
109	10	194	1118	11.0	J02MD109.SHO	J02MD109.SHM	161	15	194	1248	7.0	J02MD161.SHO	J02MD161.SHM
110	10	194	1119	9.0	J02MD110.SHO	J02MD110.SHM	162	15	194	1250	7.5	J02MD162.SHO	J02MD162.SHM
111	10	194	1119	7.5	J02MD111.SHO	J02MD111.SHM	163	15	194	1251	9.0	J02MD163.SHO	J02MD163.SHM
112	10	194	1120	7.0	J02MD112.SHO	J02MD112.SHM	164	15	194	1253	11.0	J02MD164.SHO	J02MD164.SHM
113	10	194	1121	5.0	J02MD113.SHO	J02MD113.SHM	165	15	194	1254	13.0	J02MD165.SHO	J02MD165.SHM
114	10	194	1122	3.0	J02MD114.SHO	J02MD114.SHM	166	15	194	1255	15.0	J02MD166.SHO	J02MD166.SHM
115	11	194	1123	3.0	J02MD115.SHO	J02MD115.SHM	167	15	194	1256	17.0	J02MD167.SHO	J02MD167.SHM
116	11	194	1124	5.0	J02MD116.SHO	J02MD116.SHM	168	15	194	1259	19.0	J02MD168.SHO	J02MD168.SHM
117	11	194	1125	7.0	J02MD117.SHO	J02MD117.SHM	169	15	194	1300	21.0	J02MD169.SHO	J02MD169.SHM
118	11	194	1126	7.5	J02MD118.SHO	J02MD118.SHM	170	16	194	1301	21.0	J02MD170.SHO	J02MD170.SHM
119	11	194	1127	9.0	J02MD119.SHO	J02MD119.SHM	171	16	194	1302	19.0	J02MD171.SHO	J02MD171.SHM
120	11	194	1128	11.0	J02MD120.SHO	J02MD120.SHM	172	16	194	1304	17.0	J02MD172.SHO	J02MD172.SHM
121	11	194	1129	13.0	J02MD121.SHO	J02MD121.SHM	173	16	194	1306	15.0	J02MD173.SHO	J02MD173.SHM
122	11	194	1130	15.0	J02MD122.SHO	J02MD122.SHM	174	16	194	1307	13.0	J02MD174.SHO	J02MD174.SHM
123	11	194	1130	17.0	J02MD123.SHO	J02MD123.SHM	175	16	194	1310	11.0	J02MD175.SHO	J02MD175.SHM
124	11	194	1131	19.0	J02MD124.SHO	J02MD124.SHM	176	16	194	1313	9.0	J02MD176.SHO	J02MD176.SHM
125	11	194	1132	21.0	J02MD125.SHO	J02MD125.SHM	177	16	194	1314	7.5	J02MD177.SHO	J02MD177.SHM
126	12	194	1133	21.0	J02MD126.SHO	J02MD126.SHM	178	16	194	1316	7.0	J02MD178.SHO	J02MD178.SHM
127	12	194	1134	19.0	J02MD127.SHO	J02MD127.SHM	179	16	194	1318	5.0	J02MD179.SHO	J02MD179.SHM
128	12	194	1134	17.0	J02MD128.SHO	J02MD128.SHM	180	16	194	1319	3.0	J02MD180.SHO	J02MD180.SHM
129	12	194	1135	15.0	J02MD129.SHO	J02MD129.SHM	181	17	194	1417	3.0	J02MD181.SHO	J02MD181.SHM
130	12	194	1136	13.0	J02MD130.SHO	J02MD130.SHM	182	17	194	1418	5.0	J02MD182.SHO	J02MD182.SHM
131	12	194	1137	11.0	J02MD131.SHO	J02MD131.SHM	183	17	194	1419	7.0	J02MD183.SHO	J02MD183.SHM
132	12	194	1138	9.0	J02MD132.SHO	J02MD132.SHM	184	17	194	1421	7.5	J02MD184.SHO	J02MD184.SHM
133	12	194	1139	7.5	J02MD133.SHO	J02MD133.SHM	185	17	194	1422	9.0	J02MD185.SHO	J02MD185.SHM
134	12	194	1140	7.0	J02MD134.SHO	J02MD134.SHM	186	17	194	1423	11.0	J02MD186.SHO	J02MD186.SHM
135	12	194	1141	5.0	J02MD135.SHO	J02MD135.SHM	187	17	194	1425	13.0	J02MD187.SHO	J02MD187.SHM
136	12	194	1142	3.0	J02MD136.SHO	J02MD136.SHM	188	17	194	1426	15.0	J02MD188.SHO	J02MD188.SHM
137	13	194	1144	7.5	J02MD137.SHO	J02MD137.SHM	189	17	194	1427	17.0	J02MD189.SHO	J02MD189.SHM
138	13	194	1145	7.5	J02MD138.SHO	J02MD138.SHM	190	17	194	1428	19.0	J02MD190.SHO	J02MD190.SHM
139	13	194	1146	7.5	J02MD139.SHO	J02MD139.SHM	191	17	194	1434	21.0	J02MD191.SHO	J02MD191.SHM
140	13	194	1147	7.5	J02MD140.SHO	J02MD140.SHM	192	18	195	0719	*Bdarks*	J02MC192.SHO	J02MC192.SHM
141	13	194	1148	7.5	J02MD141.SHO	J02MD141.SHM	192	18	195	0807	3.0	J02MD192.SHO	J02MD192.SHM
142	13	194	1149	7.5	J02MD142.SHO	J02MD142.SHM	193	18	195	0808	5.0	J02MD193.SHO	J02MD193.SHM
143	13	194	1150	7.5	J02MD143.SHO	J02MD143.SHM	194	18	195	0809	7.0	J02MD194.SHO	J02MD194.SHM
144	13	194	1151	7.5	J02MD144.SHO	J02MD144.SHM	195	18	195	0810	7.5	J02MD195.SHO	J02MD195.SHM
145	13	194	1151	7.5	J02MD145.SHO	J02MD145.SHM	196	18	195	0811	9.0	J02MD196.SHO	J02MD196.SHM
146	13	194	1152	7.5	J02MD146.SHO	J02MD146.SHM	197	18	195	0812	11.0	J02MD197.SHO	J02MD197.SHM
147	13	194	1153	7.5	J02MD147.SHO	J02MD147.SHM	198	18	195	0813	13.0	J02MD198.SHO	J02MD198.SHM
148	14	194	1216	3.0	J02MD148.SHO	J02MD148.SHM	199	18	195	0814	15.0	J02MD199.SHO	J02MD199.SHM
149	14	194	1217	5.0	J02MD149.SHO	J02MD149.SHM	200	18	195	0815	17.0	J02MD200.SHO	J02MD200.SHM
150	14	194	1219	7.0	J02MD150.SHO	J02MD150.SHM	201	18	195	0816	19.0	J02MD201.SHO	J02MD201.SHM
151	14	194	1221	7.5	J02MD151.SHO	J02MD151.SHM	202	18	195	0817	21.0	J02MD202.SHO	J02MD202.SHM
152	14	194	1222	9.0	J02MD152.SHO	J02MD152.SHM	203	18	195	0819	23.0	J02MD203.SHO	J02MD203.SHM
153	14	194	1223	11.0	J02MD153.SHO	J02MD153.SHM	204	18	195	0820	25.0	J02MD204.SHO	J02MD204.SHM

Table B1. (cont.) A summary of the miniNESS deployment log for SeaBOARR-98. The data are organized according to sequential casts and experiments (*Exp.*). The deployment distance from the tower is given by x, and this column is also used to indicate when the darks were recorded for the profiler and the reference together (*Bdarks*) or individually (*Pdarks* and *Rdarks*, respectively). The filenames for the profiler and reference data are in the columns with the same name. All times are in GMT.

Cast	*Exp.*	*SDY*	*Time*	x [m]	*Profiler*	*Reference*	*Cast*	*Exp.*	*SDY*	*Time*	x [m]	*Profiler*	*Reference*
205	18	195	0821	27.0	J02MD205.SHO	J02MD205.SHM	219	19	195	0839	7.0	J02MD219.SHO	J02MD219.SHM
206	18	195	0822	29.0	J02MD206.SHO	J02MD206.SHM	220	19	195	0841	5.0	J02MD220.SHO	J02MD220.SHM
207	19	195	0824	29.0	J02MD207.SHO	J02MD207.SHM	221	19	195	0846	3.0	J02MD221.SHO	J02MD221.SHM
208	19	195	0825	27.0	J02MD208.SHO	J02MD208.SHM	222	20	195	0946	3.0	J02MD222.SHO	J02MD222.SHM
209	19	195	0826	25.0	J02MD209.SHO	J02MD209.SHM	223	20	195	0947	5.0	J02MD223.SHO	J02MD223.SHM
210	19	195	0827	23.0	J02MD210.SHO	J02MD210.SHM	224	20	195	0948	7.0	J02MD224.SHO	J02MD224.SHM
211	19	195	0828	21.0	J02MD211.SHO	J02MD211.SHM	225	20	195	0949	7.5	J02MD225.SHO	J02MD225.SHM
212	19	195	0829	19.0	J02MD212.SHO	J02MD212.SHM	226	20	195	0950	9.0	J02MD226.SHO	J02MD226.SHM
213	19	195	0830	17.0	J02MD213.SHO	J02MD213.SHM	227	20	195	0952	11.0	J02MD227.SHO	J02MD227.SHM
214	19	195	0831	15.0	J02MD214.SHO	J02MD214.SHM	228	20	195	0953	13.0	J02MD228.SHO	J02MD228.SHM
215	19	195	0832	13.0	J02MD215.SHO	J02MD215.SHM	229	20	195	0954	15.0	J02MD229.SHO	J02MD229.SHM
216	19	195	0833	11.0	J02MD216.SHO	J02MD216.SHM	230	20	195	0955	17.0	J02MD230.SHO	J02MD230.SHM
217	19	195	0835	9.0	J02MD217.SHO	J02MD217.SHM	231	20	195	0956	19.0	J02MD231.SHO	J02MD231.SHM
218	19	195	0837	7.5	J02MD218.SHO	J02MD218.SHM	232	20	195	0958	21.0	J02MD232.SHO	J02MD232.SHM

Table C1. A summary of the SeaSAS deployment log for SeaBOARR-98. The data are organized according to sequential casts. The file name for each data type collected is constructed from the root name and the four extensions. Dark files and sea and sky data have SC and SS codes in the root names, respectively. All times are in GMT.

Cast	*State*	*SDY*	*Time*	*Root*	*Dir.*	*Sea*	*Sky*	*Ref.*	*Cast*	*State*	*SDY*	*Time*	*Root*	*Dir.*	*Sea*	*Sky*	*Ref.*
1	Beg.	190	0830	J02SC001	.SHD	.SHW	.SHS	.SHM	16	Beg.	191	1121	J02SS016	.SHD	.SHW	.SHS	.SHM
	End	190	0834							End	191	1124					
1	Beg.	190	0908	J02SS001	.SHD	.SHW	.SHS	.SHM	17	Beg.	191	1129	J02SS017	.SHD	.SHW	.SHS	.SHM
	End	190	0912							End	191	1132					
2	Beg.	190	0902	J02SS002	.SHD	.SHW	.SHS	.SHM	18	Beg.	191	1133	J02SS018	.SHD	.SHW	.SHS	.SHM
	End	190	0905							End	191	1136					
3	Beg.	190	0912	J02SS003	.SHD	.SHW	.SHS	.SHM	19	Beg.	191	1137	J02SS019	.SHD	.SHW	.SHS	.SHM
	End	190	0931							End	191	1140					
	Beg.	190	0933						20		191		*Aborted*				
	End	190	0938						21		191		*Aborted*				
4	Beg.	190	0939	J02SS004	.SHD	.SHW	.SHS	.SHM	22	Beg.	191	1143	J02SS022	.SHD	.SHW	.SHS	.SHM
	End	190	0942							End	191	1147					
5	Beg.	190	1257	J02SS005	.SHD	.SHW	.SHS	.SHM	23	Beg.	191	1148	J02SS023	.SHD	.SHW	.SHS	.SHM
	End	190	1316							End	191	1151					
6	Beg.	190	1317	J02SS006	.SHD	.SHW	.SHS	.SHM	24	Beg.	191	1154	J02SS024	.SHD	.SHW	.SHS	.SHM
	End	190	1320							End	191	1157					
7	Beg.	190	1322	J02SS007	.SHD	.SHW	.SHS	.SHM	25	Beg.	191	1158	J02SS025	.SHD	.SHW	.SHS	.SHM
	End	190	1325							End	191	1201					
8	Beg.	190	1339	J02SC008	.SHD	.SHW	.SHS	.SHM	32	Beg.	191	1234	J02SS032	.SHD	.SHW	.SHS	.SHM
	End	190	1342							End	191	1237					
9	Beg.	191	0750	J02SC009	.SHD	.SHW	.SHS	.SHM	33	Beg.	191	1238	J02SS033	.SHD	.SHW	.SHS	.SHM
	End	191	0753							End	191	1241					
10	Beg.	191	0855	J02SS010	.SHD	.SHW	.SHS	.SHM	34	Beg.	191	1252	J02SS034	.SHD	.SHW	.SHS	.SHM
	End	191	0905							End	191	1253					
11	Beg.	191	0906	J02SS011	.SHD	.SHW	.SHS	.SHM	35	Beg.	191	1254	J02SS035	.SHD	.SHW	.SHS	.SHM
	End	191	0909							End	191	1257					
12	Beg.	191	0909	J02SS012	.SHD	.SHW	.SHS	.SHM	36	Beg.	191	1258	J02SS036	.SHD	.SHW	.SHS	.SHM
	End	191	0914							End	191	1301					
13	Beg.	191	0915	J02SS013	.SHD	.SHW	.SHS	.SHM	37	Beg.	191	1302	J02SS037	.SHD	.SHW	.SHS	.SHM
	End	191	0918							End	191	1305					
14	Beg.	191	0919	J02SS014	.SHD	.SHW	.SHS	.SHM	38	Beg.	194	1016	J02SC038	.SHD	.SHW	.SHS	.SHM
	End	191	0922							End	194	1019					
15	Beg.	191	0922	J02SS015	.SHD	.SHW	.SHS	.SHM	39	Beg.	194	1027	J02SS039	.SHD	.SHW	.SHS	.SHM
	End	191	0925							End	194	1030					

Table C1. (cont.) A summary of the SeaSAS deployment log for SeaBOARR-98. The data are organized according to sequential casts. The file name for each data type collected is constructed from the root name and the four extensions. Dark files and sea and sky data have SC and SS codes in the root names, respectively. All times are in GMT.

Cast	*State*	*SDY*	*Time*	*Root*	*Dir.*	*Sea*	*Sky*	*Ref.*	*Cast*	*State*	*SDY*	*Time*	*Root*	*Dir.*	*Sea*	*Sky*	*Ref.*
40	Beg.	194	1032	J02SS040	.SHD	.SHW	.SHS	.SHM	67	Beg.	195	0805	J02SC067	.SHD	.SHW	.SHS	.SHM
	End	194	1035							End	195	0808					
41	Beg.	194	1036	J02SS041	.SHD	.SHW	.SHS	.SHM	68	Beg.	195	0813	J02SS068	.SHD	.SHW	.SHS	.SHM
	End	194	1039							End	195	0816					
42	Beg.	194	1041	J02SS042	.SHD	.SHW	.SHS	.SHM	69	Beg.	195	0817	J02SS069	.SHD	.SHW	.SHS	.SHM
	End	194	1044							End	195	0820					
43	Beg.	194	1047	J02SS043	.SHD	.SHW	.SHS	.SHM	70	Beg.	195	0821	J02SS070	.SHD	.SHW	.SHS	.SHM
	End	194	1050							End	195	0824					
44	Beg.	194	1052	J02SS044	.SHD	.SHW	.SHS	.SHM	71	Beg.	195	0826	J02SS071	.SHD	.SHW	.SHS	.SHM
	End	194	1055							End	195	0829					
45	Beg.	194	1104	J02SS045	.SHD	.SHW	.SHS	.SHM	72	Beg.	195	0830	J02SS072	.SHD	.SHW	.SHS	.SHM
	End	194	1107							End	195	0833					
46	Beg.	194	1108	J02SS046	.SHD	.SHW	.SHS	.SHM	73	Beg.	195	0834	J02SS073	.SHD	.SHW	.SHS	.SHM
	End	194	1111							End	195	0837					
47	Beg.	194	1112	J02SS047	.SHD	.SHW	.SHS	.SHM	74	Beg.	195	0840	J02SS074	.SHD	.SHW	.SHS	.SHM
	End	194	1115							End	195	0843					
48	Beg.	194	1116	J02SS048	.SHD	.SHW	.SHS	.SHM	75	Beg.	195	0846	J02SS075	.SHD	.SHW	.SHS	.SHM
	End	194	1119							End	195	0849					
49	Beg.	194	1122	J02SS049	.SHD	.SHW	.SHS	.SHM	76	Beg.	195	0849	J02SS076	.SHD	.SHW	.SHS	.SHM
	End	194	1126							End	195	0852					
50	Beg.	194	1126	J02SS050	.SHD	.SHW	.SHS	.SHM	77	Beg.	195	0853	J02SS077	.SHD	.SHW	.SHS	.SHM
	End	194	1129							End	195	0856					
51	Beg.	194	1131	J02SS051	.SHD	.SHW	.SHS	.SHM	78	Beg.	195	0857	J02SS078	.SHD	.SHW	.SHS	.SHM
	End	194	1134							End	195	0900					
52	Beg.	194	1135	J02SS052	.SHD	.SHW	.SHS	.SHM	79	Beg.	195	0900	J02SS079	.SHD	.SHW	.SHS	.SHM
	End	194	1138							End	195	0903					
53	Beg.	194	1151	J02SS053	.SHD	.SHW	.SHS	.SHM	80	Beg.	195	0904	J02SS080	.SHD	.SHW	.SHS	.SHM
	End	194	1154							End	195	0907					
54	Beg.	194	1155	J02SS054	.SHD	.SHW	.SHS	.SHM	81	Beg.	195	0908	J02SS081	.SHD	.SHW	.SHS	.SHM
	End	194	1158							End	195	0911					
55	Beg.	194	1200	J02SS055	.SHD	.SHW	.SHS	.SHM	82	Beg.	195	0912	J02SS082	.SHD	.SHW	.SHS	.SHM
	End	194	1203							End	195	0915					
56	Beg.	194	1208	J02SS056	.SHD	.SHW	.SHS	.SHM	83	Beg.	195	0918	J02SS083	.SHD	.SHW	.SHS	.SHM
	End	194	1211							End	195	0919					
57	Beg.	194	1212	J02SS057	.SHD	.SHW	.SHS	.SHM	84	Beg.	195	0919	J02SS084	.SHD	.SHW	.SHS	.SHM
	End	194	1215							End	195	0922					
58	Beg.	194	1217	J02SS058	.SHD	.SHW	.SHS	.SHM	85	Beg.	195	0923	J02SS085	.SHD	.SHW	.SHS	.SHM
	End	194	1220							End	195	0926					
59	Beg.	194	1221	J02SS059	.SHD	.SHW	.SHS	.SHM	86	Beg.	195	0927	J02SS086	.SHD	.SHW	.SHS	.SHM
	End	194	1224							End	195	0930					
60	Beg.	194	1225	J02SS060	.SHD	.SHW	.SHS	.SHM	87	Beg.	195	0931	J02SS087	.SHD	.SHW	.SHS	.SHM
	End	194	1228							End	195	0934					
61	Beg.	194	1229	J02SS061	.SHD	.SHW	.SHS	.SHM	88	Beg.	195	0934	J02SS088	.SHD	.SHW	.SHS	.SHM
	End	194	1232							End	195	0937					
62	Beg.	194	1233	J02SS062	.SHD	.SHW	.SHS	.SHM	89	Beg.	195	0939	J02SS089	.SHD	.SHW	.SHS	.SHM
	End	194	1234							End	195	0942					
63	Beg.	194	1241	J02SS063	.SHD	.SHW	.SHS	.SHM	90	Beg.	195	0942	J02SS090	.SHD	.SHW	.SHS	.SHM
	End	194	1244							End	195	0945					
64	Beg.	194	1246	J02SS064	.SHD	.SHW	.SHS	.SHM	91	Beg.	195	0946	J02SS091	.SHD	.SHW	.SHS	.SHM
	End	194	1249							End	195	0949					
65	Beg.	194	1250	J02SS065	.SHD	.SHW	.SHS	.SHM	92	Beg.	195	0950	J02SS092	.SHD	.SHW	.SHS	.SHM
	End	194	1253							End	195	0953					
66	Beg.	194	1254	J02SS066	.SHD	.SHW	.SHS	.SHM	93	Beg.	195	0954	J02SS093	.SHD	.SHW	.SHS	.SHM
	End	194	1257							End	195	0957					

Table D1. A summary of the WiSPER Deployment Log for SeaBOARR-98. The entries show the file names for each acquisition system associated with each CoASTS station; blank entries indicate no data collected. The WiSPER files are the processed data in the SeaWiFS Bio-Optical Archive and Storage System (SeaBASS) format (Hooker et al. 1994). The last column gives the sampling overlap between the WiSPER measurements and the DalSAS sequence numbers (Table F1).

Station		*Sample*		*File*	C_a	C_{TSM}	WS	*DalSAS*
Date	*SDY*	*Start*	*End*	*Name*	$[\mathrm{mg\,m^{-3}}]$	$[\mathrm{mg\,m^{-3}}]$	$[\mathrm{m\,s^{-1}}]$	*Sequence*
9 July	190	1302	1327	46S3.RAD	1.212	4.20	5.3	2
10 July	191	0854	0856	46S4.RAD	1.269	3.16	4.3	3
10 July	191	1126	1148	46S5.RAD	1.189	2.84	2.9	5, 6, 7
10 July	191	1201	1223	46S5A.RAD				9, 10, 11
10 July	191	1249	1311	46S5B.RAD				12
10 July	191	1323	1349	46S5C.RAD				
13 July	194	1028	1030	47S1.RAD	0.223	0.84	7.3	13
13 July	194	1106	1128	47S1A.RAD				16, 17, 18
13 July	194	1135	1158	47S1B.RAD				19, 20
13 July	194	1217	1239	47S1C.RAD				22, 23
13 July	194	1251	1313	47S1D.RAD				25
13 July	194	1430	1458	47S1E.RAD				
14 July	195	0812	0834	47S2.RAD	0.589	1.93	2.4	26, 27, 28
14 July	195	0945	1007	47S3.RAD	0.555	1.87	3.0	28, 36, 37

Table E1. A summary of the deployment logs for the AC-9, CE-318, and MFR-6 instruments during SeaBOARR-98. Also shown are the HPLC pigment, yellow substance absorption (a_{ys}), and particulate absorption (a_p) logs. The entries show the file names for each acquisition system associated with each CoASTS station; blank entries indicate no data collected. The WiSPER entries are the ASCII files associated with each station (calibrated, but unprocessed data). The processed WiSPER files are given in Table D1.

Station	*Instrument*				*Water Sample*		
Code	WiSPER	AC-9	CE-318	MFR-6	HPLC	a_{ys}	a_p
46S1	46S1.SAT	46S1.ACM	46S1.NSU	46S1.MFR	46S1.PIG	46S1.DOM	46S1.PAR
46S2	46S2.SAT	46S2.ACM	46S2.NSU	46S2.MFR	46S2.PIG	46S2.DOM	46S2.PAR
46S2a	46S2A.SAT	46S2C.ACM	46S2.NSU	46S2.MFR			
46S3	46S3.SAT	46S3.ACM		46S3.MFR	46S3.PIG	46S3.DOM	46S3.PAR
46S4	46S4.SAT	46S4.ACM		46S3.MFR	46S4.PIG	46S4.DOM	46S4.PAR
46S5	46S5.SAT	46S5.ACM	46S5.NSU	46S5.MFR	46S5.PIG	46S5.DOM	46S5.PAR
46S5A	46S5A.SAT	46S5B.ACM	46S5.NSU	46S5.MFR			
46S5B	46S5B.SAT	46S5D.ACM	46S5.NSU	46S5.MFR			
46S5C	46S5C.SAT	46S5F.ACM	46S5.NSU	46S5.MFR			
47S1	47S1.SAT	47S1.ACM	47S1.NSU	47S1.MFR	47S1.PIG	47S1.DOM	47S1.PAR
47S1A	47S1A.SAT	47S1A.ACM	47S1.NSU	47S1.MFR			
47S1B	47S1B.SAT	47S1C.ACM	47S1.NSU	47S1.MFR			
47S1C	47S1C.SAT	47S1E.ACM	47S1.NSU	47S1.MFR			
47S1D	47S1D.SAT	47S1G.ACM	47S1.NSU	47S1.MFR			
47S1E	47S1E.SAT	47S1I.ACM	47S1.NSU	47S1.MFR			
47S2	47S2.SAT	47S2.ACM			47S2.PIG	47S2.DOM	47S2.PAR
47S3	47S3.SAT	47S3.ACM			47S3.PIG	47S3.DOM	47S3.PAR

Table F1. A summary of the DalSAS Deployment Log for SeaBOARR-98. The entries show the file names for each acquisition system associated with each CoASTS station; blank entries indicate no data collected. The first column (S) is a sequential counter for each cast (C) set. Missing cast numbers indicated aborted collection events. All times are in GMT.

S	C	*State*	*SDY*	*Time*	*File Name*	*Mode*	S	C	*State*	*SDY*	*Time*	*File Name*	*Mode*
1	3	Beg.	190	0912	J02US003.SHG	Sea,Sky	10	30	Beg.	191	1226	J02US030.SHG	Sea,Sky
		End		0931	J02US003.SHI	$E_d(0^+)$,$E_d(0^+)$			End		1229	J02US030.SHI	$E_d(0^+)$,$E_d(0^+)$
	3	Beg.	190	0933	J02UP003.SHG	Plaque,Sky		31	Beg.	191	1230	J02UP031.SHG	Plaque,Sky
		End		0938	J02UP003.SHI	$E_d(0^+)$,$E_d(0^+)$			End		1233	J02UP031.SHI	$E_d(0^+)$,$E_i(0^+)$
	4	Beg.	190	0939	J02UP004.SHG	Plaque,Sky	11	32	Beg.	191	1234	J02US032.SHG	Sea,Sky
		End		0942	J02UP004.SHI	$E_d(0^+)$,$E_i(0^+)$			End		1237	J02US032.SHI	$E_d(0^+)$,$E_d(0^+)$
2	5	Beg.	190	1257	J02US005.SHG	Sea,Sky		33	Beg.	191	1238	J02UP033.SHG	Plaque,Sky
		End		1316	J02US005.SHI	$E_d(0^+)$,$E_d(0^+)$			End		1241	J02UP033.SHI	Plaque,Sky
	6	Beg.	190	1317	J02UP006.SHG	Plaque,Sky	12	35	Beg.	191	1254	J02US035.SHG	Sea,Sky
		End		1320	J02UP006.SHI	$E_d(0^+)$,$E_d(0^+)$			End		1257	J02US035.SHI	$E_d(0^+)$,$E_d(0^+)$
	7	Beg.	190	1322	J02UP007.SHG	Plaque,Sky		36	Beg.	191	1258	J02UP036.SHG	Plaque,Sky
		End		1325	J02UP007.SHI	$E_d(0^+)$,$E_i(0^+)$			End		1301	J02UP036.SHI	$E_d(0^+)$,$E_i(0^+)$
	8	Beg.	190	1339	J02UC008.SHG	Darks		37	Beg.	191	1302	J02US037.SHG	Sea,Sky
		End		1342	J02UC008.SHI	Darks			End		1305	J02US037.SHI	$E_d(0^+)$,$E_d(0^+)$
	9	Beg.	191	0750	J02UC009.SHG	Darks		38	Beg.	194	1016	J02UC038.SHG	Darks
		End		0753	J02UC009.SHI	Darks			End		1020	J02UC038.SHI	Darks
3	10	Beg.	191	0855	J02US010.SHG	Sea,Sky	13	39	Beg.	194	1027	J02US039.SHG	Sea,Sky
		End		0905	J02US010.SHI	$E_d(0^+)$,$E_d(0^+)$			End		1030	J02US039.SHI	$E_d(0^+)$,$E_d(0^+)$
	11	Beg.	191	0906	J02UP011.SHG	Plaque,Sky		40	Beg.	194	1032	J02UP040.SHG	Plaque,Sky
		End		0909	J02UP011.SHI	$E_d(0^+)$,$E_d(0^+)$			End		1035	J02UP040.SHI	$E_d(0^+)$,$E_i(0^+)$
	12	Beg.	191	0909	J02UP012.SHG	Plaque,Sky	14	41	Beg.	194	1036	J02US041.SHG	Sea,Sky
		End		0914	J02UP012.SHI	$E_d(0^+)$,$E_i(0^+)$			End		1039	J02US041.SHI	$E_d(0^+)$,$E_d(0^+)$
4	13	Beg.	191	0915	J02US013.SHG	Sea,Sky		42	Beg.	194	1041	J02UP042.SHG	Plaque,Sky
		End		0918	J02US013.SHI	$E_d(0^+)$,$E_d(0^+)$			End		1044	J02UP041.SHI	$E_d(0^+)$,$E_i(0^+)$
	14	Beg.	191	0919	J02UP014.SHG	Plaque,Sky	15	43	Beg.	194	1047	J02US043.SHG	Sea,Sky
		End		0922	J02UP014.SHI	$E_d(0^+)$,$E_d(0^+)$			End		1050	J02US043.SHI	$E_d(0^+)$,$E_d(0^+)$
	15	Beg.	191	0922	J02UP015.SHG	Plaque,Sky		44	Beg.	194	1052	J02UP044.SHG	Plaque,Sky
		End		0925	J02UP015.SHI	$E_d(0^+)$,$E_i(0^+)$			End		1055	J02UP044.SHI	$E_d(0^+)$,$E_i(0^+)$
5	16	Beg.	191	1121	J02US016.SHG	Sea,Sky	16	45	Beg.	194	1104	J02US045.SHG	Sea,Sky
		End		1124	J02US016.SHI	$E_d(0^+)$,$E_d(0^+)$			End		1107	J02US045.SHI	$E_d(0^+)$,$E_d(0^+)$
	17	Beg.	191	1129	J02UP017.SHG	Plaque,Sky		46	Beg.	194	1108	J02UP046.SHG	Plaque,Sky
		End		1132	J02UP017.SHI	$E_d(0^+)$,$E_i(0^+)$			End		1111	J02UP046.SHI	$E_d(0^+)$,$E_i(0^+)$
6	18	Beg.	191	1133	J02US018.SHG	Sea,Sky	17	47	Beg.	194	1112	J02US047.SHG	Sea,Sky
		End		1136	J02US018.SHI	$E_d(0^+)$,$E_d(0^+)$			End		1115	J02US047.SHI	$E_d(0^+)$,$E_d(0^+)$
	19	Beg.	191	1137	J02UP019.SHG	Plaque,Sky		48	Beg.	194	1116	J02UP048.SHG	Plaque,Sky
		End		1140	J02UP019.SHI	$E_d(0^+)$,$E_i(0^+)$			End		1119	J02UP048.SHI	$E_d(0^+)$,$E_i(0^+)$
7	22	Beg.	191	1143	J02US022.SHG	Sea,Sky	18	49	Beg.	194	1123	J02US049.SHG	Sea,Sky
		End		1147	J02US022.SHI	$E_d(0^+)$,$E_d(0^+)$			End		1126	J02US049.SHI	$E_d(0^+)$,$E_d(0^+)$
	23	Beg.	191	1148	J02UP023.SHG	Plaque,Sky		50	Beg.	194	1126	J02UP050.SHG	Plaque,Sky
		End		1151	J02UP023.SHI	$E_d(0^+)$,$E_i(0^+)$			End		1129	J02UP050.SHI	$E_d(0^+)$,$E_i(0^+)$
8	24	Beg.	191	1154	J02US024.SHG	Sea,Sky	19	51	Beg.	194	1131	J02US051.SHG	Sea,Sky
		End		1157	J02US024.SHI	$E_d(0^+)$,$E_d(0^+)$			End		1134	J02US051.SHI	$E_d(0^+)$,$E_d(0^+)$
	25	Beg.	191	1158	J02UP025.SHG	Plaque,Sky		52	Beg.	194	1135	J02UP052.SHG	Plaque,Sky
		End		1201	J02UP025.SHI	$E_d(0^+)$,$E_i(0^+)$			End		1138	J02UP052.SHI	$E_d(0^+)$,$E_i(0^+)$
	26	Beg.	191	1208	J02US026.SHG	Sea,Sky	20	53	Beg.	194	1151	J02US053.SHG	Sea,Sky
		End		1211	J02US026.SHI	$E_d(0^+)$,$E_d(0^+)$			End		1154	J02US053.SHI	$E_d(0^+)$,$E_d(0^+)$
	27	Beg.	191	1214	J02UP027.SHG	Plaque,Sky		54	Beg.	194	1155	J02UP054.SHG	Plaque,Sky
		End		1217	J02UP027.SHI	$E_d(0^+)$,$E_i(0^+)$			End		1158	J02UP054.SHI	$E_d(0^+)$,$E_i(0^+)$
9	28	Beg.	191	1218	J02US028.SHG	Sea,Sky		55	Beg.	194	1200	J02US055.SHG	*Aborted*
		End		1221	J02US028.SHI	$E_d(0^+)$,$E_d(0^+)$			End		1203	J02US055.SHI	*Aborted*
	29	Beg.	191	1222	J02UP029.SHG	Plaque,Sky	21	56	Beg.	194	1208	J02US056.SHG	Sea,Sky
		End		1225	J02UP029.SHI	$E_d(0^+)$,$E_i(0^+)$			End		1211	J02US056.SHI	$E_d(0^+)$,$E_d(0^+)$

Table F1. (cont.) A summary of the DalSAS Deployment Log for SeaBOARR-98. The entries show the file names for each acquisition system associated with each CoASTS station; blank entries indicate no data collected. The first column (S) is a sequential counter for each cast (C) set. Missing cast numbers indicated aborted collection events. All times are in GMT.

S	*C*	*State*	*SDY*	*Time*	*File Name*	*Mode*	*S*	*C*	*State*	*SDY*	*Time*	*File Name*	*Mode*
21	57	Beg.	194	1212	J02UP057.SHG	Plaque,Sky	29	75	End	195	0849	J02UP075.SHI	$E_d(0^+)$,$E_d(0^+)$
		End		1215	J02UP057.SHI	$E_d(0^+)$,$E_i(0^+)$	30	76	Beg.	195	0849	J02US076.SHG	Sea,Sky
22	58	Beg.	194	1217	J02US058.SHG	Sea,Sky			End		0852	J02US076.SHI	$E_d(0^+)$,$E_d(0^+)$
		End		1220	J02US058.SHI	$E_d(0^+)$,$E_d(0^+)$		77	Beg.	195	0853	J02UP077.SHG	Plaque,Sky
	59	Beg.	194	1221	J02UP059.SHG	Plaque,Sky			End		0856	J02UP077.SHI	$E_d(0^+)$,$E_d(0^+)$
		End		1224	J02UP059.SHI	$E_d(0^+)$,$E_i(0^+)$	31	78	Beg.	195	0857	J02US078.SHG	Sea,Sky
23	60	Beg.	194	1225	J02US060.SHG	Sea,Sky			End		0900	J02US078.SHI	$E_d(0^+)$,$E_d(0^+)$
		End		1228	J02US060.SHI	$E_d(0^+)$,$E_d(0^+)$		79	Beg.	195	0900	J02UP079.SHG	Plaque,Sky
	61	Beg.	194	1229	J02UP061.SHG	Plaque,Sky			End		0904	J02UP079.SHI	$E_d(0^+)$,$E_d(0^+)$
		End		1232	J02UP061.SHI	$E_d(0^+)$,$E_i(0^+)$	32	80	Beg.	195	0904	J02US080.SHG	Sea,Sky
	62	Beg.	194	1233	J02US062.SHG	*Aborted*			End		0907	J02US080.SHI	$E_d(0^+)$,$E_d(0^+)$
		End		1234	J02US062.SHI	*Aborted*		81	Beg.	195	0908	J02UP081.SHG	Plaque,Sky
24	63	Beg.	194	1241	J02US063.SHG	Sea,Sky			End		0911	J02UP081.SHI	$E_d(0^+)$,$E_d(0^+)$
		End		1244	J02US063.SHI	$E_d(0^+)$,$E_d(0^+)$		82	Beg.	195	0912	J02US082.SHG	Sea,Sky
	64	Beg.	194	1246	J02UP064.SHG	Plaque,Sky			End		0915	J02US082.SHI	Sea,Sky
		End		1249	J02UP064.SHI	$E_d(0^+)$,$E_i(0^+)$			Beg.	195	0918		*Aborted*
25	65	Beg.	194	1250	J02US065.SHG	Sea,Sky			End		0918		*Aborted*
		End		1253	J02US065.SHI	$E_d(0^+)$,$E_d(0^+)$	33	84	Beg.	195	0919	J02UP084.SHG	Plaque,Sky
	66	Beg.	194	1254	J02UP066.SHG	Plaque,Sky			End		0922	J02UP084.SHI	$E_d(0^+)$,$E_d(0^+)$
		End		1257	J02UP066.SHI	$E_d(0^+)$,$E_i(0^+)$		85	Beg.	195	0923	J02US085.SHG	Sea,Sky
	67	Beg.	195	0805	J02UC067.SHG	Darks			End		0926	J02US085.SHI	$E_d(0^+)$,$E_d(0^+)$
		End		0808	J02UC067.SHI	Darks	34	86	Beg.	195	0927	J02UP086.SHG	Plaque,Sky
26	68	Beg.	195	0813	J02US068.SHG	Sea,Sky			End		0930	J02UP086.SHI	$E_d(0^+)$,$E_d(0^+)$
		End		0816	J02US068.SHI	$E_d(0^+)$,$E_d(0^+)$		87	Beg.	195	0931	J02US087.SHG	Sea,Sky
	69	Beg.	195	0817	J02UP069.SHG	Plaque,Sky			End		0934	J02US087.SHI	$E_d(0^+)$,$E_d(0^+)$
		End		0820	J02UP069.SHI	$E_d(0^+)$,$E_d(0^+)$	35	88	Beg.	195	0934	J02UP088.SHG	Plaque,Sky
27	70	Beg.	195	0821	J02US070.SHG	Sea,Sky			End		0937	J02UP088.SHI	$E_d(0^+)$,$E_d(0^+)$
		End		0824	J02US070.SHI	$E_d(0^+)$,$E_d(0^+)$		89	Beg.	195	0939	J02US089.SHG	Sea,Sky
	71	Beg.	195	0826	J02UP071.SHG	Plaque,Sky			End		0942	J02US089.SHI	$E_d(0^+)$,$E_d(0^+)$
		End		0829	J02UP071.SHI	$E_d(0^+)$,$E_d(0^+)$	36	90	Beg.	195	0942	J02UP090.SHG	Plaque,Sky
28	72	Beg.	195	0830	J02US072.SHG	Sea,Sky			End		0945	J02UP090.SHI	$E_d(0^+)$,$E_d(0^+)$
		End		0833	J02US072.SHI	$E_d(0^+)$,$E_d(0^+)$		91	Beg.	195	0946	J02US091.SHG	Sea,Sky
	73	Beg.	195	0834	J02UP073.SHG	Plaque,Sky			End		0949	J02US091.SHI	$E_d(0^+)$,$E_d(0^+)$
		End		0837	J02UP073.SHI	$E_d(0^+)$,$E_d(0^+)$	37	92	Beg.	195	0950	J02UP092.SHG	Plaque,Sky
29	74	Beg.	195	0840	J02US074.SHG	Sea,Sky			End		0953	J02UP092.SHI	$E_d(0^+)$,$E_d(0^+)$
		End		0843	J02US074.SHI	$E_d(0^+)$,$E_d(0^+)$		93	Beg.	195	0954	J02US093.SHG	Sea,Sky
	75	Beg.	195	0846	J02UP075.SHG	Plaque,Sky			End		0957	J02US093.SHI	$E_d(0^+)$,$E_d(0^+)$

Table G1. A summary of the DalBOSS Deployment Log for SeaBOARR-98. The entries show the file names for each acquisition event. Early in the field campaign, the DalBOSS data were collected in hourly (track) files rather than as 3 minute *casts* synchronized with the DalSAS and SeaSAS instruments. All times are in GMT.

Cast	*SDY*	*Time*	*State*	*File Name*	*Cast*	*SDY*	*Time*	*State*	*File Name*	*Cast*	*SDY*	*Time*	*State*	*File Name*
Track	190	0848	Beg.	J9819008.SHA	Track	190	1300	Beg.	J9819013.SHA	Track	191	1100	Beg.	J9819111.SHA
	190	0859	End			190	1359	End			191	1143	End	
Track	190	0900	Beg.	J9819009.SHA	Track	190	1400	Beg.	J9819014.SHA		191	1144	Beg.	
	190	0959	End			190	1413	End			191	1144	End	
Track	190	1000	Beg.	J9819010.SHA	Track	191	0740	Beg.	J9819107.SHA		191	1146	Beg.	
	190	1059	End			191	0759	End			191	1149	End	
Track	190	1100	Beg.	J9819011.SHA	Track	191	0800	Beg.	J9819108.SHA		191	1150	Beg.	
	190	1159	End			191	0805	End			191	1153	End	
Track	190	1200	Beg.	J9819012.SHA	Track	191	1000	Beg.	J9819110.SHA		191	1156	Beg.	
	190	1259	End			191	1059	End			191	1159	End	

Table G1. (cont.) A summary of the DalBOSS Deployment Log for SeaBOARR-98. The entries show the file names for each acquisition event. Early in the field campaign, the DalBOSS data were collected in hourly (track) files rather than as 3 minute *casts* synchronized with the DalSAS and SeaSAS instruments. All times are in GMT.

Cast	*SDY*	*Time*	*State*	*File Name*	*Cast*	*SDY*	*Time*	*State*	*File Name*	*Cast*	*SDY*	*Time*	*State*	*File Name*
Track	191	1201	Beg.	J9819112.SHA	48	194	1117	Beg.	J02FD048.SHA	71	195	0826	Beg.	J02FD071.SHA
	191	1204	End			194	1121	End			195	0829	End	
	191	1210	Beg.		49	194	1123	Beg.	J02FD049.SHA	72	195	0831	Beg.	J02FD072.SHA
	191	1213	End			194	1126	End			195	0834	End	
	191	1216	Beg.		50	194	1127	Beg.	J02FD050.SHA	73	195	0834	Beg.	J02FD073.SHA
	191	1219	End			194	1130	End			195	0837	End	
	191	1220	Beg.		51	194	1131	Beg.	J02FD051.SHA	74	195	0840	Beg.	J02FD074.SHA
	191	1223	End			194	1134	End			195	0843	End	
	191	1224	Beg.		52	194	1135	Beg.	J02FD052.SHA	75	195	0846	Beg.	J02FD075.SHA
	191	1227	End			194	1138	End			195	0849	End	
	191	1228	Beg.		53	194	1151	Beg.	J02FD053.SHA	76	195	0850	Beg.	J02FD076.SHA
	191	1231	End			194	1154	End			195	0853	End	
	191	1232	Beg.		54	194	1155	Beg.	J02FD054.SHA	77	195	0853	Beg.	J02FD077.SHA
	191	1235	End			194	1159	End			195	0856	End	
	191	1236	Beg.		55	194	1200	Beg.	J02FD055.SHA	78	195	0857	Beg.	J02FD078.SHA
	191	1239	End			194	1203	End			195	0900	End	
	191	1240	Beg.		56	194	1208	Beg.	J02FD056.SHA	79	195	0901	Beg.	J02FD079.SHA
	191	1243	End			194	1211	End			195	0904	End	
34	191	1254	Beg.	J02FD034.SHA	57	194	1212	Beg.	J02FD057.SHA	80	195	0905	Beg.	J02FD080.SHA
	191	1255	End			194	1215	End			195	0908	End	
35	191	1256	Beg.	J02FD035.SHA	58	194	1217	Beg.	J02FD058.SHA	81	195	0908	Beg.	J02FD081.SHA
	191	1259	End			194	1220	End			195	0911	End	
36	191	1300	Beg.	J02FD036.SHA	59	194	1221	Beg.	J02FD059.SHA	82	195	0912	Beg.	J02FD082.SHA
	191	1303	End			194	1224	End			195	0915	End	
37	191	1304	Beg.	J02FD037.SHA	60	194	1225	Beg.	J02FD060.SHA	84	195	0919	Beg.	J02FD084.SHA
	191	1307	End			194	1228	End			195	0922	End	
39	194	1027	Beg.	J02FD039.SHA	61	194	1229	Beg.	J02FD061.SHA	85	195	0923	Beg.	J02FD085.SHA
	194	1030	End			194	1232	End			195	0926	End	
40	194	1032	Beg.	J02FD040.SHA	62	194	1233	Beg.	J02FD062.SHA	86	195	0927	Beg.	J02FD086.SHA
	194	1035	End			194	1234	End			195	0930	End	
41	194	1037	Beg.	J02FD041.SHA	63	194	1242	Beg.	J02FD063.SHA	87	195	0931	Beg.	J02FD087.SHA
	194	1040	End			194	1245	End			195	0934	End	
42	194	1041	Beg.	J02FD042.SHA	64	194	1246	Beg.	J02FD064.SHA	88	195	0935	Beg.	J02FD088.SHA
	194	1044	End			194	1249	End			195	0938	End	
43	194	1047	Beg.	J02FD043.SHA	65	194	1250	Beg.	J02FD065.SHA	89	195	0939	Beg.	J02FD089.SHA
	194	1050	End			194	1253	End			195	0942	End	
44	194	1052	Beg.	J02FD044.SHA	67	194	1254	Beg.	J02FD067.SHA	90	195	0943	Beg.	J02FD090.SHA
	194	1055	End			194	1257	End			195	0946	End	
45	194	1104	Beg.	J02FD045.SHA	68	195	0813	Beg.	J02FD068.SHA	91	195	0946	Beg.	J02FD091.SHA
	194	1107	End			195	0816	End			195	0949	End	
46	194	1108	Beg.	J02FD046.SHA	69	195	0818	Beg.	J02FD069.SHA	92	195	0950	Beg.	J02FD092.SHA
	194	1111	End			195	0821	End			195	0953	End	
47	194	1112	Beg.	J02FD047.SHA	70	195	0821	Beg.	J02FD070.SHA					
	194	1115	End			195	0824	End						

Table H1. A summary of the SQM-II Deployment Log for SeaBOARR-98. The DUT involved for each 3 minute each acquisition event is encoded in the file name: J2xcnnis.RAW where x is the session sequence letter, c is the DUT code, nn is a two-digit serial number, i is either L for light data or D for dark data, and s is the acquisition sequence letter. The (internal) monitor voltage is given in the V_M [mV] column. All times are in GMT.

Time	*File Name*	V_M	*Time*	*File Name*	V_M	*Time*	*File Name*	V_M	*Time*	*File Name*	V_M
	J2B (8 July)		1616	J2BR69LA.RAW	64.33	1636	J2BI30DA.RAW	64.40	1706	J2BI71DA.RAW	64.40
1600	J2BB01LA.RAW	64.36	1622	J2BR69LB.RAW	64.37	1646	J2BR46LA.RAW	64.40	1714	J2BR35LA.RAW	64.42
1605	J2BG01LB.RAW	64.36	1626	J2BR69DA.RAW		1651	J2BR46DA.RAW	64.38	1719	J2BR35DA.RAW	64.44
1609	J2BW01LA.RAW	64.36	1632	J2BI30LA.RAW	64.46	1701	J2BI71LA.RAW	64.45	1933	J2BR35LB.RAW	64.51

Table H1. (cont.) A summary of the SQM-II Deployment Log for SeaBOARR-98. The DUT involved for each 3 minute each acquisition event is encoded in the file name: `J2xcnnis.RAW` where `x` is the session sequence letter, `c` is the DUT code†, `nn` is a two-digit serial number, `i` is either `L` for light data or `D` for dark data, and `s` is the acquisition sequence letter. The (internal) monitor voltage is given in the V_M [mV] column. All times are in GMT.

Time	*File Name*	V_M	*Time*	*File Name*	V_M	*Time*	*File Name*	V_M	*Time*	*File Name*	V_M
1937	J2BR35DB.RAW	64.50	1746	J2CI93LA.RAW	64.57		*J2F (14 July)*		1459	J2HW01LA.RAW	62.49
1944	J2BI40LA.RAW	64.53	1750	J2CI93DA.RAW	64.53	1625	J2FB01LA.RAW	64.35	1504	J2HR28LA.RAW	62.47
1948	J2BI40DA.RAW	64.53	1756	J2CR09LA.RAW	64.55	1629	J2FG01LA.RAW	64.35	1509	J2HR28DA.RAW	62.41
1954	J2BR67LA.RAW	64.50	1800	J2CR09DA.RAW	64.52	1632	J2FW01LA.RAW	64.38	1521	J2HR35LA.RAW	62.49
1959	J2BR67DA.RAW	64.48	1803	J2CR64LA.RAW	64.54	1638	J2FR69LA.RAW		1526	J2HR35DA.RAW	62.52
2006	J2BI97LA.RAW	64.52	1806	J2CR64DA.RAW	64.53	1641	J2FR69DA.RAW	64.39	1533	J2HR64LA.RAW	62.51
2011	J2BI97DA.RAW	64.47	1810	J2CB01LB.RAW	64.51	1647	J2FR35LA.RAW	64.38	1538	J2HR64DA.RAW	62.52
2033	J2BI98LA.RAW	64.55	1814	J2CG01LB.RAW	64.52	1650	J2FR35DA.RAW	64.36	1544	J2HI40LA.RAW	62.59
2037	J2BI98DA.RAW	65.00	1818	J2CW01LB.RAW	64.59	1658	J2FI40LA.RAW	64.41	1549	J2HI40DA.RAW	62.59
2046	J2BR28LA.RAW	64.53	1822	J2CB01DA.RAW	-0.08	1702	J2FI40DA.RAW	64.39	1556	J2HB01LB.RAW	62.51
2053	J2BR28DA.RAW	64.51		*J2D (13 July)*		1708	J2FR28LA.RAW	64.40	1602	J2HG01LB.RAW	62.62
2108	J2BI20LA.RAW	65.43	1544	J2DB01LA.RAW	64.17	1712	J2FR28DA.RAW	64.40	1607	J2HW01LB.RAW	62.70
2112	J2BI20DA.RAW	64.50	1549	J2DG01LA.RAW	64.20	1717	J2FI99LA.RAW	64.44	1613	J2HB01DA.RAW	-0.07
2118	J2BI93LA.RAW	64.57	1553	J2DW01LA.RAW	64.20	1721	J2FI99DA.RAW	64.40		*J2I (11 August)*	
2123	J2BI93DA.RAW	64.52	1559	J2DI20LA.RAW		1727	J2FI20LA.RAW	64.42	1401	J2IB01LA.RAW	62.75
2132	J2BR09LA.RAW	64.50	1603	J2DI20DA.RAW	64.70	1731	J2FI20DA.RAW	64.40	1406	J2IG01LA.RAW	62.78
2136	J2BR09DA.RAW	64.49	1607	J2DI93LA.RAW	64.25	1734	J2FI93LA.RAW	64.43	1412	J2IW01LA.RAW	62.84
2140	J2BR64LA.RAW	64.52	1611	J2DI93DA.RAW	64.19	1737	J2FI93DA.RAW	64.42	1417	J2IR69LA.RAW	62.84
2144	J2BR64DA.RAW	64.52	1621	J2DR69LA.RAW	64.23	1744	J2FR09LA.RAW	64.45	1422	J2IR69DA.RAW	62.86
2155	J2BI99LA.RAW	64.55	1625	J2DR69DA.RAW	64.22	1747	J2FR09DA.RAW	64.45	1437	J2II30LA.RAW	62.91
2159	J2BI99DA.RAW	64.50	1638	J2DR35LA.RAW	64.23	1751	J2FR64LA.RAW	64.45	1452	J2II30DA.RAW	62.89
2209	J2BN48LA.RAW	64.56	1642	J2DR35DA.RAW	64.23	1755	J2FR64DA.RAW	64.44	1458	J2IR35LA.RAW	62.89
2213	J2BN48DA.RAW	64.50	1647	J2DI40LA.RAW	64.32	1759	J2FB01LB.RAW	64.44	1503	J2IR35DA.RAW	62.94
2217	J2BQ33LA.RAW	64.54	1651	J2DI40DA.RAW	64.28	1802	J2FG01LB.RAW	64.45	1508	J2II40LA.RAW	63.04
2221	J2BQ33DA.RAW	64.52	1659	J2DR09LA.RAW	64.31	1806	J2FW01LB.RAW	64.50	1513	J2II40DA.RAW	62.99
2227	J2BB01LB.RAW	64.50	1703	J2DR09DA.RAW	64.25	1811	J2FB01DA.RAW	-0.08	1541	J2IR28LA.RAW	63.14
2231	J2BG01LC.RAW	64.55	1707	J2DR64LA.RAW	64.27		*J2G (6 August)*		1548	J2IR28DA.RAW	63.08
2235	J2BW01LB.RAW	64.57	1711	J2DR64DA.RAW	64.26	1843	J2GB01LA.RAW	61.90	1736	J2II20LA.RAW	63.48
2241	J2BB01DA.RAW	-0.08	1717	J2DR28LA.RAW	64.28	1849	J2GG01LA.RAW	61.95	1740	J2II20DA.RAW	63.44
	J2C (9 July)		1721	J2DR28DA.RAW	64.28	1901	J2GW01LA.RAW	62.01	1744	J2II93LA.RAW	63.48
1638	J2CB01LA.RAW	64.37	1726	J2DI99LA.RAW	64.24	1907	J2GI20LA.RAW	62.04	1748	J2II93DA.RAW	63.46
1642	J2CG01LA.RAW	64.39	1730	J2DI99DA.RAW	64.21	1913	J2GI20DA.RAW	62.02	1707	J2IR09LA.RAW	63.36
1646	J2CW01LA.RAW	64.44	1736	J2DR46LA.RAW	64.20	1918	J2GI93LA.RAW	62.07	1711	J2IR09DA.RAW	63.33
1654	J2CR69LA.RAW	64.41	1739	J2DR46DA.RAW	64.19	1923	J2GI93DA.RAW	62.06	1715	J2IR64LA.RAW	63.38
1658	J2CR69DA.RAW	64.41	1743	J2DI71LA.RAW	64.24	1937	J2GR09LA.RAW	62.10	1719	J2IR64DA.RAW	63.36
1702	J2CI30LA.RAW	64.48	1746	J2DI71DA.RAW		1947	J2GR09DA.RAW	62.18	1620	J2II99LA.RAW	63.24
1707	J2CI30DA.RAW	64.43	1750	J2DB01LB.RAW	64.18	1952	J2GR69LA.RAW	62.19	1625	J2II99DA.RAW	63.22
1712	J2CR35LA.RAW	64.45	1755	J2DG01LB.RAW	64.19	1956	J2GR69DA.RAW	62.19	1638	J2IN48LA.RAW	63.31
1716	J2CR35DA.RAW	64.45	1758	J2DW01LB.RAW	64.22	2000	J2GB01LB.RAW	62.21	1644	J2IN48DA.RAW	63.29
1720	J2CI40LA.RAW	64.52	1802	J2DB01DA.RAW	-0.07	2007	J2GG01LB.RAW	62.22	1649	J2IQ33LA.RAW	63.33
1723	J2CI40DA.RAW	64.46		*J2E (14 July)*		2012	J2GW01LB.RAW	62.26	1654	J2IQ33DA.RAW	63.30
1730	J2CR28LA.RAW	64.48	1446	J2EB01LA.RAW	64.00	2018	J2GB01DA.RAW	-0.08	1753	J2IB01LB.RAW	63.49
1733	J2CR28DA.RAW	64.50	1450	J2EG01LA.RAW	64.02		*J2H (7 August)*		1759	J2IG01LB.RAW	63.49
1738	J2CI20LA.RAW	64.52	1454	J2EW01LA.RAW	64.05	1449	J2HB01LA.RAW	62.40	1804	J2IW01LB.RAW	63.54
1742	J2CI20DA.RAW	64.50	1500	J2EB01LB.RAW		1454	J2HG01LA.RAW	62.43	1810	J2IB01DA.RAW	-0.04

† The DUT codes are as follows: `B` for a black fiducial, `G` for a glass (radiance) fiducial, `I` for an OCI-200 in-water irradiance sensor, `M` for an OCI-200 in-air irradiance sensor, `N` for an OCI-1000 in-air irradiance sensor, `Q` for an OCR-1000 in-water radiance sensor, `R` for an OCR-200 in-water radiance sensor, and `W` for a white (irradiance) fiducial.

Glossary

A/D	Analog-to-Digital
AAOT	*Acqua Alta* Oceanographic Tower
AC	Alternating Current
AERONET	Aerosol Robotic Network
AMT	Atlantic Meridional Transect
AMT-5	The Fifth AMT Cruise
ASCII	American Standard Code for Information Interchange
BRDF	Bidirectional Reflectance Distribution Function
CC	Cloud Cover
CCPO	Center for Coastal Physical Oceanography
CDOM	Colored Dissolved Organic Matter
CEC	Commission of the European Communities
CERT	Calibration Evaluation and Radiometric Testing
CNR	*Consiglio Nazionale delle Ricerche* (National Research Council)
CoASTS	Coastal Atmosphere and Sea Time Series
CTD	Conductivity, Temperature, and Depth
DalBOSS	Dalhousie Buoyant Optical Surface Sensor
DalSAS	Dalhousie SeaWiFS Aircraft Simulator
DARR-94	Data Analysis Round-Robin
DAS	Data Acquisition Sequence
DATA	Not an acronym, but a designator for the Satlantic, Inc., series of power and telemetry units.
DC	Direct Current
DCP	Data Collection Platform
DIR	Not an acronym, but a designator for the Satlantic, Inc., series of directional units.
DUT	Device Under Test
DVM	Digital Voltmeter
GF/F	Not an acronym, but a specific type of glass fiber filter manufactured by Whatman.
GMT	Greenwich Mean Time
GSFC	Goddard Space Flight Center
HPLC	High Performance Liquid Chromatography
IOP	Inherent Optical Property
ISDGM	*Istituto per lo Studio della Dinamica delle Grandi Masse* (Italy)
JRC	Joint Research Centre
LoCNESS	Low-Cost NASA Environmental Sampling System
LS	Light Stability
MFR-6	Multi-Filter Rotating Shadow-Band Radiometer
METEOSAT	Meteorological Satellite
miniNESS	miniature NASA Environmental Sampling System
NASA	National Aeronautics and Space Administration
NIR	Near-Infrared
NRSR	Normalized Remote Sensing Reflectance
OCI	Ocean Color Irradiance
OCR	Ocean Color Radiance
PC	Personal Computer
PM	Particulate Matter
RMSD	Root Mean Square Difference
RSMAS	Rosenstiel School for Marine and Atmospheric Science
S/N	Serial Number
SAI	Space Applications Institute
SeaBASS	SeaWiFS Bio-Optical Archive and Storage System
SeaBOARR	SeaWiFS Bio-Optical Algorithm Round-Robin
SeaBOARR-98	The First SeaBOARR (held in 1998)
SeaBOSS	SeaWiFS Buoyant Optical Surface Sensor
SeaFALLS	SeaWiFS Free-Falling Advanced Light Level Sensors
SeaOPS	SeaWiFS Optical Profiling System
SeaSAS	SeaWiFS Surface Acquisition System
SeaSURF	SeaWiFS Square Underwater Reference Frame
SeaWiFS	Sea-viewing Wide Field-of-view Sensor
SDY	Sequential Day of the Year
SIMBIOS	Sensor Intercomparison and Merger for Biological and Interdisciplinary Ocean Studies
SIRREX	SeaWiFS Intercalibration Round-Robin Experiment
SIRREX-3	The Third SIRREX
SIRREX-4	The Fourth SIRREX
SMSR	SeaWiFS Multichannel Surface Reference
SOOP	SeaWiFS Ocean Optics Protocols
SPMR	SeaWiFS Profiling Multichannel Radiometer
SQM	SeaWiFS Quality Monitor
SQM-II	The Second Generation SQM
SS	Sea State
THOR	Three-Headed Optical Recorder
TSM	Total Suspended Matter
UPS	Uninterruptable Power Supply
WETLabs	Western Environmental Technology Laboratories (Inc.)
WiSPER	Wire-Stabilized Profiling Environmental Radiometer
WMO	World Meteorological Organization
WS	Wind Speed

Symbols

$(\breve{})$	A measurement corrected for scattering effects.
$(\hat{})$	A measurement corrected for temperature and salinity effects.
a	Absorption (of seawater).
a_p	Particulate absorption coefficient (of seawater).
A_p	The peak pigmented area.
A_s	The internal standard area.
$a_{\mathrm{ys}}(\lambda)$	The yellow substance absorption coefficient.
$A_{\mathrm{sus}}(\lambda)$	The absorbance of the equivalent particle suspension.
$A_{\mathrm{ys}}(\lambda)$	The yellow substance absorbance.
c	Attenuation (of seawater).
C	The chlorophyll concentration.
C_0	A spectral calibration constant.
C_1	A spectral calibration constant.
C_a	The concentration of chlorophyll *a*.
C_{a+a}	The concentration of chlorophyll *a* plus chlorophyllide *a*.
C_p	Pigment concentration.
C_{TSM}	The concentration of total suspended matter.
e	A regression coefficient.
E_d	Downwelled irradiance.
E_i	Indirect (diffuse) irradiance.
E_p	Plaque downwelling total irradiance.
E_u	Upwelled irradiance.

f_p The relative response factor for a particular pigment.
F_A The filter clearance area.
K_u The diffuse attenuation coefficient calculated from $L_u(z)$ data.
K_w The attenuation coefficient for pure water.
L_c The pathlength of a cuvette.
L_i Indirect (sky) radiance.
L_p Plaque radiance.
L_T Total radiance (for $z = 0^+$, right above the sea surface).
L_u Upwelled radiance.
L_W Water-leaving radiance.
$\hat{L}_W^A(0^+, \lambda)$ Water-leaving radiance derived from in-air method A.
$\tilde{L}_W^B(0^+, \lambda)$ Water-leaving radiance derived from in-water method B.
m The sea water absorption, $a(\lambda)$, or attenuation, $c(\lambda)$, measured by the AC-9 before any temperature or salinity correction.
$n_w(\lambda)$ The refractive index of seawater.
N The number of measurements.
$R_f(\lambda)$ The filter reflectance.
$R_{\rm rs}$ Remote sensing reflectance.
S Salinity.
T Temperature.
T' The temperature of water during calibration.
V_f The volume filtered.
V_M The (internal) monitor voltage.
V_w The volume of filtered water.
W_s The internal standard weight.
x The abscissa.
y The ordinate.
z The vertical coordinate.
z_0 Center depth.
α The Ångström exponent.
β The Ångström coefficient.
γ $\log\left[\rho_T^{-1}(\lambda)\right] - 0.5\log\left[\rho_T^{-1}(750)\right]$.
δ_r $L_T(\lambda_r, \phi', \vartheta)/L_i(\lambda_r, \phi', \vartheta')$.
δz $z - z_0$.
Δz The integration half interval ($\Delta z \approx 4$–$10\,\mathrm{m}$).
ΔL A correction factor for the specular reflection of sky light and the residual reflection of downwelling radiation from wave facets.
θ The solar zenith angle.
ϑ The nadir angle.
ϑ' $\pi - \vartheta$.
λ Wavelength.
λ_0 Reference wavelength.
λ_r A wavelength in the near infrared part of the spectrum.
μ The estimated mean.
$\rho(\lambda)$ The Fresnel reflectance of seawater.
$\rho_T(\lambda)$ Transmission mode reflectance.
$\rho_R(\lambda)$ Reflectance mode reflectance.
σ One standard deviation.
τ An instrument-dependent function.
ϕ The solar azimuth angle.
ϕ' $\phi \pm \frac{\pi}{2}$ (90° away from the sun in either direction, i.e., ϕ^+ or ϕ^-).
ϕ^- $\phi - \frac{\pi}{2}$.
ϕ^+ $\phi + \frac{\pi}{2}$.
φ The perturbations (or tilts) in alignment away from z.
χ_c A regression coefficient.
ψ^B The root mean square difference using in-water method B.

References

Aiken, J., D.G. Cummings, S.W. Gibb, N.W. Rees, R. Woodd-Walker, E.M.S. Woodward, J. Woolfenden, S.B. Hooker, J-F. Berthon, C.D. Dempsey, D.J. Suggett, P. Wood, C. Donlon, N. González-Benítez, I. Huskin, M. Quevedo, R. Barciela-Fernandez, C. de Vargas, and C. McKee, 1999: AMT-5 Cruise Report. *NASA Tech. Memo. 1998–206892, Vol. 2,* S.B. Hooker and E.R. Firestone, Eds., NASA Goddard Space Flight Center, Greenbelt, Maryland, 113 pp.

Austin, R.W., 1974: The remote sensing of spectral radiance from below the ocean surface. In: *Optical Aspects of Oceanography,* N.G. Jerlov and E.S. Nielsen, Eds., Academic Press, London, 317–344.

——, 1980: Gulf of Mexico, ocean color surface truth measurements. *Bound.-Layer Meteorol.,* **18,** 269–85.

——, and T.J. Petzold, 1981: The determination of diffuse attenuation coefficient of sea water using the Coastal Zone Color Scanner. In: *Oceanography from Space,* J.F.R. Gower, Ed., Plenum Press, 239–256.

Bukata, R.P., J.H. Jerome, and J.E. Bruton, 1988: Particulate Concentrations in Lake St. Clair as Recorded by Shipborne Multispectral Optical Monitoring System. *Remote Sens. Envir.,* **25,** 201–229.

——, ——, K.Y. Kondrattyev, and D.V. Pozdnyakov, 1995: *Optical Properties and Remote Sensing of Inland and Coastal Waters.* CRC Press, Boca Raton, Florida 362 pp.

Carder, K.L., and R.G. Steward, 1985: A remote sensing reflectance model of a red tide dinoflagellate off West Florida. *Limnol. Oceanogr.,* **30,** 286–298.

Ferrari, G.M., M.D. Dowell, S. Grossi, and C. Targa, 1996: Relationship between the optical properties of chromophoric dissolved organic matter and total concentration of dissolved organic carbon in the southern Baltic Sea region. *Mar. Chem.,* **55,** 299–316.

Gordon, H.R., 1981: A preliminary assessment of the Nimbus-7 CZCS atmospheric correction algorithm in a horizontally inhomogeneous atmosphere. In: *Oceanography from Space,* J.F.R. Gower, Ed., Plenum Press, 257–266.

——, and K. Ding, 1992: Self shading of in-water optical instruments. *Limnol. Oceanogr.,* **37,** 491–500.

——, and M. Wang, 1994: Retrieval of water-leaving radiances and aerosol optical thickness over the oceans with SeaWiFS: a preliminary algorithm, *Appl. Opt.,* **33,** 443–452.

Harrison, L., J. Michalsky, and J. Berndt, 1994: Automatic multifilter rotating shadow-band radiometer: An instrument for optical depth and radiation measurements. *Appl. Opt.,* **33,** 5,118–5,125.

Holben, B.N., T.F. Eck, I. Slutsker, D. Tanré, J.P. Buis, A. Setzer, E. Vermote, J.A. Reagan, Y.I. Kaufman, T. Nakajima, F. Lavenu, I. Jankowiak, and A. Smirnov, 1998: AERONET—A federal instrument network and data archive for aerosol characterization. *Remote Sens. Environ.,* **66,** 1–16.

Hooker, S.B., W.E. Esaias, G.C. Feldman, W.W. Gregg, and C.R. McClain, 1992: An Overview of SeaWiFS and Ocean Color. *NASA Tech. Memo. 104566, Vol. 1,* S.B. Hooker and E.R. Firestone, Eds., NASA Goddard Space Flight Center, Greenbelt, Maryland, 24 pp., plus color plates.

——, and ——, 1993: An overview of the SeaWiFS project. *Eos, Trans., Amer. Geophys. Union,* **74,** 241–246

——, C.R. McClain, and A. Holmes, 1993a: Ocean color imaging: CZCS to SeaWiFS. *Marine Tech. Soc. J.,* **27,** 3–15.

——, W.E. Esaias, and L.A. Rexrode, 1993b: Proceedings of the First SeaWiFS Science Team Meeting. *NASA Tech. Memo. 104566, Vol. 8,* S.B. Hooker and E.R. Firestone, Eds., NASA Goddard Space Flight Center, Greenbelt, Maryland, 61 pp.

——, C.R. McClain, J.K. Firestone, T.L. Westphal, E-n. Yeh, and Y. Ge, 1994: The SeaWiFS Bio-Optical Archive and Storage System (SeaBASS), Part 1. *NASA Tech. Memo. 104566, Vol. 20,* S.B. Hooker and E.R. Firestone, Eds., NASA Goddard Space Flight Center, Greenbelt, Maryland, 40 pp.

——, and J. Aiken, 1998: Calibration evaluation and radiometric testing of field radiometers with the SeaWiFS Quality Monitor (SQM). *J. Atmos. Oceanic Tech.,* **15,** 995–1,007.

——, and C.R. McClain. 1999. A comprehensive plan for the calibration and validation of SeaWiFS data. *Prog. Oceanogr.,* (submitted).

Jeffrey, S.W., R.F.C. Mantoura, and S.W. Wright (Eds.), 1997: *Phytoplankton Pigments in Oceanography: Guidelines to Modern Methods.* UNESCO Publishing, Paris, 661 pp.

Johnson, B.C., S.S. Bruce, E.A. Early, J.M. Houston, T.R. O'Brian, A. Thompson, S.B. Hooker, and J.L. Mueller, 1996. The Fourth SeaWiFS Intercalibration Round-Robin Experiment (SIRREX-4), May 1995. *NASA Tech. Memo. 104566, Vol. 37,* S.B. Hooker and E.R. Firestone, Eds., NASA Goddard Space Flight Center, Greenbelt, Maryland, 65 pp.

——, P-S. Shaw, S.B. Hooker, and D. Lynch, 1998: Radiometric and engineering performance of the SeaWiFS Quality Monitor (SQM): A portable light source for field radiometers. *J. Atmos. Oceanic Tech.,* **15,** 1,008–1,022.

Joint Global Ocean Flux Study, 1994: Protocols for the Joint Global Ocean Flux Study Core Measurements. Intergovernmental Oceanographic Commission, Scientific Committee on Oceanic Research. Manual and Guides, UNESCO, **29,** 91–96.

Lazin, G., 1998: Correction Methods for Low-Altitude Remote Sensing of Ocean Color. *M. Sc. Thesis,* Dalhousie University, 98 pp.

——, S. Hooker, G. Zibordi, S. McLean, and M.R. Lewis, 1998: In-water and above-water measurements of ocean color. *Proc. Ocean Optics XIV,* [Available on CD-ROM], Office of Naval Research, Washington, DC.

Lee, Z.P., K.L. Carder, R.G. Steward, T.G. Peacock, C.O. Davis, and J.L. Mueller, 1996: Remote sensing reflectance and inherent optical properties of oceanic waters derived from above-water measurements. *Proc. SPIE,* **2,963,** 160–166.

McLean, S., S. Feener, J. Scrutton, M. Small, S. Hooker, and M. Lewis, 1998: SQM-II: A commercial portable light source for field radiometer quality assurance. *Proc. Ocean Optics XIV,* [Available on CD-ROM], Office of Naval Research, Washington, DC.

Morel, A., 1980: In-water and remote measurements of ocean color. *Bound.-Layer Meteorol.,* **18,** 177–201.

——, 1988: Optical modeling of the upper ocean in relation to its biogenous matter content (Case I waters). *J. Geophys. Res.,* **93,** 10,749–10,768.

Mueller, J.L., and R.W. Austin, 1992: Ocean Optics Protocols for SeaWiFS Validation. *NASA Tech. Memo. 104566, Vol. 5,* S.B. Hooker and E.R. Firestone, Eds., NASA Goddard Space Flight Center, Greenbelt, Maryland, 43 pp.

——, and ——, 1995: Ocean Optics Protocols for SeaWiFS Validation, Revision 1. *NASA Tech. Memo. 104566, Vol. 25,* S.B. Hooker, E.R. Firestone, and J.G. Acker, Eds., NASA Goddard Space Flight Center, Greenbelt, Maryland, 66 pp.

——, B.C. Johnson, C.L. Cromer, S.B. Hooker, J.T. McLean, and S.F. Biggar, 1996: The Third SeaWiFS Intercalibration Round-Robin Experiment (SIRREX-3), 19–30 September 1994. *NASA Tech. Memo. 104566, Vol. 34,* S.B. Hooker, E.R. Firestone, and J.G. Acker, Eds., NASA Goddard Space Flight Center, Greenbelt, Maryland, 78 pp.

Robins, D.B., A.J. Bale, G.F. Moore, N.W. Rees, S.B. Hooker, C.P. Gallienne, A.G. Westbrook, E. Marañón, W.H. Spooner, and S.R. Laney, 1996: AMT-1 Cruise Report and Preliminary Results. *NASA Tech. Memo. 104566, Vol. 35,* S.B. Hooker and E.R. Firestone, Eds., NASA Goddard Space Flight Center, Greenbelt, Maryland, 87 pp.

Siegel, D.A., M.C. O'Brien, J.C. Sorensen, D.A. Konnoff, E.A. Brody, J.L. Mueller, C.O. Davis, W.J. Rhea, and S.B. Hooker, 1995: Results of the SeaWiFS Data Analysis Round-Robin (DARR-94), July 1994. *NASA Tech. Memo. 104566, Vol. 26,* S.B. Hooker and E.R. Firestone, Eds., NASA Goddard Space Flight Center, Greenbelt, Maryland, 58 pp.

Smith, R.C., and K.S. Baker, 1984: The analysis of ocean optical data. *Ocean Optics VII,* M. Blizard, Ed., SPIE **478,** 119–126.

——, and K.S. Baker, 1986: Analysis of ocean optical data II. *Ocean Optics VIII,* P.N. Slater, Ed., SPIE, **637,** 95–107.

Strickland, J.D.H., and T.R. Parsons, 1972: *A Practical Handbook of Sea Water Analysis.* Fish. Res. Board. Canada, 310 pp.

Tassan, S., and M. Ferrari, 1995: An alternative approach to absorption measurements of aquatic particles retained on filters. *Limnol. Oceanogr.,* **40,** 1,358–1,368.

Zaneveld, J.R.V., J.C. Kitchen, A. Bricaud, and C. Moore, 1992: Analysis of *in situ* spectral absorption meter data. *Ocean Optics XI,* Proc. SPIE, **1,750,** 187–200.

Zibordi, G., and M. Ferrari, 1995: Instrument self-shading in underwater optical measurements: Experimental data. *Appl. Opt.,* **34,** 2,750–2,754.

——, J.P. Doyle, and S.B. Hooker, 1999: Offshore tower shading effects on in-water optical measurements. *J. Atmos. and Oceanic Tech.,* (accepted).

The SeaWiFS Postlaunch Technical Report Series

Vol. 1

Johnson, B.C., J.B. Fowler, and C.L. Cromer, 1998: The SeaWiFS Transfer Radiometer (SXR). *NASA Tech. Memo. 1998–206892, Vol. 1,* S.B. Hooker and E.R. Firestone, Eds., NASA Goddard Space Flight Center, Greenbelt, Maryland, 58 pp.

Vol. 2

Aiken, J., D.G. Cummings, S.W. Gibb, N.W. Rees, R. Woodd-Walker, E.M.S. Woodward, J. Woolfenden, S.B. Hooker, J-F. Berthon, C.D. Dempsey, D.J. Suggett, P. Wood, C. Donlon, N. González-Benítez, I. Huskin, M. Quevedo, R. Barciela-Fernandez, C. de Vargas, and C. McKee, 1998: AMT-5 Cruise Report. *NASA Tech. Memo. 1998–206892, Vol. 2,* S.B. Hooker and E.R. Firestone, Eds., NASA Goddard Space Flight Center, Greenbelt, Maryland, 113 pp.

Vol. 3

Hooker, S.B., G. Zibordi, G. Lazin, and S. McLean, 1999: The SeaBOARR-98 Field Campaign. *NASA Tech. Memo. 1999–206892, Vol. 3,* S.B. Hooker and E.R. Firestone, Eds., NASA Goddard Space Flight Center, Greenbelt, Maryland, 40 pp.